Force Sensing and Control in Micromanipulation

LU ZHE

Department of Mechanical Engineering

A thesis submitted to the National University of Singapore

in fulfillment of the requirements for the degree of

Doctor of Philosophy

2007

Statement of Originality

I hereby certify that the content of this thesis is the result of work done by me and has not been submitted for a higher degree to any other University or Institution.

…… ……

Date LU ZHE

Acknowledgments

First and foremost, I extend my warmest and heartfelt thanks to Prof. Peter Chen Chao Yu and Dr. Lin Wei, my supervisors, for their inspiration, keen insight, unwaning enthusiasm and friendship. It is they who first introduce me to this field and give me invaluable guidance throughout the project.

I also express my special appreciation to Dr. Luo Hong, Dr. Andrew Shacklock, Dr. Liu YuChan, Dr. Lu HaiJing, Dr. Yang GuiLin, Dr. Wang ZhenFeng and other staff from the Singapore Institute of Manufacturing Technology (SIMTech) for all their constant support and help in this research.

I also express my appreciation to Dr. Etienne Burdet and Prof. Teo Chee Leong from the Department of Mechanical Engineering of the National University of Singapore, who have given me invaluable suggestions for this research.

I also express my appreciation to Prof. Franck Alexis Chollet and Mr. A Mohammed from Nanyang Technological University for their technical contributions.

I also express my appreciation to Dr. Ge RuoWen and Mr. Sheng DongLai from the Department of Biological Sciences, National University of Singapore for their assistance

in the project of the zebrafish embryos injection.

I am also grateful to the staff in the Control and Mechatronics Lab, for their assistance and kindness.

Last but not least, I wish to thank all my fellow colleagues, and in particular Anand Ganapathy, Dong JianFei, Du TieHua, Li YuanPing, Meng QingNian, Nam Joo Hoo, Sui Dan, Wang Chen, Wang WenHui, Yang Lin, Zhao GuoYong and Zheng Hao. for their help and friendships.

Finally, my most sincere thanks go to my parents for their constant encouragement and support.

I am grateful to the National University of Singapore and the Singapore Ministry of Education for the financial support, which have enabled realization of this work.

Table of Contents

Summary

In this work, the applicability of micro-force sensing and control in micromanipulation is investigated. A survey of the general field of micromanipulation reveals that the full potential of the micro-force signal has yet to be extensively utilized in current micromanipulation technology. Three experimental solutions are developed to resolve three problems on micro-force sensing and control. The first problem concerns the study on whether micro-force sensing alone could be used to provide useful information in micromanipulation. The experimental solution demonstrates that micro-force sensing can be used to facilitate characterization tasks (such as in determination of micro-surface topography and mechanical properties) in micromanipulation. The second problem concerns the improvement of position-based manipulation techniques through utilization of information obtained by force measurement. The experimental solution demonstrates the use of micro-force as a feedback to augment position control. The third problem concerns the applicability of direct force control in micromanipulation. The experimental solution shows that the direct force control represents an effective alternative to position-based force control in micro-assembly. Implementation of direct force control is needed in micromanipulation.

To implement direct force control, two main issues are addressed. The first issue concerns the design of a force transmission stage, which provides frictionless translation motion, as the force involved in micromanipulation is quite small (at level of milli-Newton or below). A compound flexure stage is designed and built to provide frictionless translation with low stiffness motion along one axis. The second issue concerns the design of a force controller which could precisely control the interaction force. An explicit force controller is designed to control the actual interaction force to follow a desired force trajectory. The direct force control is applied with the use of mechanical fixture, which is used to overcome adhesion force effects during the release of the micro-objects. The integration of the force control system with the microscopy system and micro-positioning system is demonstrated in a micromanipulation system.

Three experiments are used to illustrate the applicability of micro-force sensing and control in practical micromanipulation tasks. The first experiment is to use micro-force sensing to augment conventional approaches for fast and accurate fiber pigtailing in photonic assembly. A photonic alignment system based on the micro-force sensing is developed to facilitate coarse alignment in active fiber pigtailing in integrated optics technologies. The second experiment is to use micro-force sensing and control to automate the zebrafish embryos injection. A prototype micromanipulation system is developed for automatic batch microinjection in biological science. The third experiment to use micro-force sensing and control to automate the pick-up and assembly of the micro-part used in scaffold assembly. An explicit force-feedback control system is developed for the automation of the scaffold assembly in tissue engineering.

Publications

Journal Papers

1. Z. F. Wang, W. Cao, and Z. Lu, “MOEMS: Packaging and Testing”, Microsystem Technologies, Vol. 11, pp. 52-58, 2005.

2. Z. Lu, P. C. Y. Chen, and W. Lin, “Optimization of Hamiltonian algorithm for fiber alignment by simulation and experiment”, Opt. Eng. 44, 075002 (2005).

3. Z. Lu, P. C. Y. Chen and W. Lin, “Force Sensing and Control in Micromanipulation,” IEEE Trans. Syst., Man, and Cybern. C, Vol. 36(6), pp.713-724, 2006.

4. Z. Lu, H. Luo, P. C. Y. Chen and W. Lin, “An Integrated Probe Sensor for Micro-force Measurement”, Meas. Sci. Technol. Vol. 17, pp. 869-875, 2006.

5. Z. Lu, P. C. Y. Chen, H. Luo and W. Lin, “Micro-force Sensing for Coarse Alignment in Active Fiber Pigtailing,” Opt. Eng. 45, 075005 (2006).

6. Z. Lu, P. C. Y. Chen, A. Ganapathy, G. Y. Zhao, J. H. Nam, G. L. Yang, E. Burdet, C. L. Teo, Q. N. Meng and W. Lin, “A Force-feedback Control System for Micro-assembly,” J. of Micromech. and Microeng., 16 (2006) 1861-1868.

7. Z. Lu, P. C. Y. Chen, J. H. Nam, R. W. Ge and W. Lin, “A Micromanipulation System with Dynamic Force-Feedback for Automatic Batch Microinjection”, J. of Micromech. and Microeng., 17 (2007) 314-321.

Conference Papers

1. Z. Lu, W. Lin and P. C. Y. Chen, “A prototype system of optical fiber alignment based on Hamiltonian algorithm”, in Proc. IEEE Int. Conf. Intell. Mechatron. and Automat., 2004, pp. 1-5.

2. Z. Lu, P. C. Y. Chen, J. H. Nam, R. W. Ge and W. Lin, “A micromanipulation system for automatic batch microinjection (Video),” in Proc. IEEE Int. Conf. on Robot. and Automat. (Roma, Italy), 2007.

List of Tables

List of Figures

List of Symbols

α	angle between probe tip and the surface of the pad
β	position scaling
γ	force scaling
ε	permittivity of the dielectric medium
μN	micro-Newton
A	plate area of the capacitor
B_1	damping of the inner compound springs
B_2	damping of the outer compound springs
B_3	damping of the environment model
C	capacitance
d	distance between the sensor and substrate of the pad
d_f	deflection of the beam tip with extended fiber

d_s	deflection of the beam tip
D	distance between the plates
E	modulus of elasticity of the beam
f_c	constraint force between the mechanical fixture and the micro-object
f_m	adhesion force between the micromanipulator and the micro-object
f_s	adhesion force between the substrate and the micro-object
F_c	measured contact force
F_d	desired reference force
F_i	input force
F_t	force applied at the sensor tip
F	output force from the voice-coil actuator
h	height of the pad
I_i	input current
I	moment of inertia of the beam cross section
k	correlation between d_f and d_s
K_1	stiffness of the inner compound springs
K_2	stiffness of the outer compound springs
K_3	stiffness of the environment model

K_c	force sensitivity of the voice-coil actuator
K_d	derivative gain
K_e	estimated stiffness of the environment model
K_p	proportional gain
l_1	length of the fiber extension
l	active length of the beam
M_1	mass of the lower movable platform
M_2	mass of the upper movable platform
M	moment on the sensor tip
nN	nano-Newton
r	ratio of an index length (i.e., geometrical scale) between the macro-world and micro-world
X_i	deflection of the inner compound spring
X_o	deflection of the outer compound spring

M_2	mass of the upper movable platform
M	moment on the sensor tip
nN	nano-Newton
r	ratio of an index length (i.e., geometrical scale) between the macro-world and micro-world
X_i	deflection of the inner compound spring
X_o	deflection of the outer compound spring

Chapter 1

Introduction

1.1 Background

The last century has seen significant innovative exploration concerning the nature of micro-world [1]. The scientific results of such exploration gradually exert their influence on our understanding of natural phenomena in even increasingly smaller scale, and at the same time are beginning to revolutionize the ways new products are engineered and manufactured. One example of such engineering innovation is the advance of miniaturized intelligent devices enabled by the emergence of microengineering technologies [2]. Another impact of results from exploration of the micro-world is manifested in embryology and genetics engineering, where research at the cell level (or smaller) promises to revolutionize the practice of medicine and improve the quality and expectancy of life [3].

At the core of these emerging technologies and sciences lies a common fundamental issue: How to facilitate interaction between human and the micro-world. The simple act of observing activities in the micro-world under the microscope is highly inadequate to meet the growing desire of human to practically manipulate objects in the micro-world. In order to handle various practical tasks, whether it is to construct a complicated miniaturized structure or to perform operation on a single cell, it is necessary to manipulate objects in micro-scale with high dexterity. Such manipulation is referred to as micromanipulation.

Micromanipulation includes observation, positioning and transformation of micro-objects. Manual micromanipulation has been practiced for almost a century in invertebrates and lower animals [4]. In the last decade, micromanipulation techniques had been applied in the treatment of human disease. For example, intracytoplasmic sperm injection (ICSI), a form of micromanipulation, has recently been very successful in treating male-factor infertility by direct injection of single sperm into an egg [5] [6]. The last decade has also witnessed the trend to apply micromanipulation techniques to complement conventional techniques for fabrication of Micro Electro-Mechanical Systems (MEMS) devices [7]. Currently, conventional techniques for fabricating MEMS devices are bulk and surface silicon micromachining, laser micromachining, and LIGA [8] [9] [10]. These, however, may not be suitable in the manufacture of certain hybrid MEMS devices due to their particularity in terms of processes, materials, and geometries [11]. A viable approach to the manufacture of such devices is micro-assembly, where various parts (possibly fabricated with different techniques) are assembled discretely through micromanipulation to

yield an integrated 3D hybrid MEMS device [12].

1.1.1 Current micromanipulation techniques and the needs for micro-force sensing and control

Currently in micromanipulation, mature microscopy (for observation) and micro-positioning techniques exist. Microscopy has been successfully applied to the semiconductor industry and life sciences. Automated microscope stages were developed and used extensively for wafer inspection in semiconductor fabrication. Microscopes with automated internal controls are commercially available for use in life-science research laboratory [13]. For micro-positioning, commercial stages and motors are available to provide high stability and high resolution in multi-axis positioning. Diverse range of motion can be achieved by combining long-travel actuators (such as stepper motor) with ultraprecise actuators (such as piezoelectric actuator) [14].

Microscopy and micro-positioning techniques have been successfully applied in some micromanipulation tasks [15]-[16]. However, these techniques are not adequate for more sophisticated micromanipulation, because in these techniques only position is measured and controlled while the force that quantitively describes interaction between objects in micro-world is not considered. This category of interaction involving force includes interaction between an object being manipulated and the manipulator, and interaction between an object and its environment (e.g., substrate), etc.

The sensing and control of the force of interaction are important in micromanipulation.

For example, when manipulating objects (especially delicate structure or biological material that is usually fragile) in the micro-world, pure position control is usually not adequate in ensuring successful operation and preventing damage to the object. Force sensing is often needed to augment the position control in order to achieve safer manipulation. As another example, in certain applications (such as individual cell based diagnosis or pharmaceutical test) obtaining force information is the main objective. This will involve probing or reconstructing the state of the micro-objects through knowledge of the micro-forces interacting between the manipulator and object [17]- [18].

The nature of force in micromanipulation has its unique characteristics. In micromanipulation, the size of the manipulated object is usually much less than one millimeter in a single dimension. This leads to many problems (for manipulation through force) which are not evident in macro-world, and for which macro-world techniques alone may not be adequate to provide solutions. Undoubtedly, these problems need to be resolved.

1.1.2 Fundamental issues in micromanipulation involving force

Substantial studies to resolve specific problems related to force in micromanipulation have been reported in the literature. Generally, these studies concern two main issues. The first issue concerns the interaction between the manipulated objects and its environment through adhesion forces. Adhesion forces may arise when an object with size less than one millimeter in a single dimension is in contact (or in close proximity to) another object. In the macro-world, adhesion forces are negligible because of the dominance of gravitational and inertial forces. However, below a certain size threshold, gravitational

and inertial forces become insignificant compared to adhesion forces. The dominance of adhesion forces then introduces complication in the manipulation process. For instance, when placed by a manipulator onto a desired location on a substrate, an object may have a tendency to adhere more strongly to the gripper than to the substrate. One way to deal with adhesion forces is to examine the source of the individual adhesion forces and identify the factors that contribute to such forces. By suppressing the influence of such factors, it may be possible to reduce the adhesion forces. Another way is to directly reduce the effect of adhesion forces on manipulation through inertial forces. If inertial force can be made one order of magnitude greater than adhesion forces, then the effect of adhesion forces will become inconsequential.

The second issue concerns the challenge in measurement and control of micro-force because the magnitudes of such forces can be extremely small. In micromanipulation, the magnitude of forces may range from hundreds of mN down to tens of μN and below. Such small forces pose challenge on the design and construction of sensors that can provide measurements with high resolution and high accuracy. To meet these requirements, semiconductor and micro-fabrication techniques have been applied to build sensitive and stable micro-force sensors. Currently, the types of widely used micro-force sensors are: strain gauge, piezoelectric, capacitive, and optical sensor. Understanding of these sensors (such as their resolution and range, etc.) is necessary for their utilization in various application environments.

For practical micromanipulation involving application of desired force, detection of force alone is not sufficient. Control of interacting forces between the manipulator and

its environment is usually the ultimate objective. Force control is applied in many micro-manipulation operations, which are usually carried out using teleoperated or automatic micromanipulation system. For teleoperated systems, the force control is implemented through human. The contact forces in the micro-environment is magnified to give the operator force feedback during the execution of a manipulation task. This allows more effective use of human skills to achieve dexterous manipulation. One particular feature of teleoperated system is that information flow between macro-world and micro-worlds needs to be scaled: the movement of the master robot is scaled down for the slave robot to follow, while contact forces in the micro-environment is magnified. The position and force scaling should be scaled appropriately for human manipulation, with minimal distortion of information (such as density and viscosity). Two main approaches are developed to accomplish this need. One is based on the estimated model of micro-world and the other is based on the interaction mode between the micro-objects. For automatic micromanipulation system, currently, there exist few applications. There are three overriding concerns in these applications: one is to control the impact force so as to avoid damaging fragile micro objects (such as delicate MEMS structure or biological material); one is to regulate the micro contact force during micromanipulation; and one is to achieve a stable grasp of micro-object for micro-assembly operations.

The two issues (dealing with adhesion forces and micro-force sensing and control) are usually considered together due to their interdependency; below a certain physical scale level, any approach for micro-force sensing and control must also account for the effect of adhesion forces [19]. The interplay of these two issues underlines the fundamental

challenges in micromanipulation. (A detail literature review of these issues is presented in Chapter 2.)

1.2 Research Motivations

The two issues introduced in section 1.1 are fundamental to the development of micromanipulation techniques. Concerning the first issue, knowledge of the effect of adhesion forces on a micromanipulation process is necessary in designing methods to take advantage of this type of force (e.g., utilizing the adhesion force to facilitate picking up of a micro-object) while minimizing its adverse effect (e.g., causing a micro-object to stick to a manipulator). Concerning the second issue, using micro-force sensors to measure interaction force can provide high-resolution and stable micro-force signal, which represents an important piece of information that should be utilized to ensure a successful manipulation.

In this research, we focus on the study of micro-objects in the size around hundreds of microns range. Under this range, the effect of adhesion forces to the micromanipulation could be neglected. The scope of the resolution and measurement range in micro-force sensing could be defined to a few micro-Newton and a few milli-Newton.

A survey of the general field of micromanipulation (as reported in Chapter 2 of this thesis) reveals that the full potential of the micro-force signal has yet to be extensively utilized in current micromanipulation technology. Many important questions remain open. These include: what unique information would micro-force signal provide to

the study of the micro-object's features, and how micro-force signal could be used as feedback to facilitate the control of the micromanipulation process. In order to answer these general questions, the applicability and implementation of micro-force sensing and control in micromanipulation should be investigated. The research reported in this thesis focuses on three main problems.

1.2.1 Three problems on micro-force sensing and control studied in this thesis

The *first problem* concerns the study on whether micro-force sensing alone could be used to provide useful information in micromanipulation. When a probe is used to touch the micro-object, the force response of the micro-object to the probe can be recorded. The question is then whether this force response can be used to understand the characteristics of objects in micro-world.

The *second problem* concerns the improvement of position-based manipulation techniques through utilization of information obtained by force measurement. Currently, prevailing approaches to micromanipulation are based on position control, whereby the interaction between the micromanipulator and the micro-object is accomplished by controlling the relative positions of the manipulator and the manipulated object. When a micro-force sensor is used to measure the interaction force between the micromanipulator and a micro-object, a force profile of the interaction can be generated. In this profile, some specific features will reveal the state of the operation. Since the force profile of the

interaction is directly related to the position, the question is how to exploit these features in order to improve the effectiveness of position control.

The *third problem* concerns the applicability of direct force control in micromanipulation. In certain applications (such as in micro-assembly), position control alone is not sufficient to achieve the desired result. This can be attributed to two main limitations of pure position control. First, pure position-based method cannot directly control the interaction force between the micromanipulator and a part. Even when a correlation between the measured force (pertaining to a particular part) and the displacement of the positioning stage can be obtained, this correlation cannot be used as a uniform correlation over a batch of parts, because different parts may have different mechanical properties, thus exhibiting different force-displacement behavior. Second, the resolution of the controllable interaction force solely depends on the resolution of the positioning system. To avoid damaging the micro-objects being manipulated, the step size of the positioning system must be substantially smaller than the maximum allowable compliance of the part. Hence the speed of purely position-based assembly is limited. Due to these limitations of position-based control in micromanipulation tasks that involve force, direct force control is needed in such tasks. Implementing direct force control in micromanipulation remains a open but challenging problem.

1.3 Objectives and Methodology

The objective of this thesis is to investigate the applicability of micro-force sensing and control in micromanipulation by developing *experimental solutions* to the problems discussed in Section 1.2.1. These experimental solutions are:

(1) Characterization of micro-object's features with micro-force sensing.

(2) Augmentation of position control in micromanipulation with micro-force sensing feedback.

(3) Implementation of direct force control in micromanipulation.

1.3.1 Characterization of micro-object features with micro-force sensing

The first solution demonstrates that micro-force sensing can be used to facilitate characterization tasks (such as in determination of micro-surface topography and mechanical properties) in micromanipulation. In determining the surface topography of a miniature device, a sharp probe equipped with a micro-force sensor is used to sweep across the surface of the miniature device. By analyzing the force response of the miniature device to the probe, the surface features of the miniature device is characterized. The micro-force sensing method can be used to measure 3D surface topography at several nanometer resolution. The micro-force sensing method can also be used to measure vertical profiles, especially inside narrow and deep structures, where sophisticated high

resolution vision system is rendered ineffective by operational factors (such as physical geometrical constraints). A long and thin probe connected to a micro-force sensor is inserted into the structure to measure the profiles of the wall. For large area surface topography, an array of probes can be applied, with each probe scanning a small area.

In characterization of mechanical properties of the micro-object, micro-force sensing can be used to study the mechanical property of biosamples. A micropipette connected to a micro-force sensor is used to probe the membrane of the biosample. By exerting a force on the membrane, a quantitative relationship between the applied force (measured by the micro-force sensor) and structural deformation of the membrane can be established. Consequently, an analytical model of the biomembrane can be developed to describe the the mechanical properties of the biosample. This quantitative information can also be used to study the change of mechanical properties of biomembrane in a biosample at different developmental stages.

1.3.2 Augmentation of position control in micromanipulation with micro-force sensing feedback

The second solution demonstrates the use of micro-force as a feedback to augment position control. The key advantage of this solution is that, when augmented by force feedback, an originally position-controlled micromanipulation task can be automated. In this solution, force information obtained by direct measurement provides the crucial feedback needed to enable automation of the task. The principle and effectiveness of

this solution are demonstrated through two applications. The first involves the batch microinjection of zebrafish embryos, while the second concerns the coarse alignment of active fiber pigtailing in photonic assembly.

Currently, manual microinjection is a conventional and widespread practice in biological science research labs for tasks that involve first penetrating certain biological or organism (such as cells) then injecting certain material into the organism (using a micropipette), all done without damaging the organism itself. The success rate of manual microinjection is very low, due to the fact that to execute various steps in a manual microinjection requires fine control of both position and force, which is difficult for a human operator to accomplish consistently. One possible approach to overcome this difficulty, and consequently to enable automation of the injection process, is to use position control with force feedback. In this approach, the penetration force is measured and used as a real-time feedback to control the penetration process. This is made possible due to the fact that force information thus obtained reflects quickly and accurately the physical state of the organism (e.g., being deformed or penetrated). The measured penetration force is used to augment position control to enable process automation by dynamically determining the stopping point of the tip of the micropipette.

The particular microinjection task investigated in this first application is the batch injection of zebrafish embryos. By exploiting the unique characteristics of the force signal in the penetration process, batch injection of zebrafish embryos can be accomplished. The penetration-force profile of the zebrafish embryo was recorded and studied. The force reading was around zero before the micropipette contacted the embryo. Subsequent to

contact, the penetration force increases linearly while the embryo exhibits elastic deformation. When the penetration force reached a critical value, it dropped drastically back to zero, indicating that the embryo has been penetrated. The point at which penetration of the embryo occurs can be determined by detecting the sharp drop in the penetration force after its initial rise. By analyzing the first-order and second-order derivatives of the penetration force with respect to time, it is determined that the embryo is penetrated when the value of the first-order derivative is smaller than zero and the value of the second-order derivative is larger than zero.

In the second application, the force information is used to facilitate the coarse alignment of active fiber pigtailing, where the efficiency of search of light intensity signal is improved by using the micro-force signal. In active fiber pigtailing, the movement of the fiber typically begins with a coarse alignment called the search of first light, which aims to position the optical fiber and the optical device in such a way that at least some light will travel through the system and be received by the detector.

The method of 2-D blind raster scan is conventionally used in coarse alignment. In this method, the signal of light intensity is measured to check whether the first light is found. However, specific features of some optical devices (such as the optical path between the substrate and transparent cover) may interfere with the scanning process, resulting in poor signal content or no signal at all as the fiber traverses a large portion of the optical device input facet. This would mean that during the scanning process the signal generated is not useful most of the time in effectively directing the movement of the fiber.

To improve the efficiency of searching for the first light, force information is introduced in this second application of force-augmented position-controlled micromanipulation. A micro-force sensor with a sharp tip is used to sweep the input facet of the optical device. The resulting micro-force measured by the sensor continuously provides meaningful information about the surface features as long as the tip of the sensor is in contact with the input facet. These surface features (as characterized by the the micro-force signal in real-time) provides useful clues in guiding the fiber to rapidly locate the actual optical path of the optical device. In demonstrating this force-augmented solution for coarse alignment of active fiber pigtailing, a micro-force sensor with a sharp tip is used to sweep the surface of a optical device having a convex surface with a small hole at the center for fiber pigtailing. The ideal optical path of the optical device is at the center of the hole. As the tip of the sensor sweeps across the convex surface, the measured contact force varied continually with the curvature of the surface. When the tip happens to sweep across the center hole, it loses contact with the surface momentarily, resulting in a sharp discontinuity in the measured force signal. Such a sharp discontinuity serves as a clear indication of the existence and the location of the center hole. Once the center hole is determined, the optical fiber to be pigtailed can be moved to this position to start the search of first light in the neighboring small area.

1.3.3 Implementation of direct force control in micromanipulation

In this third solution, an explicit force-feedback control for micro-assembly is developed. Explicit force-feedback control represents an effective alternative to position-

based force control in micro-assembly. In an explicit force-feedback control system, the input signal and the measured signal are direct representations of the magnitudes of force. Consequently, limiting the magnitude of the input signal can help to prevent damaging a part during assembly. Application of explicit force-feedback control can also lead to an effective micro-assembly process based on force information. When the measured force exceeds a certain threshold (or exhibits a certain pattern), it can be judged that assembly is completed. Hence, by properly controlling the interaction force in the assembly process, automation of the assembly is possible.

Implementation of explicit force-feedback control requires effective force-transmission. The means for force transmission proposed in this research is in the form of a force-transmission stage. It is desirable that the force-transmission stage generates low frictional effect and has high immunity against noise (due to vibration, for instance). This ensures that no matter how small the output force from the actuator is, the system still exhibits a high signal-to-noise ratio. A force-transmission stage, designed and built based on a compound flexure configuration, has been developed to provide frictionless translation with low stiffness motion along one axis while exhibiting high stiffness in all other axes.

When the force-transmission stage is used to implement force control in micromanipulation, the main objective is to control the interaction force between the micromanipulator and its environment. A force controller for this purpose has been designed based on a mass-spring-damper dynamics model of the stage to achieve the objective of having the actual force follow a desired force as closely as possible. Because of its simple form,

low-pass nature, and its zero steady state error for a constant reference force, integral control has been found to be most suitable for this purpose. The effectiveness of this controller has been verified through simulation and experiments.

The developed force control system (i.e., the force-transmission stage equipped with the force controller) can serve as a subsystem in a micromanipulation system to facilitate the control of the interaction between the micromanipulator and its environment. In this solution, the force control system is integrated with a microscopy system and a micro-positioning system to create a functional micro-assembly workstation for assembly of micro-parts. The effectiveness of this workstation has been demonstrated in the task of assembling micro-parts in a tissue engineering application.

1.4 Significance

The research reported in this thesis focuses on the potential applications of force sensing and control in micromanipulation. The results could lead to fundamental advances in the emerging field of micromanipulation. The construction and integration of components for explicit force control discussed in this thesis could serve as an impetus for stimulating further interests in the subsequent generation of practical tools and systems in this field, leading to possible commercial development of components and subsystems that are instrumental in micromanipulation, such as frictionless stage, high-resolution actuator, multi-axis micro-force sensors, etc.

The prototype systems and experiments developed in this research may serve as an ex-

perimental foundation for further advancing micromanipulation techniques to a higher level, where direct and automated control of interaction processes is possible. This would allow full automation of micromanipulation tasks in the future.

This research is impactful on widening the existing domain of application for micromanipulation technologies. The prototype systems and experiments results have demonstrated the validity in the use of micro-force sensing and control systems for automation of micromanipulation tasks. This would lead to more practical applications of force-based techniques, such as in the realization of lab-level 3D hybrid MEMS devices and the automation of the volume-injection of the zebrafish eggs.

1.5 Organization of the thesis

This thesis is organized as follows:

Chapter 1 introduces the background of micro-force sensing and control in micromanipulation. Three main problems in micro-force sensing and control are raised. In order to solve these problems, the applicability and implementation of force sensing and control in micromanipulation should be investigated. The objective of this thesis is to investigate the applicability of micro-force sensing and control in micromanipulation by developing experimental solutions. The significance of this thesis is given.

Chapter 2 surveys previous studies to resolve specific problems related to force in micromanipulation. It focuses on two fundamental issues (i) techniques for dealing with

adhesion forces, and (ii) challenge in measurement and control of micro-force. It first examines two approaches for reducing the effect of adhesion forces in micromanipulation: one exploits the inherent properties of adhesion forces, while the other work deals with amplification of inertial forces involved in the manipulation process. It then discusses the basic principles and applications of four types of widely used micro-force sensors, and reviews a number of force-control approaches for both teleoperated and automatic microrobotic systems. It reveals that the full potential of the micro-force signal has yet to be extensively utilized in current micromanipulation.

Chapter 3 develops three experimental solutions to the three main problems in micro-force sensing and control. These experimental solutions are: (i)characterization of micro-object's features with micro-force sensing, (ii) augmentation of position control in micromanipulation with micro-force sensing feedback, (iii) implementation of direct force control in micromanipulation. Several examples are used to illustrate the first and the second solutions. The importance of the third solution for micromanipulation is discussed.

Chapter 4 presents the implementation of direct force control in micromanipulation (the third experimental solution), focusing on two key issues: design of force transmission stage and force controller. A compound flexure stage is designed and built to provide frictionless translation with low stiffness motion along one axis. An explicit force controller is designed to control the actual interaction force to follow a desired force trajectory. The direct force control is applied in the use of mechanical fixture, which is used to overcome adhesion force effects during the release of the micro-objects.

The integration of the developed force control system with the microscopy system and micro-positioning system is demonstrated in a micromanipulation system.

Chapter 5 presents an experiment to use micro-force sensing to augment conventional approaches for fast and accurate fiber pigtailing in photonic assembly. A photonic alignment system based on the micro-force sensing is developed to facilitate coarse alignment in active fiber pigtailing in integrated optics technologies. It illustrates that the micro-force signal provides useful clues in guiding the fiber to rapidly locate the actual optical path of the optical device (with specific geometry feature on its input surface). Using an improved piezoresistive force sensor to characterize the surface feature of an optical ferrule on a micron scale, the actual optical path of the ferrule had been located accurately and efficiently.

Chapter 6 presents an experiment to use micro-force sensing and control to automate the zebrafish embryos injection. A prototype micromanipulation system is developed for automatic batch microinjection in biological science. Such automatic batch processing is made possible by (i) the development of a machine vision algorithm to identify the number of embryos in a batch and to locate the centerline of each embryo, (ii) the integration of a piezoresistive micro-force sensor with a micropipette to measure the penetration force of the embryo in real-time, and (iii) the synthesis of a position control with dynamic force feedback by exploiting the characteristics of the force profile associated with the microinjection process. The effectiveness of this prototype micromanipulation system has been demonstrated in an experiment. The experimental results demonstrate that the technique of position control with dynamic penetration-force feed-

back is practicable for automatic batch microinjection applications.

Chapter 7 presents an experiment to use micro-force sensing and control to automate the pick-up and assembly of the micro-part used in scaffold assembly. An explicit force-feedback control system is developed for the automation of the scaffold assembly in tissue engineering. The force-feedback system is incorporated with a compound flexure stage, which is driven by a voice-coil actuator and designed to provide frictionless translation motion along one axis. A force sensor measures the interaction force between the micromanipulator and its environment, while an explicit force controller controls the interaction force to follow a desired force trajectory.

Chapter 8 summaries the contributions in this thesis and outlines directions for future research.

Chapter 2

Literature Review

This chapter surveys previous studies to resolve specific problems related to force in micromanipulation. It focuses on (i) techniques for dealing with adhesion forces, and (ii) challenges in measurement and control of micro-force.

2.1 Adhesion forces in micromanipulation

Adhesion forces may arise when an object with size less than one millimeter in a single dimension is in contact (or in close proximity to) another object. In the macro-world, adhesion forces are negligible because of the dominance of gravitational and inertial forces. However, below a certain size threshold, gravitational and inertial forces become insignificant compared to adhesion forces. The dominance of adhesion forces then introduces complication in the manipulation process. Such complication includes

seemingly erratic phenomena that do not appear in macromanipulation. For instance, when placed by a manipulator onto a desired location on a substrate, an object may have a tendency to adhere more strongly to the manipulator than to the substrate, thus preventing accurate placement [20].

Adhesion forces arise primarily from electrostatic attraction, van der Waals forces, and surface tension forces. The magnitudes of these forces depend on the size of the object under consideration. As the object becomes smaller, its mass decreases in proportion to the third power of the length, and to the second power of its cross-sectional area [21]. Since the magnitudes of adhesion forces are proportional to the size of object surface, when the size of an object is less that a certain threshold, the overall adhesion forces become greater than the gravitational force acting on the object. Figure 2.1 illustrates the difference in magnitude between adhesion forces and gravitational force as a function of the object radius. These forces are evaluated in the context of interaction between a charged spherical object and a plane which represents the tip of an end-effector. Treating the tip of the end-effector as a plane simplifies calculations and allows analytical formulations for van der Waals and electrostatic forces. The surface tension forces are evaluated by considering hydrophilic surfaces and separation distances smaller than the object radius [20]. As shown in Figure 2.1, surface tension forces dominate when the object radius is less than one millimeter. Van der Waals forces can start to be significant (with smooth surfaces) when the radius of the object is about 100 μm, while electrostatic force is larger than gravitational force when the manipulated parts are less than 10 μm in radius [22].

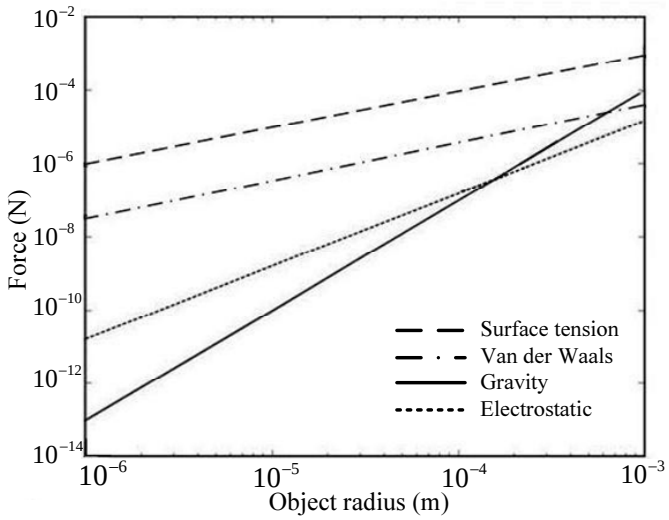

Figure 2.1: Gravitational force and the different adhesion forces as a function of the object radius.

The dominance of adhesion forces inevitably introduces complication in micromanipulation. For instance, when the end-effector of a manipulator approaches a micro object in a pick-up operation, electrostatic forces may attract the object to the extent that the object jumps towards the end-effector even before the picking operation is started [23]. Such behavior makes micromanipulation processes difficult to manage, and demonstrates the need for techniques to deal with adhesion forces.

2.1.1 Reducing adhesion forces by altering physical characteristics of object and its environment

One way to deal with adhesion forces is to examine the source of the individual adhesion forces and identify the factors that contribute to such forces. By suppressing the influence of such factors, it may be possible to reduce the adhesion forces. For instance,

by increasing the surface roughness of a microgripper [24] or reducing the humidity of manipulation environment, adhesion forces can be reduced as a consequence.

Electrostatic forces arise from charge generation or charge transfer during contact between two bodies. These forces can be active over a range in the order of the object radius. Arai *et al.* [25] derived models of electrostatic forces between a charged body and an uncharged wall, and between bodies carrying different amount of charges. A microgripper with micro-pyramidal gripping surface was designed accordingly to reduce the electrostatic forces. The micropyramids (with its sharp edges) generated a strong electric field, which is effective in reducing electrostatic forces. Experimental results showed that S_iO_2 spheres (with a diameter of 30 μm) disengage from the microgripper with a micro-pyramidal surface more easily than from one with a simple plane surface [24].

Van der Waals forces are due to instantaneous polarization of atoms and molecules when they are set close, and can be considered as a result of three additive terms: Keesom Force, Debye Force, and London Force. It is known that the London force has the largest proportion in the van der Waals forces. This force is inversely proportional to the distance between two atoms or molecules. Scheeper *et al.* [26] indicated that van del Waals forces are significant only for gaps of about 100 nm or less. One proposition to reduce van der Waals forces in micromanipulation is to increase the roughness of the contacting surfaces of the manipulator and the object. In micro-scale, a solid surface has many sharp points. Van der Waals forces are considered to be in effect at these sharp points when the gap between the sharp points on the surfaces of the two objects is less

than 100 *nm*. If all the sharp points have roughly the same height, then van der Waals forces exist on all of the points, and the sum of the forces on all these points are the total amount of van der Waals forces between the two objects. Varying the heights of the sharp points results in the situation that van der Waals forces will only arise at some of the points. Obviously, having sharp points with different heights leads to a rough surface. Arai *et al.* [23] verified this proposition, and succeeded in reducing the van der Waals forces by increasing the roughness of gripping surface [24].

Surface tension forces originate from interaction of layers of absorbed moisture on two surfaces in close proximity to each other. In micromanipulation, this interaction forms a liquid bridge between the contact surface of the manipulator and that of the manipulated object. Lamber *et al.* [27] proposed a numerical approach to compute the capillary and surface tension forces between objects linked by an axially symmetrical meniscus, i.e., the liquid bridge. The model was used to simulate a dynamic manipulation of a free object. The force exerted by the liquid bridge on the free object was computed and a method for accelerating the gripper was developed for releasing the object. In fact, ensuring a dry or vacuum manipulation environment is probably the simplest method to reduce surface tension. Tsuchitani *et al.* [28] confirmed that thermal treatment at about $200°C$ and hydrophobic treatment of the surface are effective in reducing the surface force. Menciassi *et al.* [20] assured a dry condition by dipping the tool and the object first into sulfuric acid and then into acetone, and demonstrated that it was almost impossible to pick up the sphere by relying on surface tension forces alone; when the same operation was carried out without drying the tools, however, the sphere could be

picked up consistently.

Among the three major groups of forces (i.e., the electrostatic forces, the van der Waals forces, and the surface tension forces) that make up adhesion forces, surface tension forces are the most significant for micromanipulation in an ambient environment. Electrostatic forces come into effect only when the size of the manipulated object is less than 10 μm, while van der Waals forces can be considered negligible at that scale (unless the surfaces of both the manipulator and the manipulated objects are very smooth, which is unlikely the case in practice). It is mainly due to surface tension forces that free standing micro-structures in MEMS devices tend to stick to the substrate after being released. This subsequently leads to van der Waals bonding [23]. On the other hand, if the micromanipulation could be carried out in liquid mediums, the adhesion force will decrease significantly. Gauthier *et al.* [29] proved that the micromanipulation task is easier to perform in a submerged medium than in air. Moreover, in submerged medium, the hydrodynamic forces limit the maximum micro-objects velocity, so the loss of objects is avoided in liquid medium.

The approaches discussed above demonstrate that one way for dealing with adhesion forces in micromanipulation is to alter the physical characteristics of the object and its environment so as to reduce or eliminate the adhesion forces. Another way for dealing with adhesion forces is to minimize their effect on the manipulation process. This can be done using special-purpose mechanisms or compensatory motion, such as mechanical release with needle [30] [31], or making a rolling motion during release [32] [33]. For example, a two-finger micro-hand was developed for facilitating the release of micro

object [34]. Each finger was a glass pipette whose tip was heated and then drawn to a sharp point. In the experiment, a glass ball with a diameter of 2 μm adhered to one of the finger. Using the other finger, the micro object was pushed toward the tip of the finger (to which the ball was initially adhered), resulting in successful release of the ball from that finger.

2.1.2 Reducing effect of adhesion forces on manipulation through inertial forces

When handling macro objects, adhesion forces are negligible because of the dominance of gravitational and inertial forces. If the gravitational and inertial forces can be artificially amplified and controlled such that the same dominance is maintained in a way that helps the micromanipulation process, then the effect of adhesion forces will become insignificant. In an ambient manipulation environment, it is impossible to change gravitational force. However, inertial force can be easily amplified by, for instance, generating an instantaneous acceleration [35], or increasing centripetal acceleration [36]. If inertial force can be made one order of magnitude greater than adhesion forces, then the effect of adhesion forces will become inconsequential.

Haliyo *et al.* [35] developed an one-finger end-effector to pick up and release micro objects onto a substrate solely based on effect of adhesion forces and inertial force. During release, the effect of adhesion forces between the end-effector and the object is to be overcome by sudden motion of the end-effector. Another example of using inertial ef-

fect to deal with adhesion forces was reported by Lai *et al.* [36]. In a micro-assembly task, a cantilever-like plate is to be lifted up to assemble the entire structure constrained by hinges. However, the cantilever may stick to the substrate due to surface tension forces. Moreover, if the surface tension is sufficiently strong to pull the suspended cantilever in contact with the substrate, it will lead to permanent adhesion by van der Waals bonding. Lai *et al.* [36] demonstrated that centrifugal force can overcome adhesion forces and thus be used for non-contact assembly. To study the interaction between the the micro cantilever and the substrate while both are in rotation, the cantilever-substrate structure was attached to a spinning disc. The separation of the cantilever from the substrate depended on the angular speed of the spinning disc.

These studies demonstrate that the method of using amplified inertial forces to deal with adhesion forces is effective. However, because the manipulated object is accelerated in this method, the displaced object may interfere with the manipulation process. Thus, properly constraining the displacement of the accelerated object becomes an important issue. For example, the method of instantaneous acceleration was applied to isolate a single pollen from the dense pollen powder [35]. Although the released pollen flied randomly after acceleration, it was constrained in a container for collection. In the application of non-contact assembly by centrifugal force [36], micro mirrors also automatically lock themselves to designed latches after spinning.

The ultimate objective in force control of micromanipulation is to control the interaction forces between the end-effector and its environment (which may include the manipulated object) under the influence of adhesion forces. Dealing with adhesion forces

is thus one fundamental issue in achieving such an objective. The other issue is the measurement and control of the interaction forces whose magnitudes are very small (usually in the scale of mN or less). The ability to measure such forces accurately is a pre-requisite for controlling them in micromanipulation.

2.2 Micro-force Sensors

Force sensors are commonly used to measure interaction forces between the manipulator and its environment. When external forces are applied to a force sensor, its sensing element will deform. The deformation is either detected by measuring the change in certain properties of the sensing element (e.g., change in resistance or capacitance), or directly measured by optical devices (e.g., atomic force microscope). The applied force is calculated from the established calibration between the deformation and a known force. In micromanipulation, the magnitude of forces may range from hundreds of mN down to tens of μN and below. Such small forces pose challenge on the design and construction of sensors that can provide measurements with high resolution and high accuracy. To meet these requirements, semiconductor and micro-fabrication techniques have been applied to build sensitive and stable sensing elements. Currently, the types of widely used micro-force sensors are: strain gauge, piezoelectric, capacitive, and optical sensor. Understanding of these sensors (such as their fabrication procedure and resolution, etc.) is necessary for their utilization in various application environments.

2.2.1 Strain gauge

A strain gauge has the property that its resistance changes under physical pressure or mechanical work. When a strain gauge is strained or deflected, its internal resistance will change (and remain changed) until its original shape is restored. The change in resistance is measured by an electric circuit (e.g., Wheatstone bridge). Strain gauges are usually made of a metal foil or of a semiconductor material. Semiconductor strain gauges are characterized by a much larger gauge factor than that of the metal type, which translates into a higher sensitivity (usually in the order of more than 100 times).

In practical applications, it is often the case that a strain gauge is integrated into the micromanipulator. Proper placement of the stain gauge then becomes important for ensuring accurate and repeatable measurements of micro-force. Although the optimal location to place a strain gauge is where strain occurs, the small size of a micromanipulator may make it physically impossible to place a strain gauge at the desired location. Menciassi *et al.* [37] developed a symmetrical method to place strain gauges on a microgripper structure. Four strain gauges are mounted in two pairs on the microgripper, with each pair located at a flexure joint: one strain gauge of the pair measures compression while the other one measures tension. This symmetrical configuration results in better thermal compensation and higher signal-to-noise ratio.

Another way of placing a strain gauge is to attach it to the fixed jaw of a gripper. This configuration is usually seen in the use of piezoresistive force sensor, e.g., in [38]. (Piezoresistive force sensors belong to the category of semiconductor strain gauge; they

exhibit good sensitivity due to the piezoresistive effect of silicon.) A piezoresistive cantilever is bonded to one side of the gripper. When the gripper is in contact with an object, the gripping force is detected from the deformation of the cantilever. The advantage of this approach is that the sensor so placed directly measures the force on the jaw of the gripper. It is possible to vary the measurement range and the resolution of the force sensor by selecting a cantilever with appropriate mechanical properties. The more stiff the cantilever, the higher the precision in the measurement. The piezoresistive cantilever alone can also be used as a probe or manipulator [39]- [40]. It could measure the contact force during probing or manipulation.

With proper arrangement of strain gauges, multi-axis micro-force sensing can be achieved. There are types of multi-axis micro-force sensor, such as a sensor for measuring contact forces at the tip of a microsurgical instrument in three dimensions [41] (resolution: 0:5 mN, range: 1 N), a three-axis sensor mounted on a micromanipulator in a micro-teleoperated system [42] (resolution: 0:3 mN), a three-axis tactile sensor for micro-material characterization [43], a three-axis stress sensor for dimensional metrology [44], a six-axis sensor for measuring force and moment acting on boundary particles in a turbulent liquid flow [45] and a multi-axis sensor for measuring the instantaneous ground reaction force produced by insects [46] (resolution: 0:5 mN) .

Since force sensing based on strain gauge requires measurement of deformation in the gauge, there must be enough compliance in the strain gauge to provide sufficiently large deformation. These large deformations are undesirable because they limit the frequency response of the measuring system and also introduce geometric changes into the force

measuring path which inevitably leads to measurement errors (e.g., nonlinearity and hysteresis). This problem, however, does not exist in another type of sensor, namely, the piezoelectric force sensors.

2.2.2 Piezoelectric force sensor

A piezoelectric force sensor generates a voltage when it is stressed by a force. The material for making this type of sensor exhibits high stiffness comparable to steel. Therefore, the deformation of the sensing element in a piezoelectric force sensor will be much smaller than in other measuring systems (e.g., in a strain gauge). The high rigidity of piezoelectric force sensors provides an inherently high natural frequency and short rise time. This permits the measurement of extremely fast events.

The most widely used piezoelectric force sensor is fabricated with the polyvinylidene fluoride (PVDF) film. PVDF is an ideal sensing device because of its responsiveness to a wide range of frequencies, high mechanical strength, and high sensitivity. Kim *et al.* [47] designed and fabricated a PVDF force sensor, which can be integrated into a tweezerstype microgripper. This PVDF sensor enables the microgripper to sense gripping forces with magnitudes under 100 μN.

A PVDF sensor can be directly installed on the grasping surface of a gripper (as reported in [47] and [48]). It can also be integrated into a probe-tip to detect the contact force exerted at the tip. This configuration is useful for measuring contact force or injection force in micromanipulation. For example, Kim *et al.* [18] bonded a micro injection

pipette on the tip of a PVDF force sensor, and used it as an one-axis force sensor (with a resolution in the order of μN) to characterize the mechanical properties of the membrane of zebrafish eggs. Shen *et al.* [49] designed a one-axis PVDF force sensor with sub-micron resolution based on the same approach. This micro-force sensor has been used to detect impact forces during lifting of micro mirrors.

A key characteristic of piezoelectric sensors is that the electrical signal generated by the piezo-element decays rapidly after the application of force. This renders piezoelectric sensors unsuitable for detecting static force (as is demonstrated in [50]). To measure static forces, strain gauges are suitable, while another type of sensor, namely, the capacitive force sensor, offers an alternative.

2.2.3 Capacitive force sensor

Capacitive force sensors make use of change in capacitance between two metal plates due to application of force. When a force is applied, the distance between the plates or the effective surface area of the capacitor will change. Since the capacitance C between two parallel plates is given by $C = A\varepsilon/D$ (where A is the plate area, D is the distance between the plates, and ε is the permittivity of the dielectric medium), a change in A or D will cause a change in capacitance. The applied force can then be calculated based on measurement of such change in capacitance by a bridge circuit. Compared to strain gauges and piezoelectric force sensors, capacitive force sensors are more stable and sensitive, and exhibit no hysteresis [51].

Capacitative force sensors have been successfully used for investigation of properties of biological materials through force measurement. In the work reported by Sun *et al.* [52], a two-axis capacitive force sensor was used to study the mechanical properties of mouse zona pellucida during fertilization. The device is capable of sensing forces applied to the cell, as well as tangential forces resulted from the miss-aligned probe. It can measure forces as small as 25 μN with a resolution as low as 0.01 μN.

For cell manipulation with capacitive sensing, a pipette (such as injection pipette [52] or holding pipette [53]) is usually attached to the probe tip of the sensor. However, displacement limitation of pipette reveals one disadvantage of capacitive force sensor. The signals in capacitive displacement sensing are proportional to the surface area of the elements while surface area decreases very drastically with miniaturization [54]. This leads to limited measurement range for capacitive force sensors. To solve this problem, electrostatic microactuators are integrated to enable the sensor to operate in an active servo mode, in which system stiffness is modulated using force compensation [55].

In capacitive force sensors, piezoelectric force sensors, and strain gauges, the sensing elements measure through contact the strain of the micromanipulator (such as a gripper or probe). However, there may be cases where the manipulator is too small (compared to the miniaturized force sensor) for the force sensor to be integrated into the manipulator. For such cases, non-contact sensing is needed. Optical sensor is an effective method for non-contact force measurement.

2.2.4 Optical sensor

For micro force sensing the technique of optical beam deflection shows great potential, due to its electromagnetic immunity and high resolution (down to *nN*) [56]. A primary advantage of this technique is that it can be used in a non-contact mode if certain structural members within a micro-device can be designed with appropriate stiffness so that they deflect a measurable amount without compromising the structural integrity of the overall device. One of the applications of this technique is the atomic force microscope (AFM).

An AFM mainly consists of a manipulator integrated with nano-scale force sensing to characterize features on various kinds of surfaces (from the micrometer scale to the nanometer scale). Besides its capabilities as a nano-scale characterizer, AFM can also be used as a nano-scale robot, i.e., for modifying surfaces or manipulating structures such as nano-particles and nano-rods [57] [58] [59] [60] [61] [62] [63]. As the cantilever (with a sharp tip at its end) in an AFM scans over a sample at distances on the order of a few nanometers, inter-atomic forces (in the order of *nN*) occur between the tip and the sample. This small force is reflected in the deflection of the cantilever, and is measured by a laser diode and a photodiode. Light from a laser diode is focused on the tip of a cantilever and deflected onto a quad-photodiode. As the cantilever bends and twists during contact with its environment, the laser beam on the quad-photodiode will move accordingly. The four voltage output from the photodiode are used to measure changes in the deflection of the beam [64].

In certain applications, force sensing using an AFM has limitations in terms of accuracy and range. When an AFM is used in aqueous mediums where biological cells survive, the reflection and refraction of the transmitted light may reduce the accuracy the measurement. Another limitation is that the photodiode can only detect deflection within a small range. As a result, force measurement range of AFM sensor is constricted.

Each of the four types of force sensing techniques discussed above has its advantages and disadvantages. Certain technique is more suitable in a particular application than others. Strain gauges are easy to use, but their proper placement is crucial to obtaining good results. Piezoelectric force sensors are best at detecting forces that vary quickly, but are not fit for static force measurement. Capacitive force sensors are more sensitive than the above two types, but their measurement range is usually limited. Finally, AFM has the highest sensitivity and may be used in non-contact force detection, but it has rather limited measurement range and requires additional force signal compensation.

2.2.5 Calibration of micro-force sensor

Calibration is usually necessary before proper application of a micro-force sensor. Calibration is a process for establishing the relationship between the output signal of a force sensor and a standard load. In this process, a known force is applied to the sensor, which produces a corresponding output signal (this signal is said to equate the known load). With a number of known forces that approximate the load range of the force sensor, an interpolation can be done between 0 load and the known maximum load to determine the actual force range that matches the sensor output range. For sensor integrated on a

micro-gripper, the load cell could be used in calibration by opening the micro-gripper against the load cell [65]. For sensor with a probe or cantilever to detect injection force or pressing force, the micro-balance can be used by first mounting the force sensor on a high precision stage and then pressing it against the micro-balance [40]. Another method to calibrate micro-force sensor without load cell is based on vision measurement. Greminger and Nelson [66] demonstrated a method to visually measure the force distribution applied to a linearly elastic object using the contour data in an image.

For practical micromanipulation involving application of desired force, detection of force alone is not sufficient. Control of interacting forces between the manipulator and its environment is usually the ultimate objective. Accurate force sensing is only the initial step towards achieving this objective. The next step is to design controllers that utilize the force measurement in order to achieve precise application of the desired force on the manipulated object or environment.

2.3 Control of Micromanipulation Forces

Force control has been applied in many micromanipulation operations, such as cell manipulation [18] [67] [68] and peg-hole assembly [69] [70] [71]. These operations are usually carried out using micromanipulation systems. These systems often consist of high precision stages, high resolution visual devices, and dexterous manipulators. Such systems can be classified as teleoperated or automatic. For teleoperated systems, the main issue is force scaling.

2.3.1 Force scaling in micro-teleoperated system

In a micro-teleoperated system, the human operator operates a master robot in the macro-world to control a slave robot in the micro-world. One particular feature of such systems is that information flow between macro-world and micro-worlds needs to be properly scaled: the movement of the master robot is scaled down for the slave robot to follow, while contact forces in the micro-environment is magnified to give the operator force feedback during the execution of a manipulation task [72]. This allows more effective use of human skills to achieve dexterous manipulation. Micro-teleoperated systems have already been developed for various applications, such as in tele-manipulation of biological cells [73] [74] [75] and microscopic surgery [76] [77] [78].

For example, Fukuda and Arai [73] designed a prototype teleoperated system for 3D bio-micromanipulation. In the slave system, a micromanipulator is mounted on a 3DOF (Degrees of Freedom) fine positioning stage. The fine positioning stage is fixed on a 3DOF coarse positioning stage, A three-axis micro-force sensor (strain gauge type) is integrated into the tip of the manipulator. A microscope is used to observe the bio-object under manipulation. The positioning system plus the micromanipulator with micro-force sensing function and microscope constitute a complete slave system.

In the design of micro-teleoperated system, the selection of position and force scaling is an important issue. In general, the operator should work in a magnified micro-environment with a scale appropriate for human manipulation, with minimal distortion of information (such as density and viscosity). One method to accomplish this is to ap-

ply an impedance scaling to reshape the environment [79]. Colgate [80] proposed the concept of "impedance shaping bilateral control" by adding a model-based impedance controller between the output of β (position scaling) and input of γ (force scaling). This approach of impedance shaping is based on the geometrical similarity on an estimated model of the environment, which means the selection of β and γ are dependent on the geometric scale between the macro and micro worlds.

A shortcoming of this approach is that the force information is calculated from the velocity and acceleration of the slave system, thus rendering the approach less suitable for real-time implementation in practice. Kaneko *et al.* [81] developed another impedance shaping method. They argued that not only geometrical scale but also dynamic scale should be used to select the position and force scaling. The geometrical scale was used to determine the force scaling and the dynamic scale was used to select position scaling. Their proposed control scheme is based on a force feedback control that does not require velocity or acceleration information, and is therefore well suited for real-time implementation.

It is noted that application of the impedance shaping approach requires an accurate model of the micro-world. Both Colgate [80] and Kaneko *et al.* [81] modelled the micro-world as a simple linear mass-spring system. Such a model may not be sufficient since in micromanipulation adhesion forces are dominant with nonlinear effect. Hence, methods that support treatment of adhesion forces should be applied to augment this approach.

Another approach for selection of force scaling, proposed by Goldfarb [82], uses dimen-

sional analysis techniques. The dimensional analysis methods do not require an exact environment model. Without the need for an exact dynamic or geometric model, this approach is suitable for dealing with both nonlinear and linear systems. The objective of this method is to find a force scaling that preserves dynamic similarity and minimizes the distortion (such as density and velocity) [72]. Two classes of force scaling have been generalized. One is characterized by structure-dominated interaction (such as the interaction associated with a simple cantilever beam), for which γ is set to be equal to r^2 (with $r >> 1$). Another is characterized by surface-dominated interaction (such as the interaction generated from surface tension), for which $\gamma = r$. However, these settings are not suitable for interactions involving a soft environment or a flexible manipulator (or both), due to the fact that in such cases the extent of geometrical deformation is disproportionally greater than that of variation in the interaction force [83].

Even if the issue of force scaling is completely resolved, teleoperated systems still have limited application simply because of their inherent need for human intervention. Such intervention leads to various operational issues that hinder system performance. For instance, cell injection is conventionally conducted manually; however, long training, disappointingly low success rates from poor reproducibility in manual operations, plus possible contamination, all call for the reduction or even elimination of direct human involvement. Moreover, in cell toxicology where hundreds of cells are to be injected, the need for an automatic micromanipulation system is self-evident.

2.3.2 Force controller design in automatic micromanipulation system

Currently, there exist few applications of automatic micromanipulation. Such applications mainly focus on (i) reduction of impact force at the tip of the probe or pipette (e.g., [84] and [85]), (ii) control of contact force at the tip of the manipulator [86], and (iii) control of gripping force at the tip of the gripper (e.g., [67] [87] and [88]). There are three overriding concerns in these applications: one is to control the impact force so as to avoid damaging fragile micro objects (such as delicate MEMS structure or biological material); the second is to regulate the micro contact force during micromanipulation; and the third is to achieve a stable grasp of micro object for micro-assembly operations.

In the case of impact force control, both position and force information need be taken into consideration (e.g., [89]). One approach is to design a controller that switches between position control and force control (e.g., [84] and [85]). The condition for switching is based on the current position and force signals. These signals are in fact the input to the controller that controls the speed of the manipulator. The controller applies position control prior to impact. When the distance between the manipulator and the object is smaller than a pre-set threshold and the measured force is greater than the minimum contact force allowed, the controller switches to force control. This switching control strategy has been demonstrated to be effective for reduction of impact force in micromanipulation [84].

In the case of contact force control, the micro-force on the tip of the manipulator is

regulated to a desired value. One approach is to design a hybrid force/position controller. Shen et al. [86] developed a micro-robotic system. A linear motor was used to move the PVDF sensor tip to contact a glass surface. Because the sensor structure installed at the end of micromanipulator was a soft beam, when manipulation was performed, the cantilever beam was considered as an infinite dimensional flexible link. A hybrid micro contact force/position control scheme was developed on the basis of an infinite dimension system approach. The force controller is used to control the contact force on the glass surface to maintain a desired force (along constrained direction), while the position controller is used to control the sensor tip to move on the glass surface (along unconstrained directions). Experimental results verified the performance of the developed micro-force sensing and hybrid control scheme.

In the case of grasping force control, the aim is to obtain a stable grasp on a micro object without damaging it. Design of such a controller requires careful analysis of the dynamics of the grasping motion. Eisinberg *et al.* [67] proposed a procedure based on the frequency response of the manipulation system. First, a piezo-actuated gripper excited by a small step voltage was closed with the object absent (i.e., the idling condition). The frequency response of the system was obtained based on principle component analysis techniques [90], and the corresponding transfer function was obtained. The same process was repeated for the case of grasping a sample object (i.e., the grasping condition). A controller was then synthesized based on the frequency response of the system under idling condition and grasping condition.

2.4 Concluding Remarks of Literature Review

In this chapter, previous studies to resolve specific problems related to force in micromanipulation have been reviewed, specifically on the (i) techniques for dealing with adhesion forces, and (ii) challenges in measurement and control of micro-force. Concerning the first issue, various techniques were examined for reducing adhesion forces by altering physical characteristics of the manipulated objects and the conditions of their environment. These techniques in general are not sufficient for dealing with adhesion forces as a whole, because they are mainly effective in reducing certain components of adhesion forces. Moreover, implementing such techniques may be costly since it requires fabrication of complicated micromanipulation tools. An alternative approach based on the concept of reducing the effect of adhesion forces by amplifying inertial force was then examined. It was pointed out that in practical implementation potential difficulties may arise in the handling of the displacement of the manipulated object (which could be subject to significant acceleration and thus may interfere with the manipulation process).

Concerning the second issue, a collection of micro-force sensing techniques was surveyed first. Specifically, four types of sensors were examined, with examples showing their applicability. This could serve as a guide for selecting force sensors for various tasks and types of environment. Significant results have been reported in the literature on various applications using piezoresistive force sensors. However, few works have been done to specifically deal with the design or modification of piezoresistive-based probe sensors for applications that exploit the particular advantages of these types of

sensors. The issue of force control in micromanipulation was examined in the context of teleoperated systems and automated manipulation process. Further analysis of force scaling with the existence of nonlinear adhesion forces is needed. Finally, force-feedback control for automatic micromanipulation was reviewed. It was pointed out that current approaches mainly deal with controlling impact, contact and grasping forces.

The survey of the two issues reveals that the full potential of the micro-force signal has yet to be extensively utilized in current micromanipulation technology. Many important questions remain open. These include: what unique information would micro-force signal provide to the study of the micro-object's features, and how micro-force signal could be used as feedback to facilitate the control of the micromanipulation process. In order to answer these general questions, the applicability and implementation of micro-force sensing and control in micromanipulation should be investigated.

Chapter 3

Applicability of Micro-force Sensing and Control in Micromanipulation

This chapter investigates the applicability of micro-force sensing and control in micromanipulation. Three problems in micro-force sensing and control are to be studied. The *first problem* concerns the study on whether micro-force sensing alone could be used to provide useful information in micromanipulation. The *second problem* concerns the improvement of position-based manipulation techniques through utilization of information obtained by force measurement. The *third problem* concerns the applicability of direct force control in micromanipulation. Three experimental solutions are developed to resolve these problems.

3.1 Characterization of micro-object's features in micro-scale by micro-force sensing

The first experimental solution demonstrates that micro-force sensing can be used to facilitate characterization tasks (such as in determination of micro-surface topography and mechanical properties) in micromanipulation.

3.1.1 Characterization of surface topography of miniature devices

3D surface topography with high resolution measurement in the range of submicron is required in micro-system technology. The conventional optical measuring system can only measure the structures in two dimensions at measurement resolution of about one micron. Micro-force sensing can be deployed to compensate for this deficiency. In determining the surface topography of a miniature device, a sharp probe equipped with a micro-force sensor is used to sweep across the surface of the miniature device. By analyzing the force response of the miniature device to the probe, the surface features of the miniature device is characterized. The micro-force sensing method can be used to measure 3D surface topography at several *nm* resolution [91].

For example, the surface topography of a wire bonding pad can be measured by this method. The probe tip of the micro-force sensor sweeps across the surface of the pad (by back-and-forth), as shown in Figure 3.1(a). The output of the force sensor is first plotted against the corresponding positions on the moving X and Y axis. A correlation

between the sensor bending and the height of the measured surface (h) exists. This correlation is established by taking into account the distance (d) between the sensor and substrate of the pad, and the fact that the probe tip is used at an angle α, as shown in Figure 3.1(b). By considering the amount of bending of the sensor beam to be linear to the force acting on it, analyzing the force signals yields the corresponding height measurements (h). The 3D surface topography of the wire bonding pad is then obtained by replacing the force reading with the corresponding height value in the plot of force vs. XY positions.

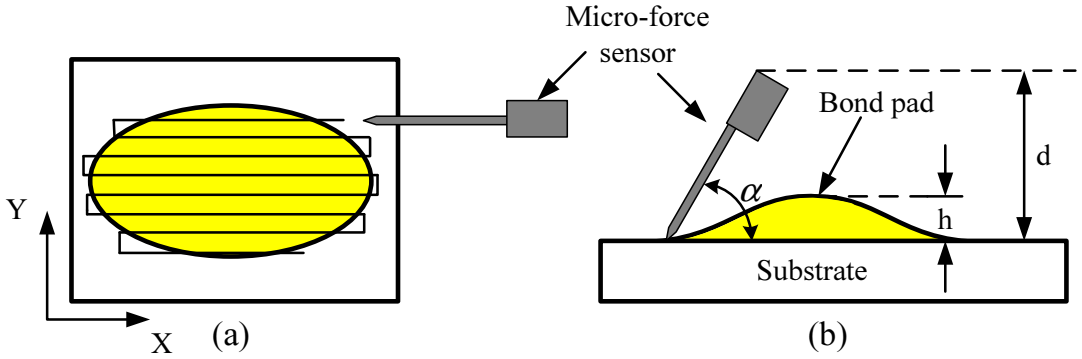

Figure 3.1: Sweep across the surface of a wire bonding pad using the probe tip of micro-force sensor (by back-and-forth). (a) Top view; (b) Side view.

The measurement resolution of the micro-force sensing method greatly depends on the sharpness of the probe tip of the micro-force sensor. A sharp tip is preferred to avoid problems such as scanning topography distortion. This type of problem arises when the radius of curvature of the tip is comparable with, or greater than, the size of the feature being imaged, and will influence the accuracy of characterization result. Figure 3.2 illustrates this problem. When the probe tip scans over a specimen which has small hole and bump on its surface, a sharp tip (as indicated in Figure 3.2(a)) will precisely measure the profiles of these features, while a blunt tip will not (Figure 3.2(b)). Currently, the

tips with radius of curvature of tens of *nm* are available.

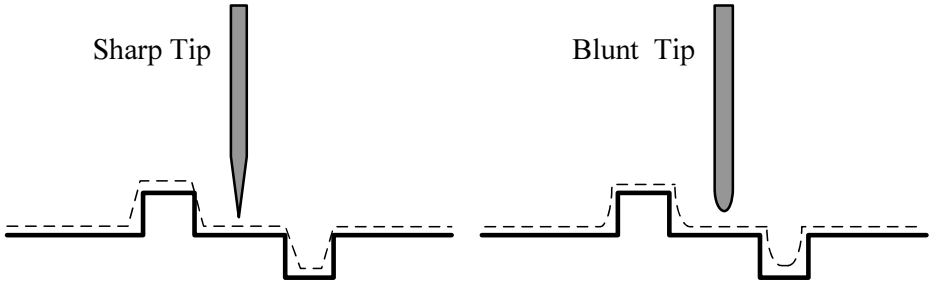

Figure 3.2: Scanning topography distortion caused by tip size: solid line is the real surface profile, while dashed line is the measured surface profile. (a) Probe with sharp tip; (b) Probe with blunt tip.

The micro-force sensing method can also provide profiles in applications where sophisticated high resolution vision system is rendered ineffective by operational factors. For example, optical measurement is inappropriate for the measurement of vertical profiles, especially inside narrow and deep structures [92]. As shown in Figure 3.3, in order to measure the profiles of wall inside a narrow micro-hole, the micro-force sensing method can be used. A long and thin probe connected to a micro-force sensor is first inserted into a micro-hole. Then the probe is used to sweep across the wall, while the bending of the probe due to contact is measured by the micro-force sensor. The profiles of the wall can be measured.

In order to reduce the time required to scan a large area, an array of probes (equipped with micro-force sensors) can be used [93]. For example, in the inspection of hundreds of micro-bumps on a wafer, an array of sharp probes (tip diameter around a few microns) equipped with micro-force sensors can be applied to scan the micro-bumps together, with each probe scanning a small area, as shown in Figure 3.4. However, the probes used in this method are all connected to a common base, excessive deflection in one

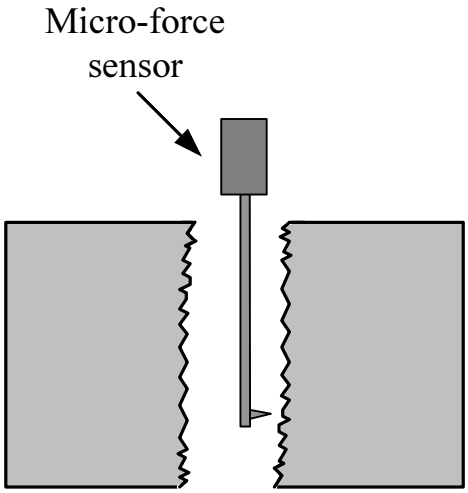

Figure 3.3: Measuring profiles inside long and narrow micro-hole.

probe can cause unwanted deflections in the other probes. It is necessary to know the maximum topographical variation that a single probe can scan over without adjusting adjacent probes.

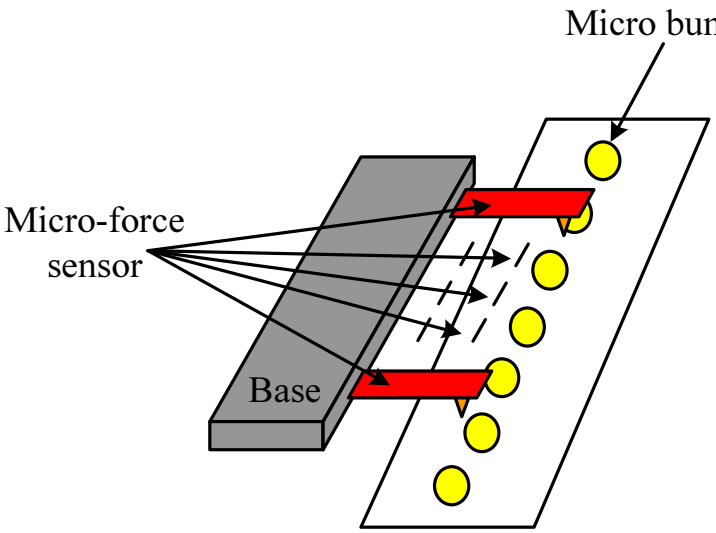

Figure 3.4: Using probe arrays to scan a row of micro-bumps.

Compared to optical measurement method, the micro-force sensing method can be used to facilitate characterization 3-D surface topography of miniature devices. It can measure vertical profiles where optical measurement method is rendered ineffective. While

in certain applications (such as individual cell based diagnosis or pharmaceutical test), the sensing of interaction force at micro-scale is the main objective. This would involve characterizing the mechanical properties of the samples through knowledge of the micro-forces interacting between the probe and the samples.

3.1.2 Characterization of mechanical properties of biosamples

Analyzing individual biosample rather than averaged properties over a large population is a major step toward understanding the fundamental elements of biological systems [94]. Micro-force sensing can facilitate single biosample studies because it can provide not only qualitative, but also quantitative information in the cellular and subcellular level. By exerting a force on the biomembrane of the biosample, a quantitative relationship between the applied forces (measured by the micro-force sensor) and biomembrane structural deformations can be established. Consequently, an analytical model of the biomembrane can be developed to describe the mechanical properties of the biosample [52]. The quantitative information can also be used to study the change of mechanical properties of biomembrane in a biosample at different developmental stages [18].

For example, zebrafish is widely used as a model for studying vertebrate development and genetics [95], [96], [97]. In the study of zebrafish, a micropipette, which is connected to a micro-force sensor, is used to penetrate the chorion layer of the zebrafish embryo. Figure 3.5(a)-(c) shows the sequential pictures of the penetration of the zebrafish embryo, while Figure 3.5(d) shows the force trajectory (with respect to time) of this penetration process. As shown in Figure 3.5(d), the force reading was around

0 *mN* before the tip of the micropipette contacted the chorion of the embryo. After the contact, the penetration force increased linearly, while the chorion exhibited elastic deformation, until point *a*. At that point the penetration force reached 1 *mN*, and then dropped drastically to below 0 *mN* at point *b*, indicating that the chorion was penetrated.

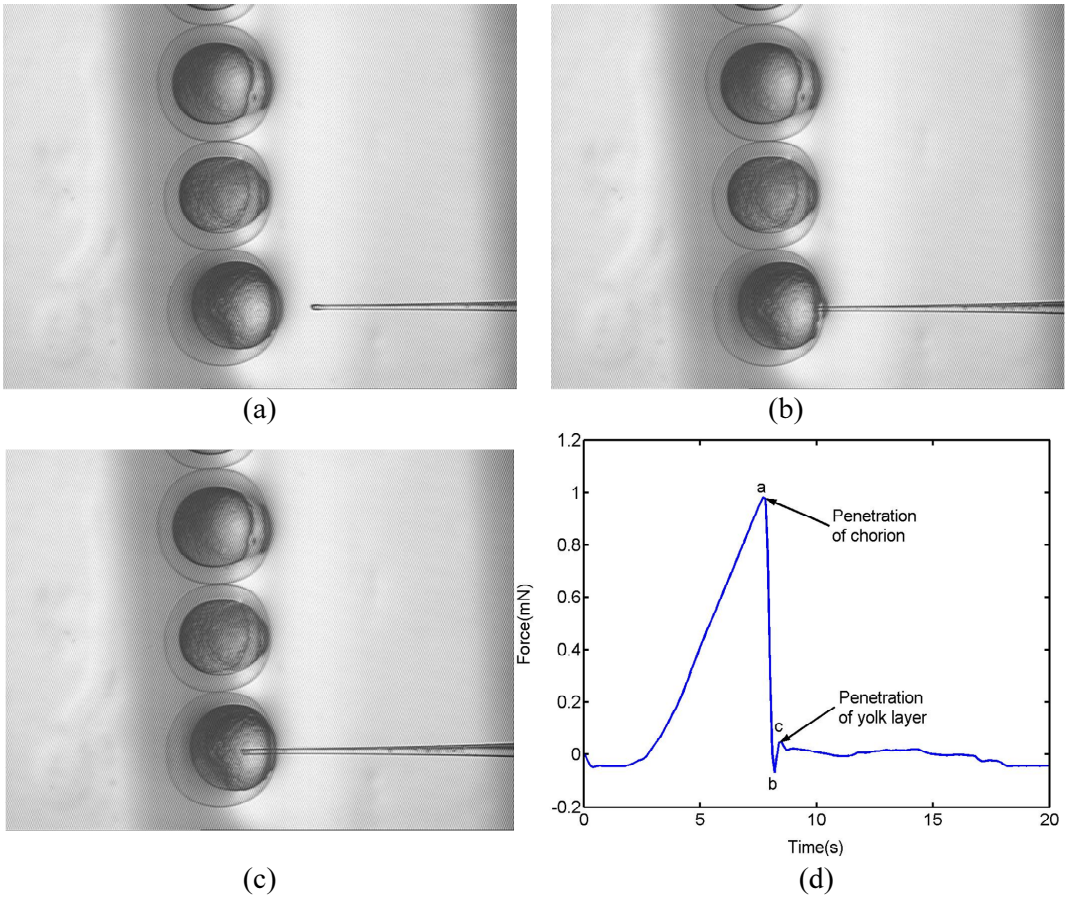

Figure 3.5: Penetration of zebrafish embryo (a) before contact (b) contact (c) penetration (d) force trajectories of the penetration process.

The zebrafish embryos shown in Figure 3.5 are at the stage of 4 to 6 hours after fertilization. The maximum penetration force is 1 mN . It is a quantitative value to describe the "hardness" of the chorion layer of the zebrafish embryo at this stage. Different penetration forces of the chorion layer can be measured at different developmental stages of the zebrafish embryos. The change of the penetration forces can be used to understand

the “chorion softening” problems in the embryo development of zebrafish [18].

This section indicates that micro-force sensing alone can be used to provide useful information in micromanipulation. When a probe is used to touch the micro-object, the force response of the micro-object to the probe is measured. The measured force can be used to facilitate characterization tasks (such as in determination of micro-surface topography and mechanical properties) in micromanipulation. For micromanipulation involving the need to control the interaction between the micromanipulator and the micro-object, measuring force alone is not sufficient. The information obtained by force measurement should be used to facilitate the direct and automated control of interaction processes.

3.2 Augmentation of position control in micromanipulation with micro-force sensing feedback

The second experimental solution demonstrates the use of micro-force as a feedback to augment position control. Currently, prevailing approaches to micromanipulation are based on position control, whereby the interaction between the micromanipulator and the micro-object is accomplished by controlling the relative positions of the manipulator and the manipulated object. When a micro-force sensor is used to measure the interaction force between the micromanipulator and a micro-object, a force profile of the interaction can be generated. In this profile, some specific features will reveal the state of the operation. Since the force profile of the interaction is directly related to the position, these features could be used to improve the effectiveness of position control.

The key advantage of this solution is that, when augmented by force feedback, an originally position-controlled micromanipulation task can be automated. In this solution, force information obtained by direct measurement provides the crucial feedback needed to enable automation of the task. The principle and effectiveness of this solution are demonstrated through two applications. The first involves the batch microinjection of zebrafish embryos, while the second concerns the coarse alignment of active fiber pigtailing in photonic assembly.

3.2.1 Using Force-feedback to Facilitate Microinjection of Zebrafish Embryo

The microinjection is a common technique in genetic engineering for transferring genetic material into a cell [98]. Microinjection of DNA materials into zebrafish embryo help the study of vertebrate development and genetics. In the injection of zebrafish embryos, the tip of the micropipette is first moved slowly towards the embryo. When the tip of the micropipette slightly touches the chorion of the embryo, it is driven to produce a quick thrust movement, resulting in an initial penetration of the chorion of the zebrafish embryo. Upon this initial penetration, the micropipette will be continuously moved until the tip of the micropipette enters the yolk of the embryo. At that point, genetic material can be injected into the embryo.

There are several strategies to control the penetration process [99]. The simplest to implement is pure position control without any feedback. However, in this approach,

there is no feedback during the process to indicate whether the penetration is successful. For instance, sometimes the micropipette may just slip on the surface of the chorion and does not penetrate it. Although vision feedback may be implemented to monitor the penetration process, the practicality of such a vision-based method is hindered by the difficulty in identifying the tip of the micropipette correctly and quickly, because of the difficulty in determining whether the tip is inside or outside (but laying on the surface of) the transparent chorion, and the high computational load associated with real-time image processing.

One possible approach to overcome this difficulty, and consequently to enable automation of the injection process, is to use position control with force feedback. In this approach, the penetration force is measured and used as a real-time feedback to control the penetration process. The advantage of using micro-force sensing as feedback is that it reflects quickly and accurately the state of the embryo (e.g., being deformed or penetrated). The measured penetration force could be used to augment position control strategy by dynamically determining the stopping point of the tip of the micropipette.

This is done by exploiting the unique characteristics of the force signal in the penetration process. For example, the penetration force profile of the zebrafish embryo (as shown in chapter 3.1.2) was studied. The force reading was around zero before the micropipette contacted the embryo. Subsequent to contact, the penetration force increases linearly while the embryo exhibits elastic deformation. When the penetration force reached a critical value, it dropped drastically back to zero, indicating that the embryo has been penetrated.

The critical value 1 *mN* (at point *a*) is a significant feature in the penetration force profile as shown in Figure 3.6. However, it should not be used as a universal threshold to determine the success of a penetration of the chorion. This is because different zebrafish embryos have different mechanical properties. Even for the same zebrafish embryo, the thickness of the chorion layer will change when the embryo evolves from one stage to the next. The specific and consistent characteristic of the force profile, however, suggests that the point at which penetration of the chorion occurs can be determined by detecting the sharp drop in the penetration force after its initial rise (e.g., between points *a* and *b* in Figure 3.6).

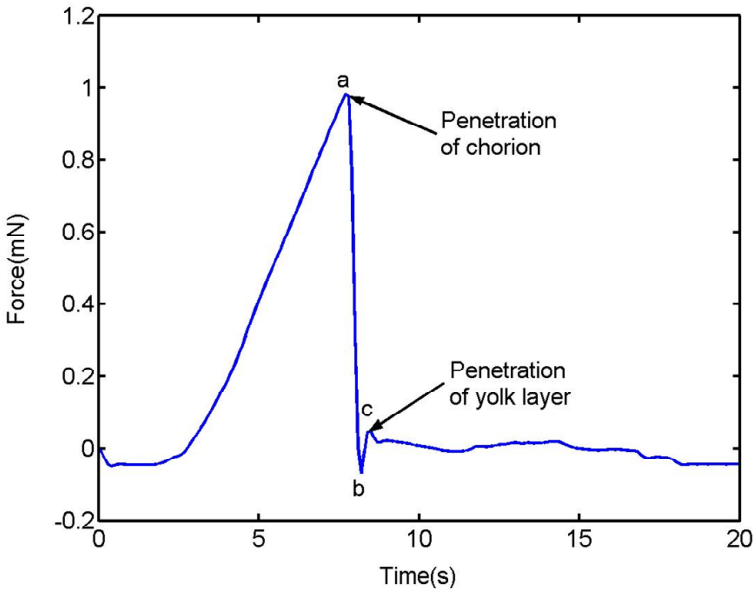

Figure 3.6: Force trajectory of the penetration process.

This can be achieved by analyzing the first-order and second-order derivatives of the penetration force with respect to time, as shown in Figures 3.7(a) and 3.7(b), respectively. When the value of the first-order derivative is smaller than 0 (point *d*) and the value of the second-order derivative is larger than 0 (point *e*), the corresponding force is

between point *a* and *b* shown in Figure 3.6. This brief interval (between *a* and *b*) indicates that the chorion is being penetrated, with *b* signifying the end of the penetration.

In implementing this force-augmented position control, the position of the micropipette and penetration force are sampled in two different real-time processes, with the force sampled at a much higher frequency. The first-order and second-order derivatives of the penetration force are computed in real-time. When their values meet the requirements, the position control will command the micropipette to stop. As a result, the stopping position is inside the embryo, slightly further inward from the point of penetration.

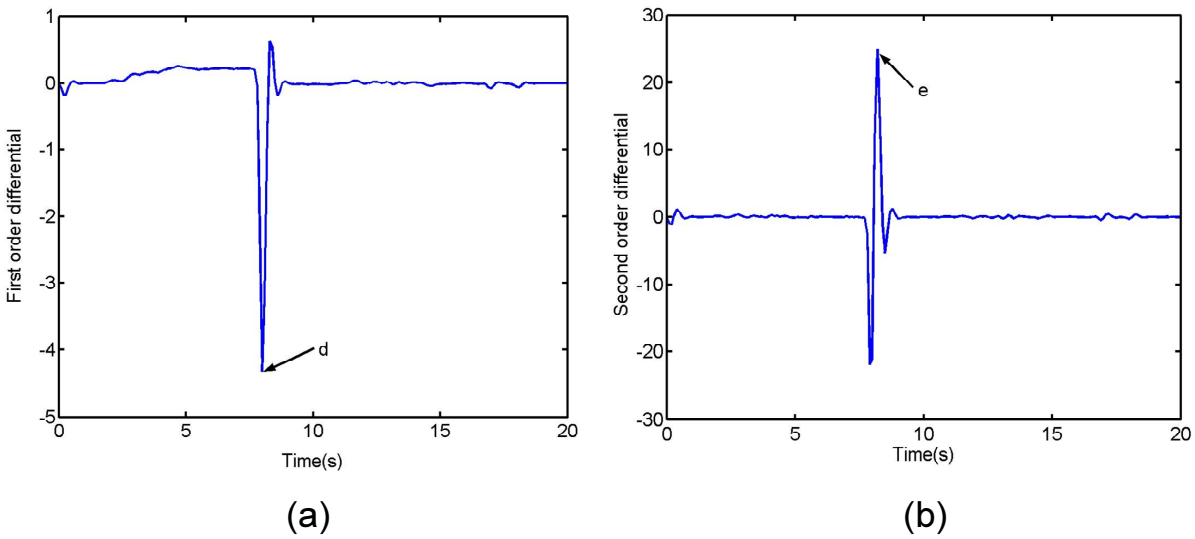

Figure 3.7: Derivative of penetration force (a) first order derivative (b) second order derivative.

In the control of the penetration process of zebrafish embryo, micro-force sensing feedback is used because the interaction force reflects quickly and accurately the state of the embryo (e.g., being deformed or penetrated). While in the applications where the interaction force is not apparently useful, as long as there exists contact between the micromanipulator and the micro-object, micro-force feedback could still be used to facilitate

the control of the micromanipulation process. For example, the force information could be used to facilitate the coarse alignment of active fiber pigtailing, where the search of light intensity signal was improved by using the micro-force signal.

3.2.2 Using Force-feedback to Facilitate Coarse Alignment in Active Fiber Pigtailing

Assembly of optical fiber onto optical device with high accuracy of alignment is the core process in packaging of photonic systems [100]. Currently, active fiber pigtailing is one general approach because of its low excess loss, good loss uniformity and high yield [101]. Active fiber pigtailing is conducted based on the integrity of light coupling between the optical fiber and the optical device. This involves moving the fiber in very fine incremental motion until a maximum coupling in term of light intensity is achieved. The movement of the fiber typically begins with a coarse alignment called the search of first light, which aims to position the optical fiber and the optical device in such a way that at least some light will travel through the system and be received by the detector.

The method of 2-D blind raster scan is usually used in coarse alignment. In this method, the signal of light intensity is measured to check whether the first light is found. The fiber scans (by back-and-forth search or rectangular spiral search) over an area where it is assumed that the input channel of the optical device is located. Estimation of position and area size of the search directly affects the efficiency of this method. However, the estimation is difficult to make. Moreover, specific features of some optical devices

(such as the optical path between the substrate and transparent cover) may interfere with the scanning process, resulting in poor signal content or no signal at all as the fiber traverses a large portion of the optical device input facet. This would mean that during the scanning process the signal generated is not useful most of the time in effectively directing the movement of the fiber.

For example, in pigtailing of single-mode fiber, the diameter of the fiber core is only about 8 or 9 microns. In order to differentiate the “first light” signal from noise, the sampling interval of fiber’s movement is limited to a few microns. Such a small sampling interval would lead to long searching time in coarse alignment. Moreover, if the input facet of the optical device is opaque, the detector receives no signal unless the optical paths of single-mode fiber and optical device are coincidentally close to each other.

A new approach using force information could be applied to locate this small area. A micro-force sensor with a sharp tip is used to sweep the input facet of the optical device. The resulting micro-force measured by the sensor will continuously provide useful information about the surface features as long as the tip of the sensor is in contact with the input facet. These surface features (as characterized by the the micro-force signal in real-time) provide useful clues in guiding the fiber to rapidly locate the actual optical path of the optical device. Figure 3.8 illustrates one application scenario for using this approach to locate the optical path.

As shown in Figure 3.8, a micro-force sensor with a sharp tip sweeps the surface of the optical device, which has a convex surface with a small hole at the center of the surface for fiber pigtailing. It can be inferred that the optical path of the optical device

is very close to the center of the hole. As the tip of the sensor sweeps across the convex surface, the measured contact force varies continually with the curvature of the surface. If the tip happens to sweep across the center hole, it will lose contact with the surface momentarily, resulting in a sharp discontinuity in the measured force signal. Such a sharp discontinuity serves as a good indication of the existence and the location of the center hole. Once the center hole is determined, the optical fiber to be pigtailed will be moved to this position and start the search of first light in the adjacent small area. To apply this approach in practice requires an efficient search technique to guide the sweeping movement of the sensor tip across the surface of the optical facet.

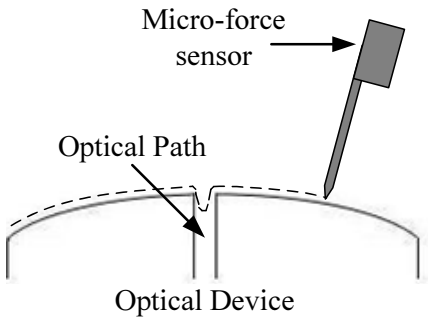

Figure 3.8: Using a micro-force sensor to sweep the surface of an optical device.

Figure 3.9 illustrates a simple but efficient search technique. From a randomly selected initial point at the edge of the facet surface, the sensor tip first sweeps across the device surface in a randomly selected direction. The peak of this characterized arc is marked. Then another sweep is performed in a similar fashion but perpendicular to the first arc. The new arc is made to pass through the first peak point. By the fact that the directions of these two arcs are perpendicular to each other, the center of the new arc is taken to be the center of the insertion hole. This search technique permits a coarse sampling interval, where the force signal provides meaningful information for rapidly locating the

area containing the optical path.

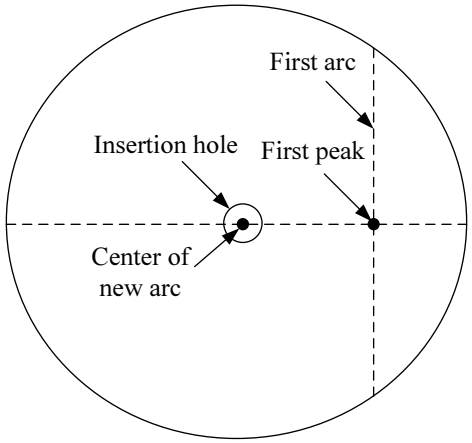

Figure 3.9: Search path for finding the center of an insertion hole.

For integrated optical devices such as waveguides, this method is applicable to the one with a socket in the end face of the planar structure directly at the end of the guiding region [102]. For example, Gibson et al. developed a new technique to etch the doped guiding core region of the waveguide. A pure-silica cladding-based buried channel waveguide possesses a doped guiding core region for the propagation of light. This doped core region is found to etch at a greater rate because of the increase in solubility compared with that of the surrounding pure-silica region. This selective etching thus could form a socket (20μm with a mean width of 10μm) for fiber pigtailing. Figure 3.10 shows a schematic graph of the waveguide end face after etching. Such remarkable socket could be easily found based on force information.

This section indicates that the position-based micro-manipulation techniques could be augmented through utilization of information obtained by micro-force measurement. Micro-force information can provide the crucial feedback needed to enable automation of the micromanipulation task. However, in some applications, position-based micro-

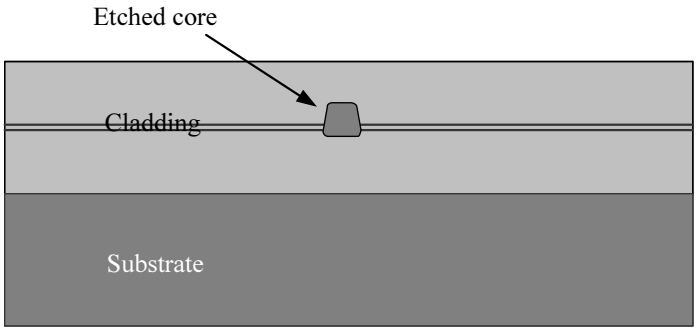

Figure 3.10: Schematic graph of the waveguide end face after etching.

manipulation is not sufficient to control the process of micromanipulation, such as in micro-assembly. Direct force control is needed in such tasks.

3.3 Implementation of direct force control in micromanipulation

The *third problem* in micro-force sensing and control concerns the applicability of direct force control in micromanipulation. The experimental solution shows that the direct force control represents an effective alternative to position-based force control in micro-assembly. Implementation of direct force control is needed in micromanipulation.

Research and development of technologies for micro-assembly have been reported in the literature [7] [11] [103] [56] [104]. The common practice is to conduct micro-assembly using a workstation, which usually consists of a micromanipulator, a micro-force/micro-position sensor, a set of microscopes, and several high-precision positioning stages. Assembly is usually carried out by precise positioning of parts. The positioning

stages provide long-range (in the order of millimeters) conveyance of parts, and support short-range (in micron scale) part-handling and assembly operation.

This type of pure position-based assembly approach is not suitable for dealing with interaction forces that inevitably arise during assembly for two reasons. First, in a short-range part-handling and assembly operation, pure position-based method cannot directly control the interaction force between the micromanipulator and a part. Even if a micro-force sensor is mounted at the tip of the micromanipulator to measure the interaction force, a correlation between the measured force (pertaining to a particular part) and the displacement of the positioning stage needs to be calibrated first. Then by controlling the displacement of the positioning stage, the manipulator can be maneuvered to exert a desired interaction force. Since different parts may have different mechanical properties, such a method of position-based force control may not produce consistent result in repetitive assembly tasks. This is mainly due to the fact that sometimes it is difficult to find a uniform correlation (for a batch of parts) between the displacement of the positioning stage and the measured force. Even for the same part, this correlation may also change at different assembly stages.

Second, the resolution of the controllable interaction force solely depends on the resolution of the positioning system. In micro-assembly, the parts are generally very fragile. To avoid damaging the parts, the magnitude of the interaction force may need to be controlled down to the level of milli-Newton or below. This in turn places a restriction on the maximum step size of the positioning system. The step size of the positioning system must be substantially smaller than the maximum allowable compliance of the

part. Hence the speed of the pure position-based assembly is limited.

Direct force-feedback control represents an effective alternative to position-based force control in micro-assembly. In direct force-feedback control system (also called ”explicit force-feedback”), the input signal and the measured signal are direct representations of magnitudes of force. Consequently, limiting the magnitude of the input signal can help prevent damage to a part during assembly.

Application of explicit force-feedback control can also lead to an effective micro-assembly process based on force information. For instance, consider the task of assembling a part onto a base plate, wherein the gap between the part and the plate indicates the degree of completeness of the assembly. Traditionally, this gap is observed by a vision system. However, sometimes it is difficult to set up this vision system in micro-assembly, because of (i) the need for unobstructed camera view, proper lighting, and sufficient space for camera mounting, and (ii) the constraints imposed by the limited field of view and limited depth of focus of the microscope. One way to deal with these problems is to use explicit force control system.

When a micromanipulator (equipped with a micro-force sensor) contacts a part, the resulting force measured by the sensor will continuously provide information as long as the micromanipulator is in contact with the part. When the measured force exhibits a certain pattern, it can be judged that the part is completely assembled onto the base plate. Hence, by properly controlling the interaction force in the assembly process, effective assembly is possible.

In order to implement explicit force-feedback control in practice, two main issues need to be resolved. The first issue concerns the design of a force transmission stage, which could provide frictionless translation motion, as the force involved in micromanipulation is quite small (at level of milli-Newton or below). The second issue concerns the design of a force controller which could precisely control the interaction force. These two issues will be discussed in detail in the next chapter.

3.4 Conclusion

In this chapter, the applicability of micro-force sensing and control in micromanipulation is investigated. Three experimental solutions are developed to resolve the three main problems in micro-force sensing and control. The first experimental solution demonstrates that micro-force sensing can be used to facilitate characterization tasks (such as in determination of micro-surface topography and mechanical properties) in micromanipulation. The second experimental solution demonstrates the use of micro-force as a feedback to augment position control. The third experimental solution shows that it is needed to implement direct force control in micromanipulation. Several examples are used to illustrate the first and the second solutions. The importance of the third solution for micromanipulation is discussed. The next chapter will present how to realize the third solution.

Chapter 4

Implementation of Explicit Force Control in Micromanipulation

To implement explicit force control in micromanipulation poses challenges on the design, selection, and integration of various components, including actuators, stages, sensors, and controllers. The developed force control system would serve as a subsystem in a micromanipulation system to facilitate the control of the interaction between the micromanipulator and the environment. The force control system should be adaptively integrated with microscopy system and micro-positioning system.

In this chapter, the development of the key component to implement force control - force-transmission stage is reported first. Then the design of force controller to precisely control the interaction force between the micromanipulator and the environment is discussed. The direct force control is applied in the use of mechanical fixtures, which

are used to overcome adhesion force effects during the release of the micro-objects. Finally, the integration of the force control system with the microscopy system and micro-positioning system is shown in a prototype structure of micromanipulation system.

4.1 Design of Force-transmission Stage

In order to implement high precision force control in micromanipulation, specific stage should be developed. The stages used in micromanipulation are platforms to support the micromanipulator and the manipulated objects. Currently, micro-positioning stages are available to provide high-precision positioning. Usually, these stages have bearings (with balls or rollers, etc.) and are driven by stepper motors or piezoelectric actuators which are generally controlled in position. These actuators are not suitable to generate force with adjustable magnitude. While DC motors can output adjustable force with different current inputs, only those DC motors with high resolution of output force (in the order of a few milli-Newtons or less) can be used in force control in micromanipulation. However, such high resolution motors tend to have small force range, and are usually incapable of directly driving the bearing-type positioning stages, as these stages require a large driving force to ensure high positioning accuracy. This manifests the need for a new type of stage that, when subject to a very small force, can still move and (in doing so) transmit the input force to the point of interaction accordingly.

The force-transmission stage is developed to meet such requirements. The force-transmission stage is designed to generate low frictional effect and has high immunity against noise

(due to vibration, for instance). This ensures that no matter how small the output force from the actuator is, the system still exhibits a high signal-to-noise ratio. The voice coil actuator is used to generate a small force (with a resolution of a few milli-Newtons or less) to directly drive the force-transmission stage. The voice coil actuators are direct drive, limited motion devices that utilize a permanent magnet field and coil winding to produce a force that is proportional to the current applied to the coil.

A one-axis force-transmission stage has been designed and built (based on a compound flexure configuration) to demonstrate the applicability of this device in force control. The stage provides frictionless translation with low stiffness motion along one axis while exhibiting high stiffness in all other axes. The structure of the compound flexure stage is illustrated in Figure 4.1, while a photo of the actual device is shown in Figure 4.2.

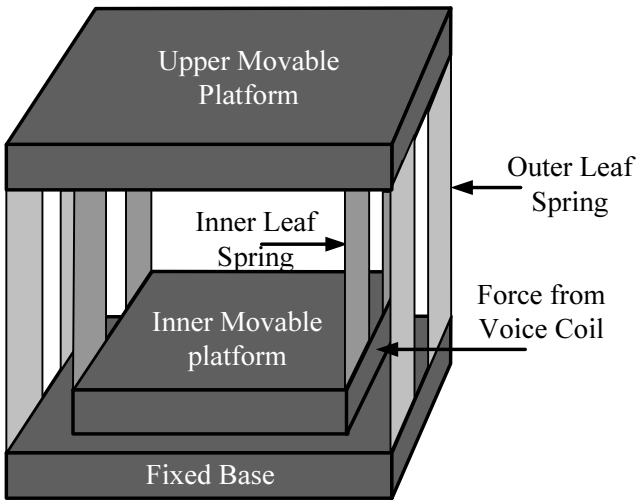

Figure 4.1: Structure of compound flexure stage.

The stage consists of two movable platforms, each supported by a set of four leaf springs in parallel. This double compound four-bar-linkage configuration enables the stage to provide frictionless translation with low stiffness motion along one axis (while exhibit-

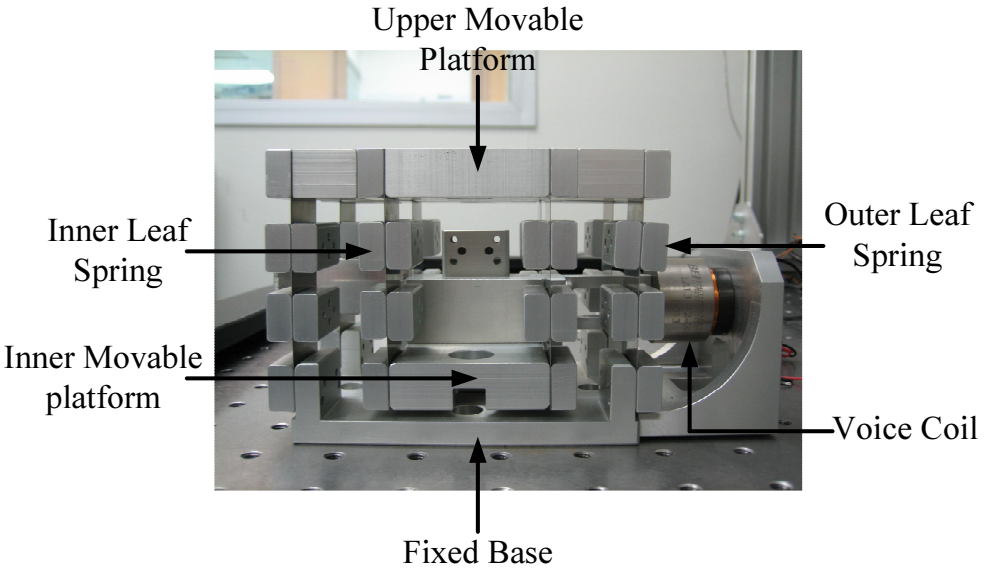

Figure 4.2: Photo of compound flexure stage.

ing high stiffness in all other axes) as well as resistance to shock and vibration. Since the springs have the same geometry and are made of the same material, they can be considered as one "compound" spring with four times the individual stiffness. Figure 4.3 illustrates the working principle of this stage. The lower platform is used to receive the force from the actuator. The inner compound spring is used to provide compliance between the input force and the upper movable platform. The upper platform is used to hold the micromanipulator. The outer compound spring is used to levitate the platform and provide frictionless movement. Each set of inner leaf springs and outer leaf springs is simplified to one compound spring. Since the inner and outer leaf springs are connected in series, both compound springs will experience the same applied force. A force F acting on the lower movable platform that deflects the inner compound spring by X_i and the outer compound spring by X_o will cause the lower movable platform to be displaced by $(X_i + X_o)$.

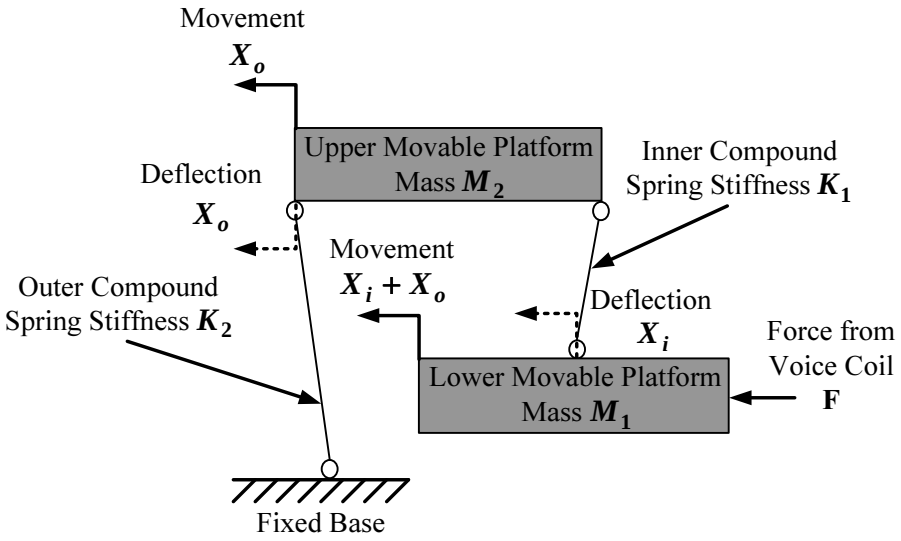

Figure 4.3: Force and displacement in flexure stage.

The stage was calibrated to determine the stiffness of the inner and outer compound springs. A force, incremented with a step of 50 mN, was applied on the lower movable platform through a voice-coil actuator and the corresponding deflections X_i and X_o of the inner and the outer compound springs were measured using a laser position sensor with a resolution of 0.5 μm. The results of the calibrations (shown in Figure 4.4) indicate a linear relationship between the applied force and the deflection of each compound spring. From these results, the stiffness of the inner and outer compound springs were estimated to be $K_1 = 1042.72$ mN/mm (with a standard deviation of 22) and $K_2 = 765.2$ mN/mm (with a standard deviation of 2), respectively.

The force-transmission stage could be used for short range micro-object picking and releasing in one translational axis. A micromanipulator (such as a probe or a pipette) is mounted on the upper movable platform of the force-transmission stage. A force sensor measures the interaction force between the micromanipulator and its environment, while an explicit force controller controls the interaction force to follow a desired force

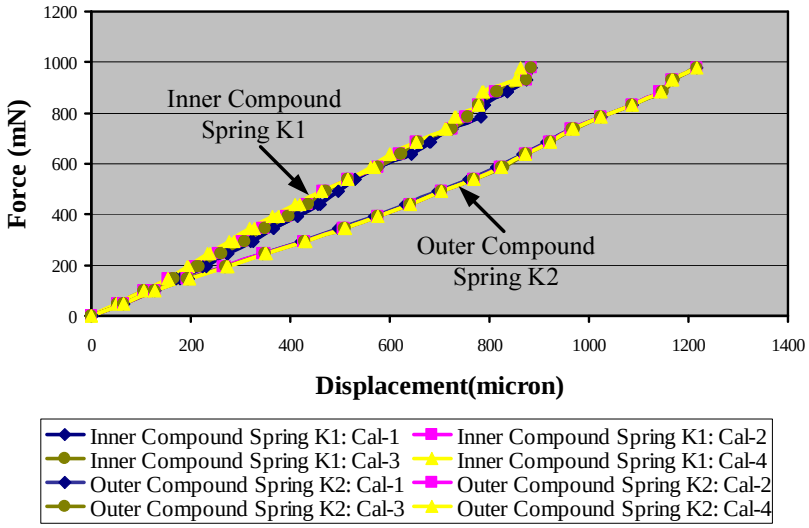

Figure 4.4: Stiffness calibration inner compound and the outer compound spring.

trajectory.

4.2 Design of Force Controller

When the force-transmission stage is used to implement force control in micromanipulation, the main objective is to control the interaction force between the micromanipulator and the environment. A force controller for this purpose was designed based on dynamic model of the stage. The model (as shown in Figure 4.5) is in the form of a mass-spring-damper system, where I_i is the input current to the voice-coil actuator, F is the output force from the voice-coil actuator and directly drives the flexure stage, K_c is the force sensitivity of the voice-coil actuator, M_1 is the mass of the lower movable platform, M_2 is the mass of the upper movable platform with the micromanipulator, K_1 and K_2 are the stiffness of the inner and outer compound spring, respectively, and B_1 and B_2 are the corresponding damping coefficients.

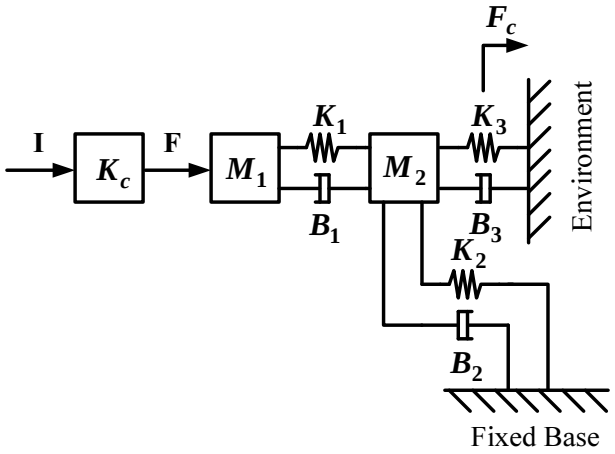

Figure 4.5: Dynamics model of force-transmission stage and its environment.

The environment is modelled as a spring-damper system, with stiffness K_3 and damping coefficient B_3. When the micromanipulator and the environment are in contact, the environment and the fixed base of the stage are in parallel. The interaction force F_i between the environment and the micromanipulator is measured by a force sensor. Based on this model, explicit force control is applied with the objective of having the actual force follow a desired force as closely as possible.

Controllers for explicit force control are often some variants of PID control. We first designed and evaluated a proportional and derivative control law:

$$I_i = \frac{1}{K_c}\left(F_i(1+a) + b\left(K_p\Delta_f + K_d\dot{\Delta}_f\right)\right),$$

where $a = K_2/K_e$, $b = M_2/K_e$, $\Delta_f = F_d - F_i$, and F_d is the desired reference force, K_e is the estimated stiffness of the environment. The controller was tested in a simulation using MATLAB, with the parameter values listed in Table 4.1.

Figure 4.6 shows the simulation results. When the the estimated stiffness of the environ-

Table 4.1: Values of simulation parameter set in the controller.

F_d	500 mN
K_c	1 mN/mA
M_1, M_2	0.5 kg, 1 kg
K_1, K_2	1042.72 mN/mm, 765.2 mN/mm
B_1, B_2	0.1, 0.1
K_3	4000 mN/mm
B_3	1
K_p, K_d	100, 20

ment K_e was exactly same as the actual stiffness K_3, the desired force was achieved, as indicated by the solid line. Error in the estimation adversely affected the force-tracking performance, and possible stability of the system. The force sensitivity of the voice-coil actuator K_c was also found to be a key factor affecting both performance and stability. For instance, the dotted line and dash line associated with K_c indicated that even a small error in the estimation of K_c would cause system to exhibit either large steady-state error or instability. This is due to the fact that the sensitivity of the voice-coil actuator was only valid in a very small range of displacement. It is clear that the feedback action in the PD control is unable to compensate for the estimation error. To overcome this problem, application of integral control was investigated.

Because of its simple form, low-pass nature, and its zero steady state error for a constant reference force [105], integral control is usually considered more suitable for explicit force control. An integral control law was designed as:

$$I = \frac{1}{K_c}\left(K_i \int_0^t (F_d - F_c)\, dt\right).$$

where F_c is the measured contact force. The only uncertain parameter in this controller

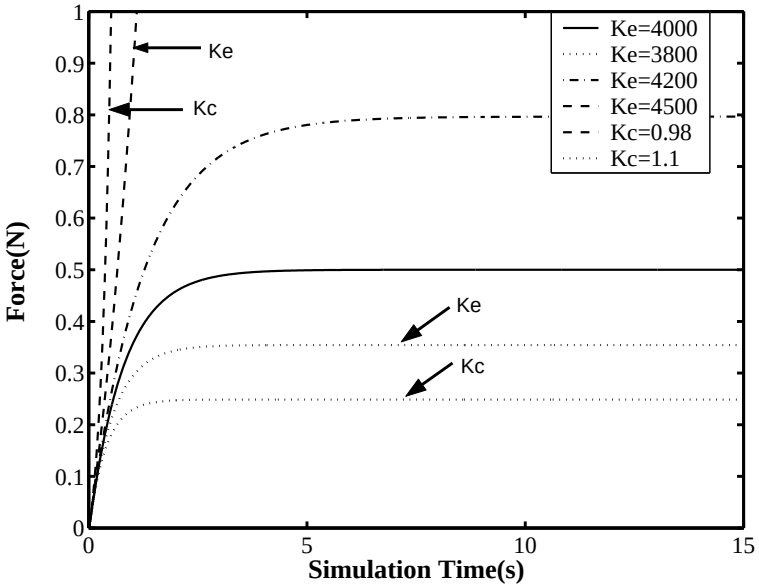

Figure 4.6: Simulation of PD force control.

is K_c. The controller was tested in a simulation using the same parameter values as those for the case of PD control. Figure 4.7 shows the simulation results, with fixed at $K_i = 0.8$ for different values of K_c. The results indicated that even with a large variation in K_c, the system still tracked the desired force satisfactorily.

The integral control is proved to be effective in force trajectory tracking in the explicit force control. The contact force between the micromanipulator and its environment could be precisely controled to reach a desired value. However, in the control of the micromanipulation process, the effect of adhesion forces should be considered, especially in the pick-up and release tasks of the micro-objects. The dominance of adhesion forces introduces complication in the manipulation process. One approach to overcome adhesion force effects is to use the mechanical fixtures, where the direct force control could be applied.

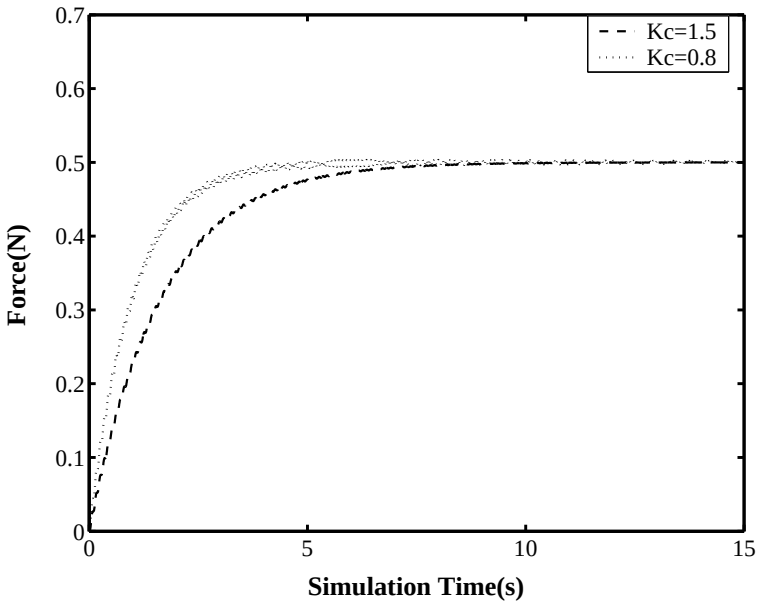

Figure 4.7: Simulation of integral force control.

4.3 Using Mechanical Fixtures to Overcome Adhesion Force Effects

In macro-world, adhesion forces are negligible because of the dominance of gravitational and inertial forces. However, below a certain size threshold, gravitational and inertial forces become insignificant compared to adhesion forces. The dominance of adhesion forces introduces complication in the manipulation process. For instance, when placed by a manipulator onto a desired location on a substrate, an object may have a tendency to adhere more strongly to the manipulator than to the substrate, thus preventing accurate placement [20]. It is possible to take advantage of the adhesion forces for pick-up, using a micromanipulator with high surface energy and low surface roughness [33]. In this case, a micro-object can be picked up by simple contact. The obvious problem in this case is the release, as it is necessary to overcome the adhesion forces between the

micromanipulator and the micro-object.

During release, the forces acting on the micro-object includes the adhesion force f_m between the micromanipulator and the micro-object; the adhesion force f_s between the substrate and the micro-object; and the gravity of the micro-object *mg* (as shown in Figure 4.8). When f_m - (f_s + mg) $>$ 0, the micro-object will stick to the manipulator. In order to overcome the effect of adhesion, the mechanical fixtures are used.

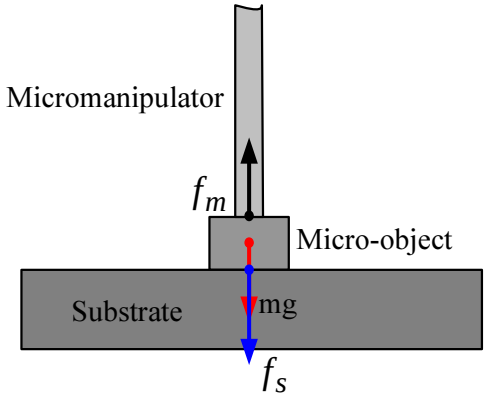

Figure 4.8: Forces acting on the micro-object during release.

A constraint force f_c (between the micro-object and the mechanical fixture) could be generated to constrain the movement of the micro-object. Compared to the adhesion force, which are usually less than several hundred micro-Newtons, the magnitudes of constraint force f_c could be one order larger than the adhesion forces by properly choosing the materials and the design of the mechanical fixtures. Different mechanical fixtures can be designed to generate the constraint force f_c. For example, the constraint force arises when an interlocking mechanism is used, as shown in Figure 4.9.

The micro-object and the substrate are designed with interlocking mechanism. When the micro-object is pushed by the micromanipulator, the jaw on the substrate will open.

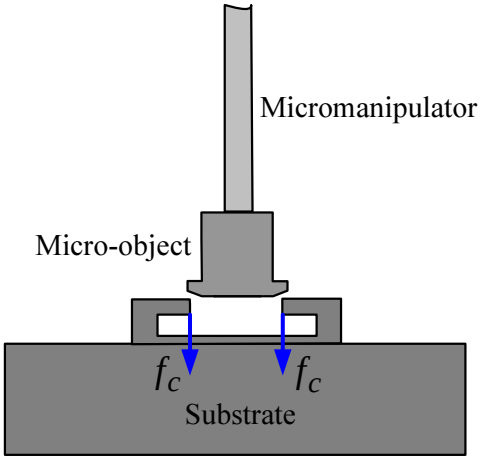

Figure 4.9: Example of interlocking mechanism.

The teeth on the micro-object will move in until it interlocks with the jaw. If a micro-force sensor is connected to the micromanipulator and measure the pushing force, a continuous rising force following by a sharp drop after certain threshold will be shown in the force profile. The force profile could be used as a feedback in real-time control of the releasing process. The transient change(drop of the force) indicates the teeth are fixed into the jaw, where the constraint force f_c is activated.

Another example using constraint force to overcome the effect of adhesion is based on friction force. Notches are fabricated on the side of the micro-object. The purpose of the notch is to enable the micro-object to be fixed onto the substrate by mating the notch with the pre-fabricated walls on the substrate, as shown in Figure 4.10. A micromanipulator is designed to push the micro-object down onto the wall on the substrate such that the notch at the bottom of the micro-part fitted onto the wall. A micro-force sensor is used to measure the friction force between the notch of the micro-object and the wall on the substrate. When the measured force reaches a threshold value, the notch fully engages

the wall, where the constraint force f_c is activated. It is noted that simply retracting the micromanipulator would result in its extraction from the micro-object, because by design the friction force between the notch of the micro-part and the wall on the substrate is much larger than the adhesion force between the micromanipulator and the micro-object.

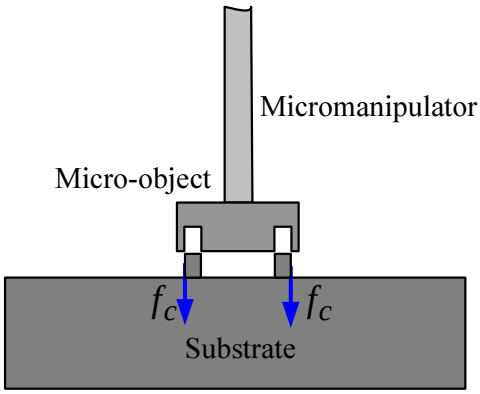

Figure 4.10: Example of notch mechanism.

The release of the micro-object could be achieved by using the mechanical fixtures, which would generate the constraint force f_c to overcome the adhesion forces. Force control is applied in this process to judge whether the constraint force is activated. The voice coil actuator, force-transmission stage, micro-force sensor, explicit force controller and mechanical fixture form a force control system for micromanipulation. The system can be used in the applications such as micro-assembly. However, the force control system alone is not enough because it can only deal with one-axis, short range handling of the micro-object. It is necessary to make the force control system adaptively integrated with the microscopy and micro-positioning systems to fulfill the requirements in the whole process of micromanipulation.

4.4 Integration of Force Control System with Microscopy System and Micropositioning System

To implement a complete process of micromanipulation requires the identification, pick-up, conveyance and release of the micro-objet. This needs the effective integration of the microscopy, micropositioning and force control systems. For example, in a micro-assembly task, the micro-parts fabricated on a wafter need to be picked up and placed on a substrate. In this process, the microscopy system first identifies the micro-part. Then the force control system is used to pick up the micro-part by controlling the picking up force. After the micro-part is picked up, the micro-positioning system conveys the micro-part to the area of the substrate. The microscopy system then locates the position where the micro-object should be placed. Finally, the force control system is used to release the micro-part by controlling the releasing force.

The integration of the force control system with the microscopy and micro-positioning systems is shown in a prototype structure of micromanipulation system (Figure 4.11). The main translation stages are the positioning stage and the force-transmission stage. The positioning stage, usually with three-axis movement in a range of tens of millimeters and a resolution of a few microns or higher in each axis, is used for long-range conveyance and precise positioning of the micro-object. The force-transmission stage is used for short range micro-object picking and releasing in one translational axis. The microscopy system is used to observe the position of the micro-object. The microscopy information is feedback to a position controller to guide the movement of the micro-

positioning system.

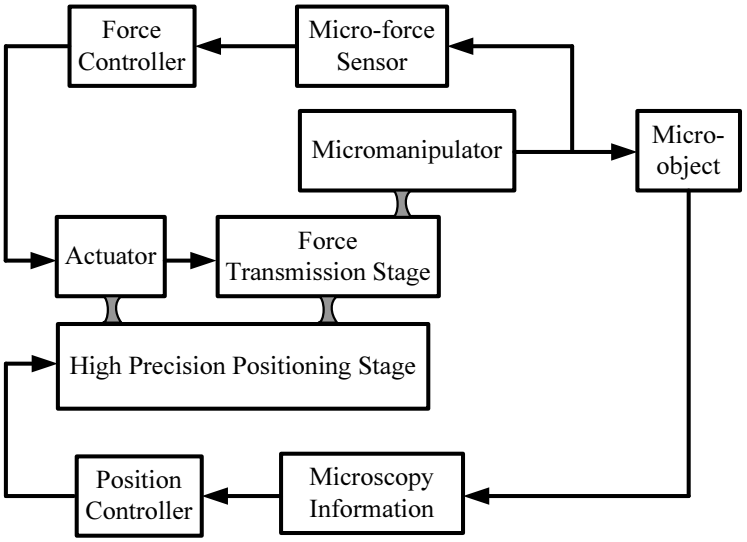

Figure 4.11: Structure of micromanipulation system consists of force control system, microscopy system and micropositioning system.

In the development of force control system, the selection and design of micro-force sensor and micromanipulator are important issues. Generally, the design of micro-force sensors can be categorized to four types: strain gauge (piezoresistive), piezoelectric, capacitive and optical sensors, each with its own characteristics in terms of resolution, measurement range, and applicability. Similarly, the micromanipulator used in a particular micromanipulation system may need to have specific capabilities due to the requirement of the micromanipulation process [106] [107]. It is usually the case that custom-built micro-force sensor and micromanipulator are used to meet specific micromanipulation requirements. By changing different groups of micro-force sensor and micromanipulator, the prototype structure of micromanipulation system shown in Figure 4.11 could be used as a base to apply into different micromanipulation tasks. The effectiveness of this prototype force-control system will be demonstrated in an experi-

mental application in the chapter 7, where micro-parts were picked up and assembled under explicit force-feedback control in scaffold assembly in tissue engineering.

4.5 Conclusion

In this chapter, the implementation of the explicit force control in micromanipulation is presented. The key components to implement force control - a frictionless force-transmission stage and an explicit force controller are developed to facilitate the implementation of force control in micromanipulation. The integration of the force control system with the microscopy and micro-positioning systems is shown in a prototype structure of micromanipulation system.

In the following chapters, three experiments are used to illustrate the applicability of micro-force sensing and control in practical micromanipulation tasks. In each experiment, a prototype system is developed to solve certain problems in micromanipulation. The integration of the force sensing and control system with the microscopy system and micro-positioning system is illustrated in each prototype system. The experiment results demonstrate the effectiveness of micro-force sensing and control in the micromanipulation.

Chapter 5

Experiment I: A Photonic Alignment System for Coarse Alignment in Automatic Fiber Pigtailing

This chapter presents an experiment to use micro-force sensing to augment conventional approaches for fast and accurate fiber pigtailing in photonic assembly. A photonic alignment system based on the micro-force sensing is developed to facilitate coarse alignment in active fiber pigtailing in integrated optics technologies. It illustrates that the micro-force signal provides useful clues in guiding the fiber to rapidly locate the actual optical path of the optical device (with specific geometry feature on its input surface).

5.1 Background

Assembly of optical fiber onto optical device with high accuracy of alignment is the core process in packaging of photonic systems. Currently, there are two general approaches for fiber pigtailing: active and passive. In passive alignment a V-grooved substrate is used to fix the optical fibers. Though cost-effective in providing adequate assembly quality for some applications, the accuracy of passive alignment is limited by the dimensional tolerance of the V-grooves as well as the uniformity of the fibers. Active alignment, on the other hand, is conducted based on the integrity of light coupling between the optical fiber and the optical device. This involves moving the fiber in very fine incremental motion until a maximum coupling in term of light intensity is achieved. The advantages of active alignment are low excess loss, good loss uniformity and high yield [101].

To gain such advantages requires optimization of the movement of the fiber in search for satisfactory light coupling. This search typically begins with a coarse alignment called the search of first light, which aims to position the optical fiber and the optical device in such a way that at least some light will travel through the system and be received by the detector. Following coarse alignment is fine alignment, in which an optimized path is used to search for the maximum light coupling in the shortest time. Various optimization algorithms for fine alignment have been proposed and well studied. For instance, the hill climbing, Hamiltonian [108] and Nelder-Mead Simplex [109] algorithm have been developed and thoroughly investigated. In contrast, optimization of coarse alignment seems to have received little attention. This is particularly unfortu-

nate because coarse alignment is actually a very important step in fiber pigtailing. It is the prerequisite to successful fine alignment. When the apparent separate processes of coarse alignment and fine alignment are taken as a whole, a properly optimized coarse alignment process could greatly enhance the efficiency of fiber pigtailing. It is therefore desirable to develop optimization methods for coarse alignment.

Two common methods used in coarse alignment are 2-D machine vision and 2-D blind raster scan. In the first method, a vision system first identifies the features of the optical fiber and optical device, and then directs the fiber to a location where is assumed that the optical paths of fiber and device are approximately aligned. However, the vision method needs unobstructed camera view, proper lighting and sufficient space for camera mounting. This method is also constrained by the limited field of view and limited depth of focus of the microscope.

The method of 2-D blind raster scan provides an alternative when using machine vision is not possible or practical. In this method, the fiber scans (by back-and-forth search or rectangular spiral search) over a small area where is assumed that the input channel of the optical device is located. Estimation of position and area size of search directly affect the efficiency of this method. However, the estimation is difficult to make without any assistances. Moreover, specific features of some optical devices (such as the optical path between the substrate and transparent cover) may interfere with the scanning process, resulting in poor signal content or no signal at all as the fiber traverses a large portion of the optical device input facet. This would mean that during the scanning process the signal generated is not useful most of the time in effectively directing the movement of

the fiber.

Another complication arises when the input facet of an optical device has multiple layers, such as a waveguide with optical path lying between the substrate and transparent cover. In such cases, local maximum of light intensity exists. This can easily result in a fiber being positioned at a location away from the actual optical path (where global maximum of light intensity occurs). Figure 5.1 illustrates this situation. As shown in the figure, the global peak represents the position where the maximum light intensity is coupled between the fiber and the optical device. This global peak is surrounded by (possibly) multiple local peaks. Simply judging from a light intensity signal, it is difficult to tell whether this signal belongs to the global peak region or to one of the local peak regions. In order to resolve this problem, the estimated location of the optical path should be correctly confined to a very small area.

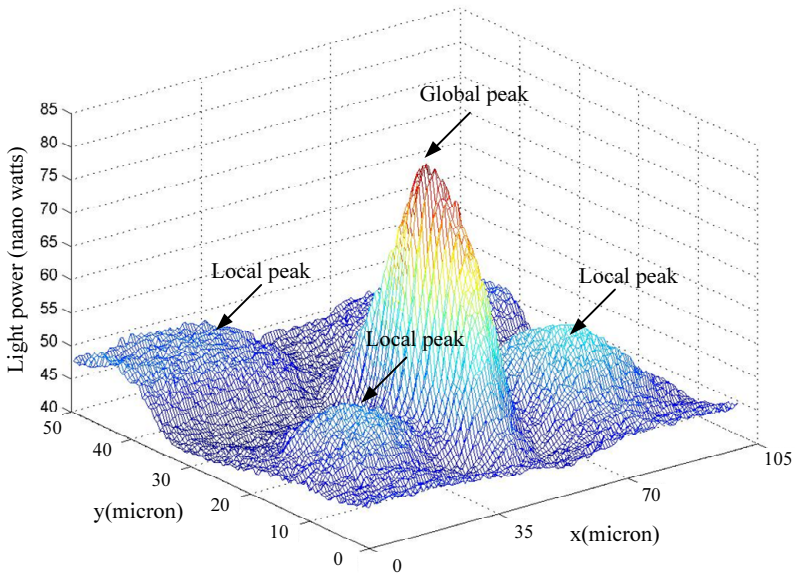

Figure 5.1: Waveguide profile of local peak and global peak.

5.2 Methodology

To achieve fast coarse alignment, we propose a novel approach by micro-force sensing. A customized micro-force sensor with a sharp tip is used to sweep the input facet of the optical device. The resulting micro force measured by the sensor will continuously provide useful information about the surface features as long as the tip of the sensor is in contact with the input facet. These surface features (as characterized by the the micro-force signal) provide useful clues in guiding the fiber to rapidly locate the actual optical path of the optical device. We demonstrated the effectiveness of this approach through an experiment on a photonic alignment system. A piezoresistive micro-force sensor was developed with a sharp tip to find the center of the insertion hole on the surface of a commercial optical ferrule. When a single-mode optical fiber is inserted into this hole thus located, its optical path is supposed to pass through the center of the hole. In demonstrating that (by employing micro-force sensing) the center of the insertion hole could be exactly located.

Figure 5.2 illustrates one application scenario for using this approach to locate the optical path. As shown in Figure 5.2, a micro-force sensor with a sharp tip sweeps the surface of the optical device, which has a convex surface with a small hole at the center of the surface for fiber pigtailing. It can be inferred that the optical path of the optical device also passes through the center of the hole. As the tip of the sensor sweeps across the convex surface, the measured contact force varies continually with the curvature of the surface. If the tip happens to sweep across the center hole, it will lose contact with the surface momentarily, resulting in a sharp discontinuity in the measured force signal.

Such a sharp discontinuity serves as a good indication of the existence and the location of the center hole.

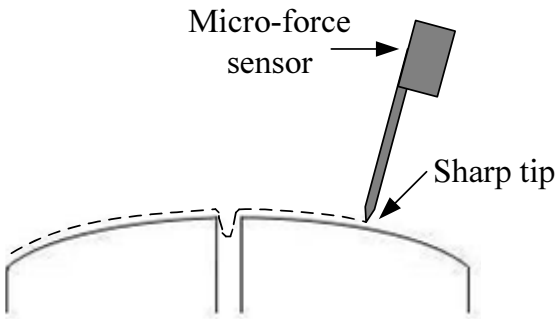

Figure 5.2: Using a micro-force sensor to sweep the surface of an optical device.

An important issue in implementing this force-sensing approach is the selection of suitable micro-force sensors. Two key issues involved in the selection are measurement range and probe-tip geometry. Suitable measurement range is dictated by the fact that forces exerted by the scanning probe on the optical device are usually limited to be in the order of milli-Newtons or lower (with micro-Newton resolution). This is because most of structures in an optical device are very delicate and fragile. Exerting such a small force avoids damaging the structure. Concerning probe-tip geometry, to properly characterize the surface feature of the optical device, a sensor with sharp tip at its end is preferred in order to avoid problems such as scanning topography distortion.

5.3 Sensor Design and Characterization

Among the various types of sensors available for measuring forces in micro-scale [19], some have been fabricated with sharp probes at their tips [110] [18] [49]. However, these

sensors are of the piezoelectric or capacitive type, and as such, have inherent limitations for the application of coarse alignment based on force sensing. Piezoelectric force sensors are best at detecting forces that vary quickly, but are not suitable for static force measurement. Under static loading condition, the reading of the sensor will return to its original value after several seconds [50]. Capacitive force sensors have high sensitivity at micro-Newton level, but the displacement range of the tip of such sensor is limited to only a few microns. Therefore, when the application requires not only accurate static force measurement but also an allowable probe-tip bending range in tens to hundreds of microns, piezoelectric and capacitive force sensors are not suitable. Piezoresistive force sensors, however, do not suffer from such limitations.

A piezoresistive force sensor has the property that its resistance changes under physical pressure or mechanical work. When a piezoresistive force sensor is strained or deflected, its internal resistance will change (and remain changed) until its original shape is restored. This enables it to measure static forces. The change in resistance is measured by an electric circuit (e.g., a Wheatstone bridge). A piezoresistive force sensor can be designed to exhibit a large gauge factor, which implies a high sensitivity. Its measurement range is in hundreds of milli-Newtons and its resolution could reach sub-milli-Newton. The bending range of the sensor tip can reach tens of microns or more.

5.3.1 Core sensor

Currently, there is no ready-made piezoresistive-based probe force sensor. To reduce development cycle time, a commercial piezoresistive force sensor, upon evaluation, was

found to be suitable for re-engineering into an integrated force sensing probe, and thus selected for modification. This particular sensor, the AE801 made by SensorOne® Technologies Corporation, has a sensing elements consisting of a silicon cantilever beam and a header to which the beam is mounted. The beam is made of single crystal N-type silicon and has one ion-implanted P-type resistor on each side. When the tip of the beam is deflected, the resistance of the resistor on the compressed side will decrease, while that on the other side will increase. Each resistor is connected to two pins on the header. The pins serve both as mechanical mount and as electrical connections for the resistors. Table 6.1 summaries the specifications of this sensor.

Table 5.1: Specifications of piezoresistive force sensor.

beam dimensions($l \times w \times h$)	5mm×0.95mm×0.15mm
modulus of elasticity	1.6×10^5 N/mm^2
spring constant at full length	2000 N/m
deflection of the beam at full scale	$\sim$70 μm
maximum allowed load at tip of the beam	120 mN
hysteresis	$\pm$0.1%
non-linearity	$\pm$0.25%

5.3.2 Modification

The sensor as described in Table 6.1 has a beam width of 950 μm. At this size, it may not be suitable for direct application in performing certain delicate micromanipulation tasks. For example, it is difficult to use the sensor beam alone to measure injection force acting on cell membrane. A micro-pipette is needed to contact the cell membrane instead and transfer the injection force to the sensor beam. Usually, the diameter of the micro-pipette tip is around 10 μm. In order to upgrade the core sensor for more

versatile micromanipulation tasks, a probe with a smaller diameter needs be integrated to the sensing beam as an extension. An important consideration in adding an extension to the core sensor is that the mechanical property of the probe should be close to that of the piezoresistive force sensor. This is to ensure that the extension is strong enough to transfer forces from the measurement to the sensor without affecting its frequency response. A single-mode optical fiber meets this requirement. The standard single mode optical fiber has a cladding around 125 μm in diameter. As most of the optical fibers are made with 99% of silica glass, their diameter can be reduced through etching. In particular, the modulus of elasticity of the optical fiber is close to that of the sensor; specifically, the former is 7.2×10^4N/mm^2 (for silica), while the latter is 1.6×10^5N/mm^2 (for silicon).

To prepare the optical fiber for attachment to the sensing element, the single-mode optical fiber with 125 micron diameter cladding was first etched in Buffer Oxide Etch (BOE) solution at room temperature. The BOE solution contains a mixture of HF and NH4F at a ratio of 6:1. A length of about 1.5 *cm* of the tip of the fiber was dipped into the BOE solution in a plastic container, since HF reacts with glass and the BOE solution is corrosive. The etching rate was found to be around 15 microns per hour. With an initial diameter of about 125 μm and a target diameter of 60 μm, the etching time is estimated to be $(125-60)/15 \approx 4.3$ hours.

Once the desired diameter of the fiber is obtained after etching, the next step is to properly place the etched fiber onto the deflection beam of the sensor. A suitable placement of the etched fiber is shown in Figure 5.3. The top view in Figure 5.3(b) shows that

the etched fiber is located at the center of the deflection beam. This ensures that, when a force acting on the etched fiber is perpendicular to the direction of beam deflection, the beam will bend but not twist. The relatively short fiber extension, as shown in the side view in Figure 5.3(a), ensures that the fiber probe is sufficiently stiff to transfer measured force to the sensor.

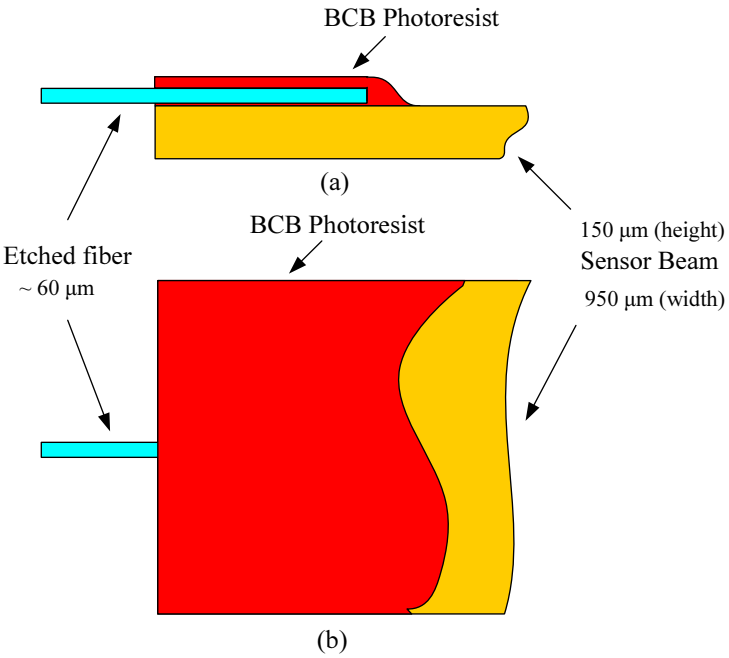

Figure 5.3: Schematic diagram of integrated probe sensor. Bonding a 60 μm etched optical fiber to the center of deflection beam of piezoresistive sensor: (a) side view; (b) top view.

After a proper placement for the fiber is decided, the next step is to bond the fiber to the sensor beam. For the type of materials involved, an appropriate means for bonding is to use a photoresist to glue the fiber directly onto the beam. The reason to use photoresist as adhesive is because it exhibits good adhesiveness and is in liquid form at room temperature. Thus even the photoresist is already applied to the etched fiber and sensor beam, the position of the etched fiber can still be adjusted before firmly set at a higher

temperature. In selecting a suitable photoresist among different types available, the one having a strong adhesiveness, light weight, and ease of application is preferred. Three candidate photoresists, i.e., AZ, DUV and BCB, were evaluated for their effectiveness in bonding the fiber to the beam. To subject the bonding to a threshold load, the tips of the bonded fibers with different photoresists were moved against a weight balance respectively. The bonding section between fiber and beam was then inspected for any sign of fracture. Results of such tests showed that AZ and DUV photoresist were not strong enough to fix the etched fiber to the sensor beam, while BCB photoresist proved effective, but required the glued part with BCB to be dried in an oven at 150°C for one hour. Figure 5.4 is a photograph showing the side view (a) and the top view (b) of an etched fiber bonded to the sensor beam by BCB photoresist.

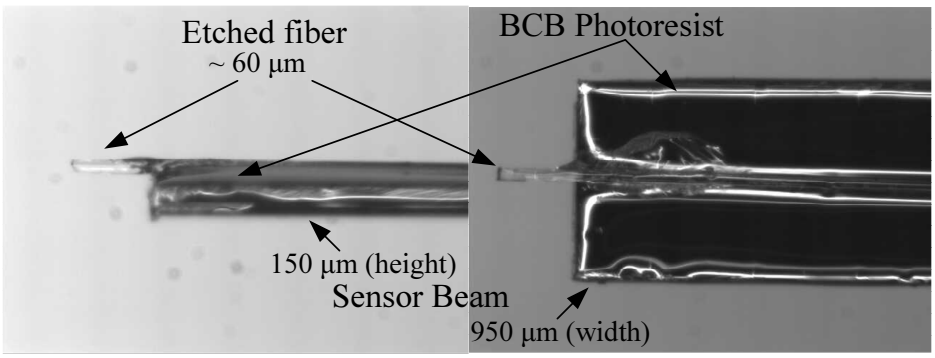

Figure 5.4: Photograph of integrated probe sensor: (a) side view; (b) top view.

5.3.3 Modelling

According to the elastic bending theory, the deflection of the cantilever beam is linear to the force perpendicularly acting on the beam. This relationship can be modelled

analytically. Such an analytical model is useful, as it can be used to determine the theoretical value of critical force that needs to be observed when using the sensor. This critical force arises due the fact that loading condition of the tip of the beam will be more severe with an integrated fiber extension than without. To prevent overloading (and thus causing damage to) the sensor requires careful analysis of the maximum allowable force at the tip of the sensor beam.

When a force is applied directly to the tip of the beam of the core sensor, the deflection of the beam (denoted by d_s) can be expressed as:

$$d_s = \frac{F_t l^3}{3EI} \tag{5.1}$$

where F_t is the force applied at the sensor tip, $l = 4\ mm$ is the active length of the beam, E is the modulus of elasticity of the beam (made of silicon), and I is the moment of inertia of the beam cross section. When the maximum allowed load of 120 mN is applied to the tip of the beam, the corresponding full-scale deflection at the tip of the beam is calculated to be 59.9 μm. This establishes the maximum deflection range of the sensor without the fiber extension. When the etched fiber is fixed to the sensor beam, the maximum deflection of the beam tip is greater than that for the case when the maximum load is applied to the beam alone. The deflection of the beam tip in this case (denoted by d_f) is the result of the force F_t and a moment $M = F_t l_1$, where l_1 is the length of the fiber extension (i.e., excluding the part of the fiber that is bonded to the beam). It can be

modelled:

$$EI\frac{d^2y}{dx^2} = M + F_t x; \tag{5.2}$$

Let $x = l$, $y = 0$, $\frac{dy}{dx} = 0$;

$$EIy = \frac{Mx^2}{2} + F_t\frac{x^3}{6} - (Ml + \frac{F_t l^2}{2}x) + (\frac{Ml^2}{2} + \frac{F_t l^3}{3}); \tag{5.3}$$

For $x = 0$,

$$y = \frac{1}{EI}(\frac{Ml^2}{2} + \frac{F_t l^3}{3}) \tag{5.4}$$

Since $M = F_t l_1$

$$d_f = \frac{F_t l^2}{6EI}\left(3l_1 + 2l\right). \tag{5.5}$$

For a fiber extension of $l_1 = 0.5$ *mm*, the correlation between d_f and d_s, denoted by k, is:

$$k = \frac{d_f}{d_s} = \left(1 + \frac{3l_1}{2l}\right) = 1.1875\,. \tag{5.6}$$

Equation (5.3) indicates that if a force is applied at the tip of the etched fiber, the tip of the sensor beam will deflect more (by a factor of 1.1875, in fact) than it does when the same force is applied to the tip of the sensor beam directly. In order to ensure that the deflection of the sensor beam stays within its limit so as to prevent the beam

from breaking, the maximum allowed load at the tip of the etched fiber needs to be reduced by a factor of 1.1875 to 101.1 mN. The above theoretical analysis was verified by an ANSYS simulation. Figure 5.5 shows the simulation results. In the figure, line 1 represents the beam deflection when a 120 mN force is applied at the tip of sensor beam; the deflection of the tip is 59.9 μm. Line 2 represents beam deflection when a force of the same magnitude is applied at the tip of the etched fiber. In this case, the deflection of the beam tip increases to 71.1 μm, which clearly exceeds the limit. Line 3 shows the deflection of the beam when the load is reduced to 101 mN; the deflection of the beam tip restores to 59.8 μm. In lines 2 and 3, the deflections corresponding to the length between 4 and 4.5 mm are that of the etched fiber. Under a load of 101 mN, the deflection of the tip of the integrated probe is 78 μm.

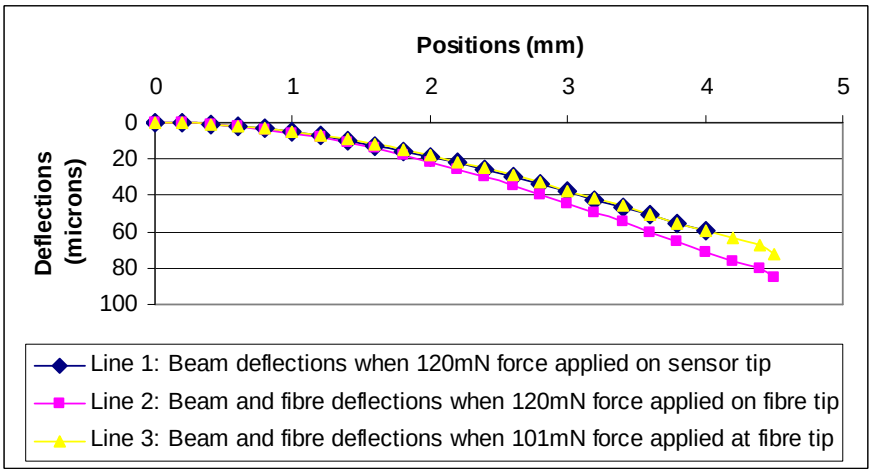

Figure 5.5: Simulated deflection of beam tip under different loading conditions.

5.3.4 Calibration

Calibration is usually necessary before proper application of a micro-force sensor. Calibration is a process for establishing the relationship between the output signal of the force sensor and a standard load. In this process, a known force is applied to the sensor, which produces a corresponding output signal (this signal is said to equate the known load. With a number of known forces that approximate the load range of the force sensor, a linear interpolation between the output signal of the sensor and the actual force can be obtained.

The integrated probe sensor was calibrated by moving the tip of the probe against an Ohaus Scout ® digital balance (model number 506-362, with a full scale of 200 g and an accuracy of 0.01 g). At each given load, the reading of the digital balance was plotted against the reading of the sensor output, which was generated as follows. As the load caused the sensor beam to deflect, the deflection led to a small difference in resistance between the two resistors on the opposite sides of the beam. This difference was detected by a whetstone bridge. The bridge excitation voltage was set to 6 V. The output signal of the bridge was acquired by a 16-bit PCI-6025E data acquisition card (DAQ) made by National Instruments. Figure 5.6 shows the results of three calibration trials. Through linear fitting, the sensitivity of the integrated probe sensor was estimated to be 0.7964 mV/mN with a standard deviation of .0027. The results also show good linearity of the sensor (with non-linearity being under 0.3%). In the calibration, the maximum load was set to 50 mN. This was done intentionally for the purpose of reducing the chance of damaging the etched fiber tip. Thus the maximum allowed deflection

of the integrated probe was estimated to be 39 μm. Since the output of the sensor is analogue, its resolution strongly depends on the noise level of amplifier and the bridge configuration of the sensor. With our current bridge configuration (half-bridge without temperature compensation), the detection limit of our sensor is 1 mN.

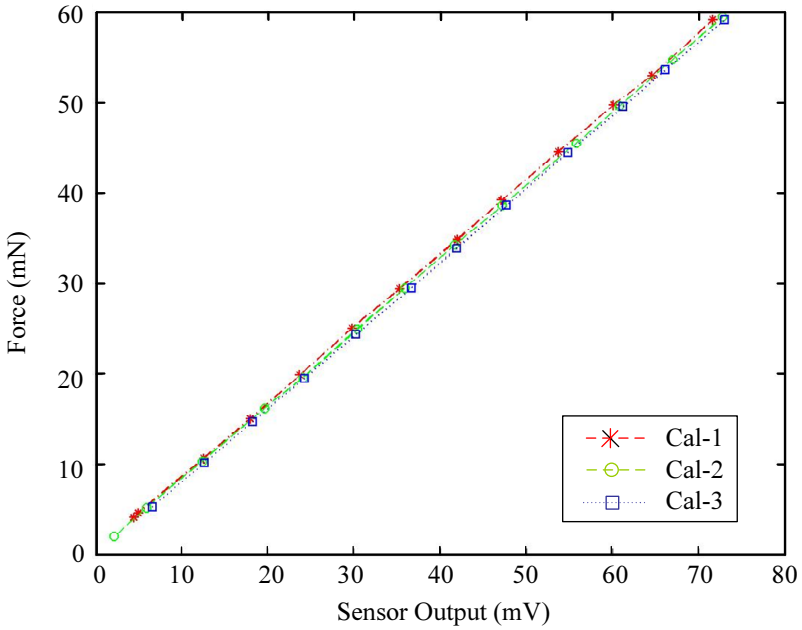

Figure 5.6: Results of calibration under static loads.

5.4 Experiment Setup and Results

We demonstrated the micro-force sensing method in an experiment on a prototype laboratory photonic alignment system. The objective of the experiment is to find the center of the insertion hole on the surface of an optical device.

5.4.1 Experiment Setup

The insertion hole is designed for the pigtailing of optical fiber. We used an optical ferrule to simulate this situation. The optical ferrule has two sides. One side has a chamfer to guide the insertion of fiber, and the other side has a polished facet. There is a hole on the center of the polished facet. The inserted fiber can come out from this hole. In the experiment, we attempted to pigtail the fiber from the polished side. One single-mode fiber was inserted from the chamfer side and the other end of the fiber was connected to a light source. Thus the optical ferrule simulated an optical device with an optical path in its center axis. It can be inferred that this optical path passes through the center of the insertion hole: If the center of the insertion hole is exactly located, then the optical path of the device is found.

The experiment was implemented on a photonic alignment system. The system was composed of a modified piezoresistive force sensor, an optical ferrule, two sets of high precision stages and an imaging unit. All the instruments were mounted on a vibration isolation table. Figure 5.7 shows the overall view and a close view of the photonic alignment system.

The modified piezoresistive micro-force sensor, fixed to a specifically designed force sensor holder, was mounted on a three degrees-of-freedom (DOF) high precision stage. The stage has a travel range of 4 *mm* in each of the X, Y, and Z axis with a step resolution of 25 *nm*. The optical ferrule was mounted on a 6-DOF high precision stage. The travel range of XYZ axis is 4 *mm* with a step resolution of 37.5 *nm* in the X and Y axis, and

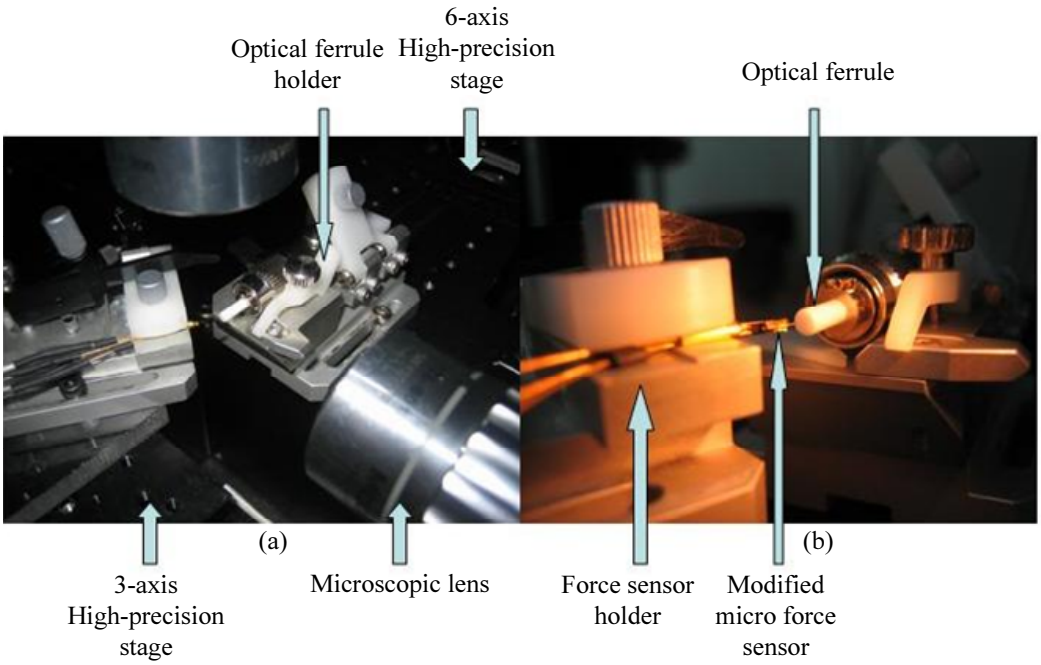

Figure 5.7: The photonic alignment system: (a) distant view, (b) close view.

25 *nm* in the Z axis. The rotation range of θ_x, θ_y, and θ_z is 6 degrees with a resolution of 25 seconds. The imaging unit included two set of microscopes with CCD cameras. The CCD camera has a high resolution of 1300(h)$\times$1030(v) pixels. Based on current setup of microscopic lens and camera, the resolution of each pixel was around 2.08 μm. The two cameras were set perpendicular to each other to monitor the photonic alignment process.

5.4.2 Verifying Repeatability

To ensure accuracy of subsequent experiments, the following procedure was first performed using the experiment setup to verify the repeatability of the system. In this procedure, the sensor beam was fixed at an angle of α to the Y axis (in x-y plane) of the

3-DOF stage, as illustrated in Figure 5.8. The optical ferrule facet was adjusted to be parallel to the *Y* axis of the 6-DOF stage. By setting the *Y* axis of the 3-DOF stage and the *Y* axis of the 6-DOF stage to be parallel, the internal angle between the sensor beam and the optical ferrule facet would also be α. With the help of the side camera, the tip of the sensor and the center of the optical ferrule facet were closely aligned with the *Z* axis. The initial position of the sensor tip was then set at the right edge of the ferrule facet in the *Y* axis.

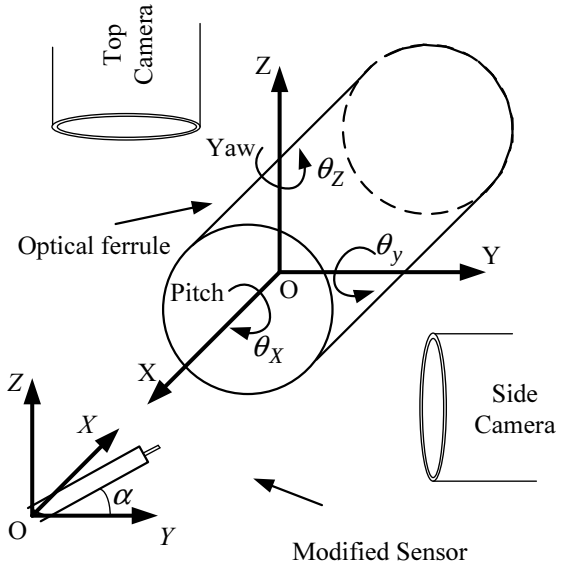

Figure 5.8: Illustration of experiment procedure.

With the top camera providing visual feedback, the sensor was moved along the *X* axis until the sensor tip came into contact with the ferrule edge, as shown in Figure 5.9, upon which all axes of the 6-DOF stage were fixed, while the *Y* axis of the 3-DOF stage was moved automatically from right to left with a step size of 5 μm. The sensor tip thus swept the facet of optical ferrule and measured force response at each stopping point. The force signal was recorded by a DAQ card at 1 *kHz*. At each stop, 100 samples were

captured and their mean value was taken as the sensor output for that particular stop.

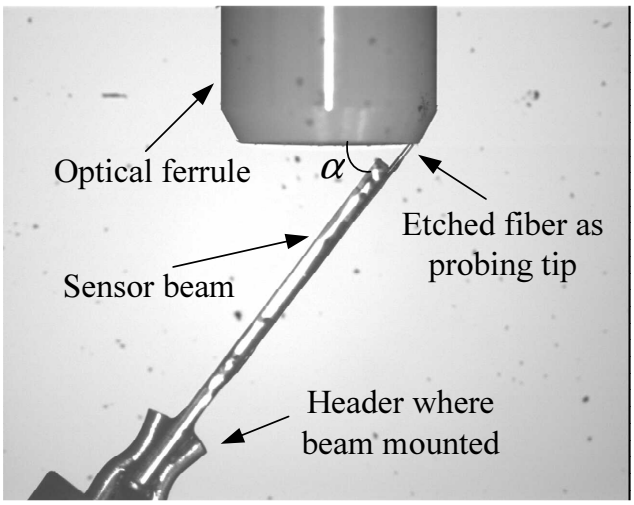

Figure 5.9: Top view of the modified sensor sweeping the surface of the optical ferrule.

Three trials were completed. In each trial, the sensor tip, starting from the exact same location, swept across the ferrule surface from right to left following the same randomly selected path. The output of the force sensor was then plotted against the moving step. Figure 5.10 shows the force-motion profiles of the ferrule facet obtained from these trials. These profiles unvaryingly indicate that the optical ferrule has a convex surface. It is noted that these force-motion profiles contain no discontinuity (which would indicate the existence of a hole on the ferrule surface). This is because the path that the sensor tip swept through in these trials was randomly selected and in this case did not happen to come across the center hole. What is significant is that, from the uniformity of these profiles, it can be concluded that the repeatability of the experiment setup is satisfactory.

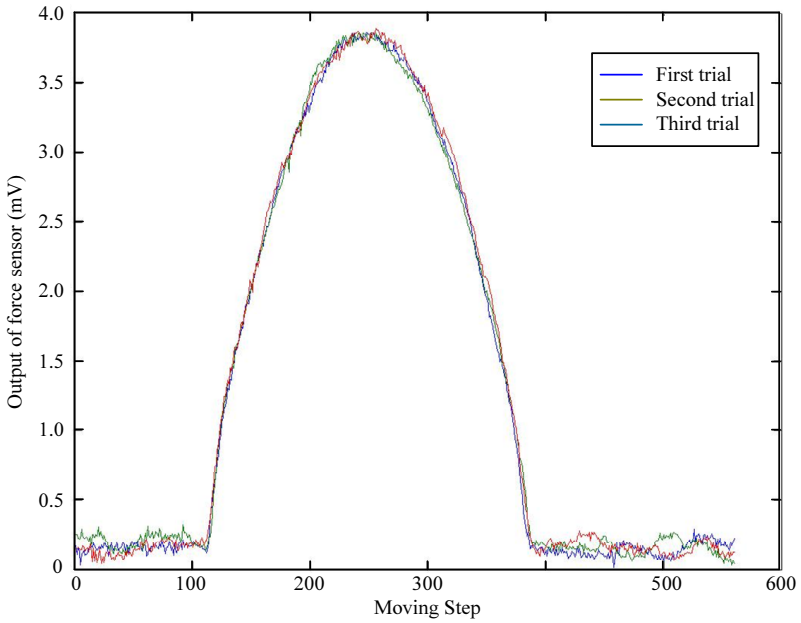

Figure 5.10: Output of the force sensor v. s. moving step.

5.4.3 Determining Optical Path

With the repeatability of the setup verified, the next experiment attempts to determine the optical path of a device by locating the insertion hole on the facet of an optical ferrule. In this experiment, the values of the X and Y coordinates of the starting position of the sensor tip were first fixed. The value of the Z coordinate was allowed to vary with a step size of 50 μm. With an approximate guide from side camera, in less than 5 trials (each trial around one minute), a gap was found on the ferrule surface by the appearance of an obvious discontinuity on the force-motion profile of the device, as shown in Figure 5.11.

However, as is indicated in Figure 5.11, the gap was shown to be off-center on the optical ferrule surface. From the known specifications of the optical ferrule, the maximum deviation of the hole to the center of the optical ferrule is 1.5 μm. This apparent incon-

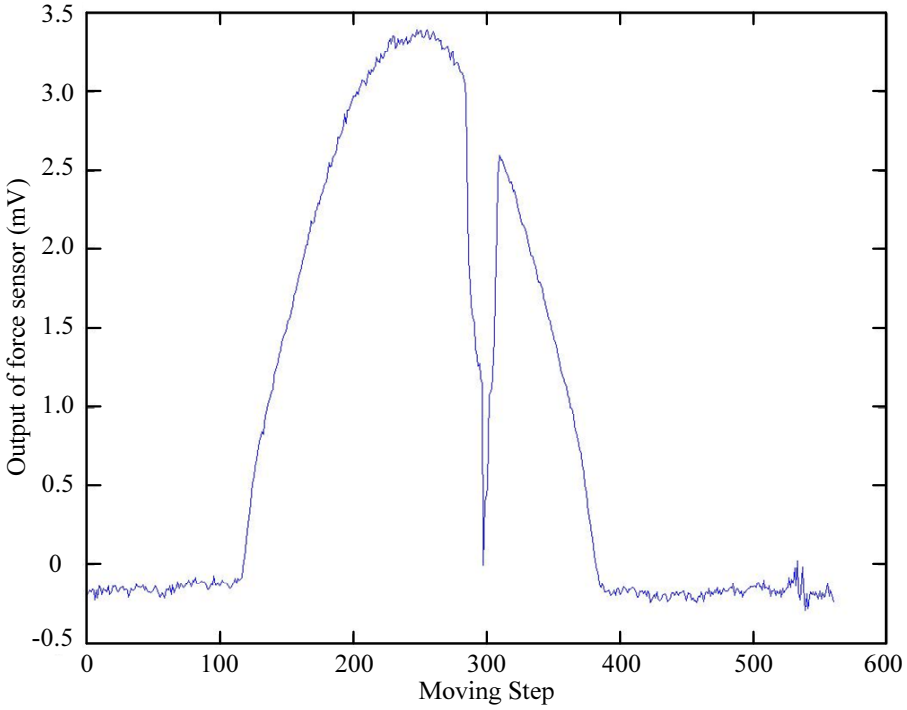

Figure 5.11: Deviation of detected hole position.

sistency between the experimental result and the specification was explained by the fact (later discovered) that the Y axis of the 3-DOF stage and the Y axis of the 6-DOF stage were not actually parallel. By adjusting the yaw axis to eliminate an angle of 0.29° between the Y axis of the 3-DOF stage and the surface of the optical ferrule, the gap then appeared at the center of the force-motion profile, indicating the location of the hole, as shown by the curve with the label $Z = 0$ in Figure 5.12.

The discontinuities in the force-motion profiles (as shown in Figure 5.12) indicate the existence of the hole on the ferrule surface. As discussed earlier, the center of this hole is taken to be the optical path needed in fine alignment. The following experiment was conducted to locate this center. While keeping the values for the X and Y coordinates the same as in the case for $Z = 0$ (as described earlier), four other values (i.e., 50, 200,

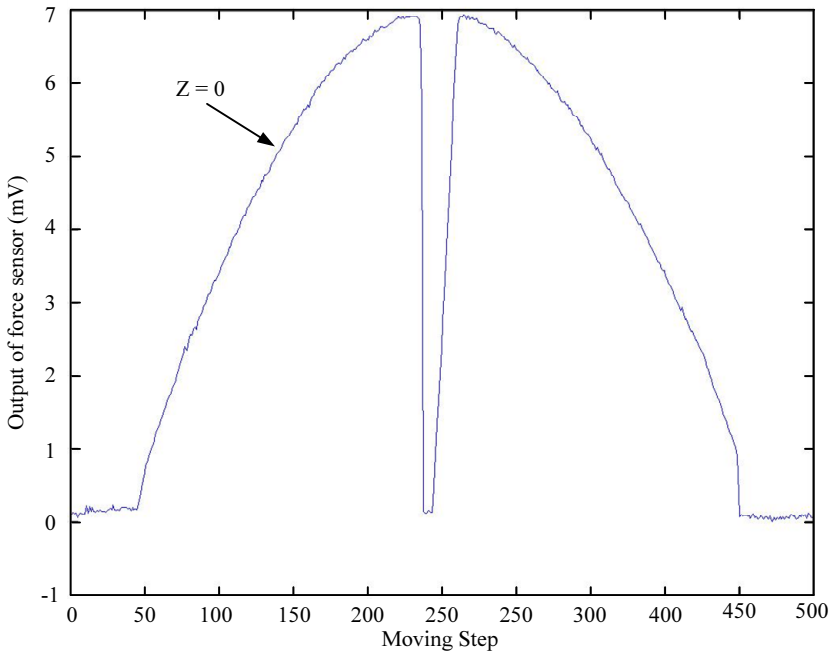

Figure 5.12: The correct hole position after adjustment.

380, and 530, all in μm) were randomly selected for the Z coordinate to form four initial points. Four sweeps of the ferrule facet were made following parallel paths starting from those four initial points. The force-motion profiles associated with these paths are as shown in Figure 5.13.

The fact that these five force-motion profiles as shown in Figure 5.13 are convex (ignoring the V-shape discontinuity in two of them for the moment) corresponds to the geometric shape of the ferrule facet. It can be seen that the value of the sensor output at the same motion-step decreases as the value of Z increases. This is because the larger the value of Z, the smaller the curvature of the arc that the sensor swept across, and consequently, the lesser the degree of bending experienced by the sensor tip.

Of the five profiles, the one corresponding to $Z = 0$ has the most convex curvature, and the sharpest discontinuity (as compared to the other profile, corresponding to $Z =$

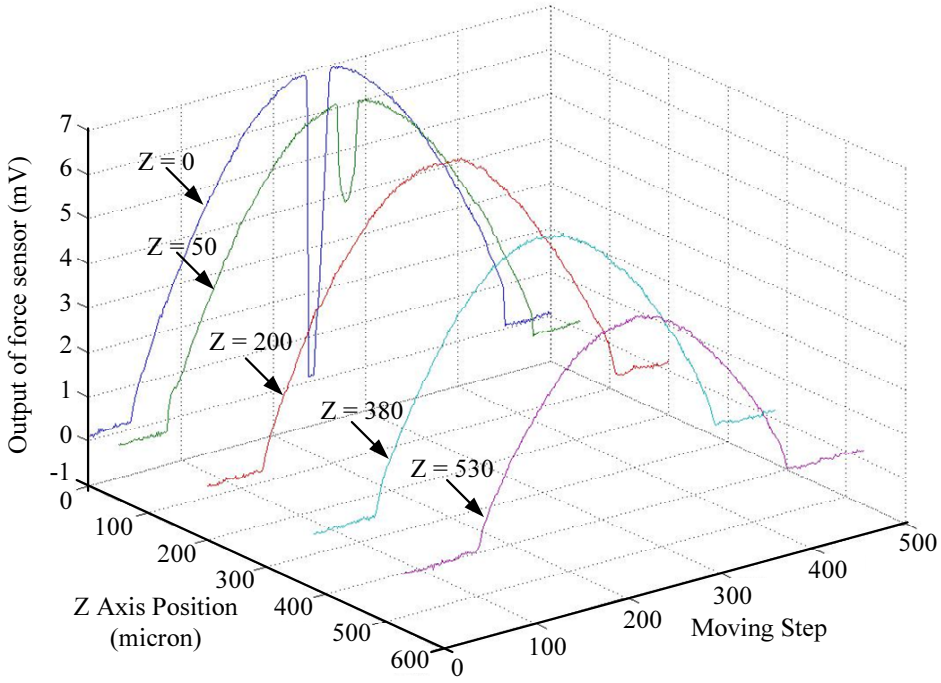

Figure 5.13: Five paths across the ferrule facet with different Z values.

50, that also contains a discontinuity). Since the sweeping path defined with $Z = 0$ is supposed to be a diametral arc on the ferrule facet, it is expected that the hole be found at the mid-point of this arc. This is supported by the $Z = 0$ force-motion profile. As shown in Figure 5.13, at the discontinuity the sensor output declined drastically from 7 mV to almost 0 mV, indicating that the sensor tip dropped into the hole. Since the interval during which the sensor output remained near 0 mV lasted for 7 steps (with a step size of 5 μm), it can be determined that the sensor tip lost contact with the inside wall of the insertion hole for a distance of 35 μm. Noting that the difference in the diameters of the sensor tip and the insertion hole is about 60 μm, it is reasonable to infer that the mid-point of the arc defined with $Z = 0$ is very close to the center of the insertion hole on the ferrule surface. This is in contrast to the case where $Z = 50$, in which the sensor tip also appeared to sweep across (part of) the hole. As indicated in Figure 5.13, at the

edge of the insertion hole, the output of the sensor only declined from 6.5 mV to 4.3 mV. This offers evidence that the sensor tip was still in contact with the inside wall of insertion hole as it swept across the hole.

To locate the center of the insertion hole more accurately, the data associated with the V-shape discontinuity in the $Z = 0$ force-motion profile were further analyzed. Figure 5.14 shows a magnified segment of the V-shape discontinuity. Starting from point *a*, the output signal of force sensor declined drastically, indicating that the tip had began to drop (from one side) into the insertion hole of the optical ferrule surface. The sensor tip lost contact starting from point *b*, and regained contact at point *c*. At point *d* the sensor tip had emerged from the insertion hole. The asymmetry between the segments *ab* and *cd* was due to the fact that the sensor beam was fixed at an angle α (as explained earlier in Section 3.2) to the optical ferrule facet. There are 26 data points between *a* and *d* (including these two end points), encompassing a total of 25 steps. The diameter of the hole was thus evaluated to be $25 \times 5 = 125\ \mu m$, with the center of the hole estimated to be between point *e* (the 13^{th} point) and point f (14^{th} point).

5.5 Summary and Discussion

In this chapter, we have reviewed existing methods of coarse alignment in active fiber pigtailing, and showed that the limitations of light intensity signal used in the traditional methods can be overcome by a novel approach of micro-force sensing. We have illustrated that the micro-force signal provides useful clues in guiding the fiber to rapidly

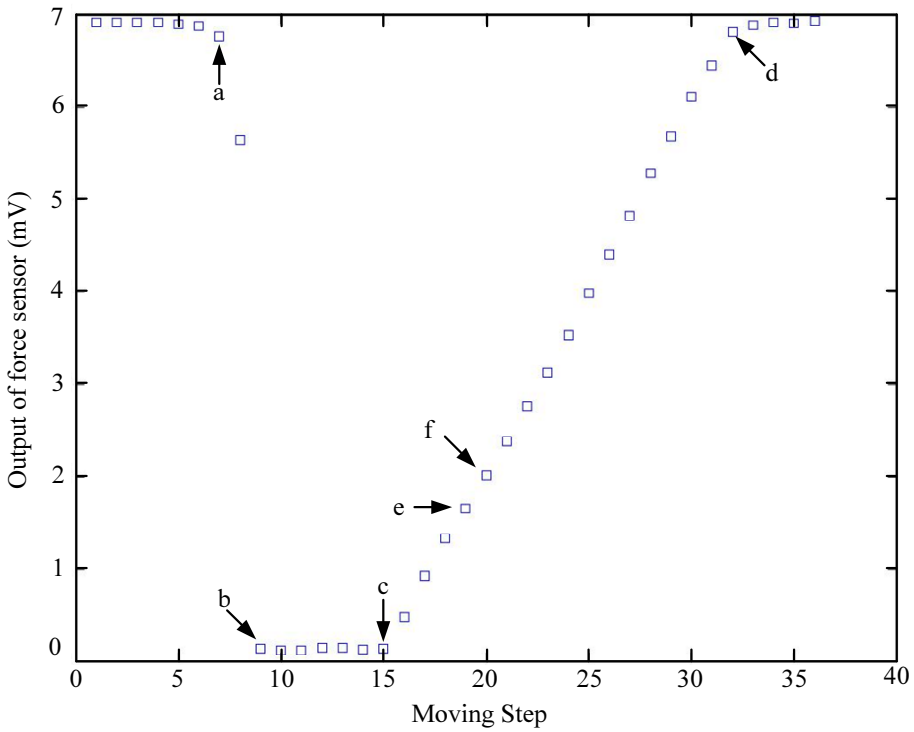

Figure 5.14: Force-motion profile between steps 230 and 265.

locate the actual optical path of the optical device (with specific geometry feature on its input surface), and demonstrated the effectiveness of this approach on a photonic alignment system. Using an improved piezoresistive force sensor to characterize the surface feature of an optical ferrule on a micron scale, the actual optical path of the ferrule had been located accurately and efficiently. These results affirm that micro-force sensing can be an effective technique in augmenting conventional approaches for fast and accurate fiber pigtailing in photonic assembly.

To fully utilize this approach, two issues need to be resolved. The first issue concerns the search along the Z axis for the path that passes through the center of the insertion hole. In the experiments described in Section 3, the search along the Z axis was not optimized. This is because the force sensor used in the experiment can detect force with

only one degree of freedom. When a 2-D force sensor is developed for this type of pigtailing applications in the future, the surface characteristics, obtained through such more sophisticated sensors, will provide better information for the alignment process to locate the actual optical path more efficiently.

The second issue concerns the smooth switch to fine alignment from coarse alignment. Once the optical path is determined after coarse alignment, the optical fiber to be pigtailed needs to be moved to this position. In an ideal situation, the tip of the fiber should take up the position of the sensor tip. This can be realized by mounting both the optical fiber and the micro-force sensor on a fixture actuated by a 3-DOF stage. By properly calibrating the position of the tip of the fiber and that of the sensor, such smooth switching to fine alignment can be achieved.

Chapter 6

Experiment II: A Micro-injection System for Automation of the Embryos Injection Process

This chapter presents an experiment to use micro-force sensing and control to automate the zebrafish embryos injection. A prototype micromanipulation system is developed for automatic batch microinjection in biological science. It demonstrates the use of micro-force as a feedback in force augmented position control. When augmented by force feedback, the manual microinjection is automated.

6.1 Background

The microinjection is a common technique in genetic engineering for transferring genetic material into a cell [98]. It is normally performed on a micromanipulation system that usually consists of an inverted microscope, a micromanipulator, a micropipette and an injector. Manual microinjection is a conventional and widespread practice in biological research. For example, in the injection of zebrafish embryos, a human operator first identifies (through an inverted microscope) the embryos in a petri dish, and then guides the tip of the micropipette slowly towards the embryo. When the tip of the micropipette slightly touches the chorion of the embryo, the operator will manually drive the micromanipulator to produce a quick thrust movement, resulting in an initial penetration of the chorion by the micropipette, which is fixed on the micromanipulator. Upon this initial penetration, the operator will continue driving the micromanipulator until the tip of the micropipette enters the yolk of the embryo. At that point, genetic material can be injected into the embryo through the injector.

In such a manual microinjection process, the skill and experience of the operator play a crucial role in achieving a successful injection. It usually takes several months of training and practice for an operator to become proficient in performing such a task. However, even for an experienced operator, the success rate of such manual microinjection may still be very low. This is mainly due to the fact that to execute various steps in a manual microinjection requires fine control of both position and force, which is difficult for a human operator to accomplish consistently.

Achieving successful penetration in a microinjection involves three key factors: a proper injection point, sufficiently high penetration speed, and an appropriate penetration trajectory. Ideally, the micropipette should start penetration at the center of the embryo; otherwise the micropipette may risk either slipping on the surface of the chorion without penetrating it, or missing the yolk after penetrating the chorion. A high speed of penetration enables the micropipette to quickly pierce the chorion without causing excessive deformation to the embryo. Lastly, an appropriate penetration trajectory will reduce the time required to complete an injection. This is especially important for situations where a large number of embryos are to be injected. For an human operator, it is very difficult to consistently deal with the last two factors effectively in a manual microinjection. Another reason for the low success rate of manual microinjection is that in general manual manipulation has poor repeatability. In a research laboratory, for instance, it is not uncommon to require more than a hundred embryos be injected one after another in quick succession. The repetitive maneuvers associated with such a high throughput microinjection process inevitably cause fatigues in the human operator, and so may easily lead to a low success rate. Automating these maneuvers is a desirable means of improving success rate for batch microinjection.

Few studies on the research and development of micromanipulation systems for microinjection have been reported in the literature. These works mainly focus on two issues. The first concerns the incorporation of a haptic device into the micromanipulation system to enable the operator to feel the penetration force so that the operator can achieve better control over the microinjection process [111] [112] [113]. The second is-

sue concerns the measurement of penetration force associated with some specific types of cells (such as zebrafish embryo and mouse oocyte) for the purpose of characterizing the cells' mechanical properties [52] [114]. In the works that deal with these issues, the micromanipulation system is aimed only for single-cell operation, where a cell is held in place by a holding pipette for manipulation. Obviously, such a system is not suitable for batch microinjection. Moreover, the measured penetration force is not utilized to automate the microinjection process. Although information obtained by machine vision information can be used to control the penetration process [115] [116], it is usually less effective compared to force information because the direct force information usually reflects the changes in the physical behavior of the cell (such as deformation or extent of penetration) more quickly and accurately.

6.2 Design and Implementation

To achieve batch microinjection of zebrafish embryos, the micromanipulation system is designed to handle multiple embryos without holding them separately. This is achieved by using parallel V-grooves (made on the gel in a petri dish) to array and hold the embryos in multiple rows. The petri dish is mounted on a tilted holder, as illustrated in Figure 6.1. This setup ensures that the embryos will not be dislodged from their prearranged location in the V-groove when in contact with the micropipette during injection.

The holder is mounted on a high-precision motion stage, which can be maneuvered so that at the start of the automatic microinjection process the left end of the top row of the

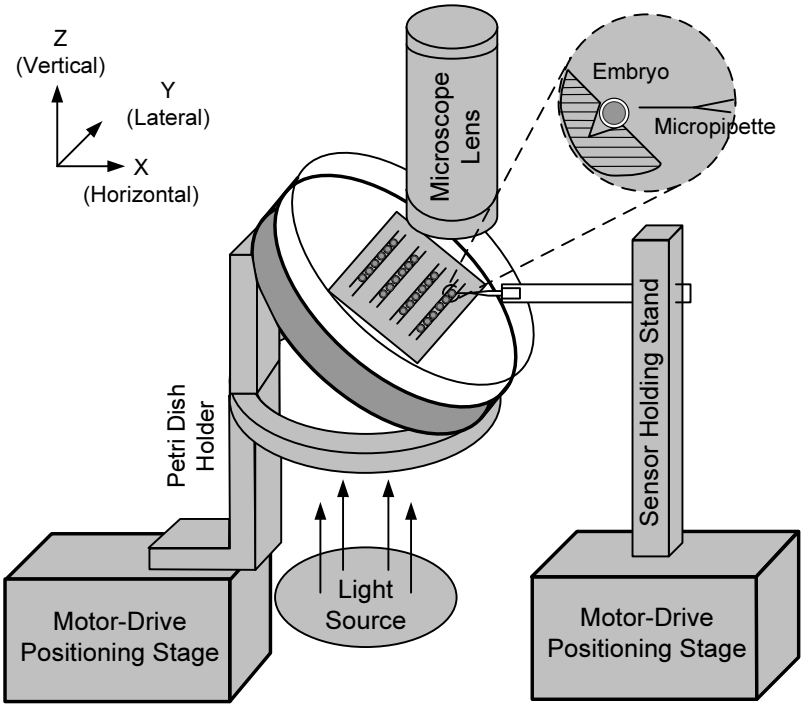

Figure 6.1: Schematic illustration of the batch microinjection system.

arrayed embryos can be focused by the microscope. Another positioning stage is used to move the micropipette. When the tip of the micropipette and the viewable embryos appear together in the local view of the microscope, their images are captured by a CCD camera. A machine vision algorithm then determines the number of embryos and marks the centerline of each embryo and the centerline of the micropipette. The micropipette is moved laterally to align itself with the centerline of the first embryo in a row, at which point penetration starts with the micropipette moving horizontally towards and then into the embryo at constant speed. A piezoresistive micro-force sensor measures the penetration force, which is then used by a force controller to decide whether the chorion layer is penetrated, the extent of penetration, and when to stop the micropipette. Upon successful penetration and injection, the micropipette retracts and moves to the next embryo and performs the penetration and injection again. This procedure is repeated

with the entire batch of embryos are processed.

The three main issues in the development of in this micromanipulation system are: position detection of zebrafish embryo and micropipette, development of piezoresistive micro-force sensor, and synthesis of force control strategy.

6.2.1 Position Detection of Zebrafish Embryo and Micropipette

Zebrafish embryos have a universal diameter of about 1 *mm*, with the yolk (which appears opaque) located at the center of the embryo and surrounded by a transparent membrane (i.e., the chorion). The yolk is a prominent feature of an embryo, and can be easily identified by machine vision.

The normalized two-dimensional cross-correlation algorithm is used to identify the yolk of an embryo. This algorithm computes the normalized cross-correlation of two matrices: a "template" matrix and a "graph" matrix. The result is another matrix containing the correlation coefficients whose values may range from -1 to 1.0. The graph matrix is orderly segmented to small parts, which are the same size as the template matrix. If the parts totally match the template, the correlation coefficient is 1. In general, the larger the value of these coefficients, the more likely the template appears in the graph. In the identification of the zebrafish embryo, the isolated yolk of the embryo is selected as the template (as shown in Figure 6.2(a)), while the image taken by the CCD camera is used as the graph. The corresponding cross-correlation is used to calculate all possible positions of the yolks in the image. The same method is applied to locate the possible

positions of the micropipette, whose template is as shown in Figure 6.2(b).

(a) (b)

Figure 6.2: Template of (a) zebrafish yolk and (b) micropipette.

The possible positions of the yolks thus calculated are grouped and averaged. The number of yolks in the image is then determined and the centerline of each yolk is marked. As an example, Figure 6.3 shows the centerline (labelled with EP1, EP2 and EP3) of three embryos identified by the vision algorithm. These lines define the lateral (with respect to the tilted petri dish) starting position of each injection. The centerline of the micropipette is also determined and marked, as indicated by the label MP in Figure 6.3.

To start penetration, the centerline of the micropipette must first be aligned with the centerline of an embryo. This involves moving the micropipette laterally by a certain distance. Since the distance information extracted from the image is measured in pixels, the following procedure is applied to calibrate the visual distance measured in pixels to the actual distance measured in microns. Taking the current lateral position of the micropipette as the baseline for reference, the micropipette is moved by the motor-driven positioning stage laterally by a known distance. The image showing the new lateral position of the micropipette is then recorded, and the visual distance corresponding to the completed motion is determined. By multiplying the visual distance between MP and

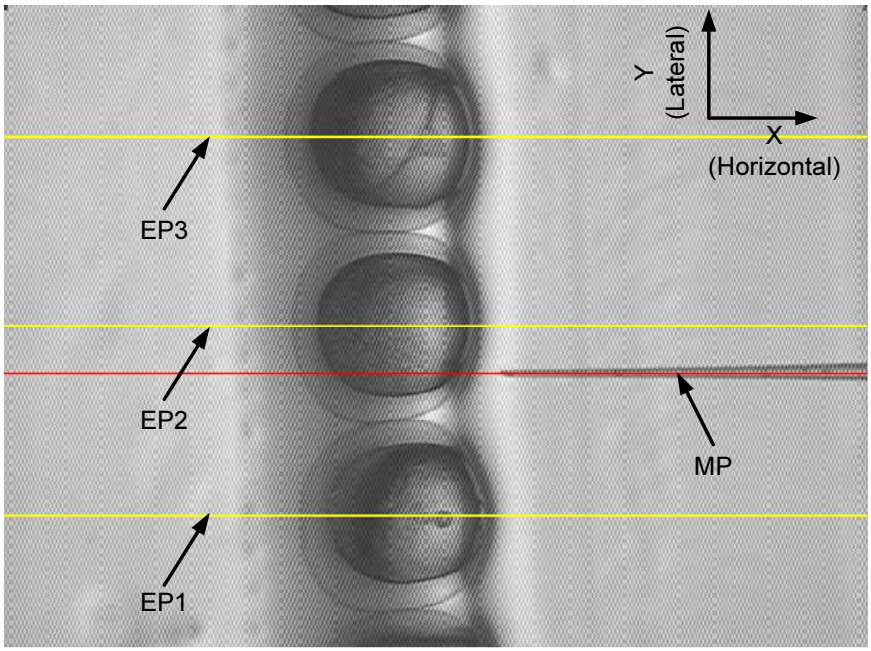

Figure 6.3: Centerlines of zebrafish embryos and micropipette.

EP1 (for instance) with the ratio between the actual known distance and the corresponding visual distance, the desired actual distance by which the micropipette must be moved in order to be aligned with the embryo at the bottom can be determined. Since the row of the injected zebrafish embryos are perpendicular to the micropipette, the horizontal starting position of the micropipette tip is same for all the injection of the embryos in the same row. The value of the horizontal starting position of the micropipette tip can be arbitrarily set as long as the alignment between the micropipette and the embryo is maintained.

Once aligned with the centerline of the embryo, the micropipette is moved along the centerline of (and towards) the embryo at a constant speed to a point where the tip is several hundred microns away from the chorion of the embryo. The actual penetration process can now be started, with the penetration force being measured to monitor the

penetration process.

6.2.2 Development of Piezoresistive Micro-force Sensor

The force required to penetrate a zebrafish embryo has been found to be in the order of hundreds of micro-Newtons [111] [114]. To measure such a small force requires a sensor with a resolution in that order. Comparing to the piezoelectric and capacitive micro-force sensor, the piezoresistive force sensor has the advantage of providing accurate and stable force signal in a large measurement range. A piezoresistive force sensor has the property that its resistance changes under physical pressure or mechanical work. When a piezoresistive force sensor is strained or deflected, its internal resistance will change (and remain changed) until its original shape is restored. The change in resistance is measured by an electric circuit (e.g., a Wheatstone bridge). Since the output of the piezoresistive sensor is analogue (i.e., a voltage signal), its resolution strongly depends on the noise level of the amplifier and the bridge configuration of the sensor. The piezoresistive force sensor has been applied in AFM to measure the atomic force change which is at the nano-Newton level [117] [118].

Currently, there is no ready-made micropipette with a built-in piezoresistive micro-force sensor. A commercial one-axis piezoresistive micro-force sensor (Model AE801, SensorOne Technologies Corporation) was modified to be used in the micromanipulation system. This sensor has a deflection beam of the dimension $4mm \times 950\mu m \times 150\mu m$. Its modulus of elasticity is $1.6 \times 10^5\ N/mm^2$ and its spring constant at full length is 2000 N/m. The modification involved bonding a micropipette (with its tip suitably cut

for penetration) to the free end of the sensor beam along its centerline. Figure 6.4 shows a photo of the modified piezoresistive force sensor with a micropipette.

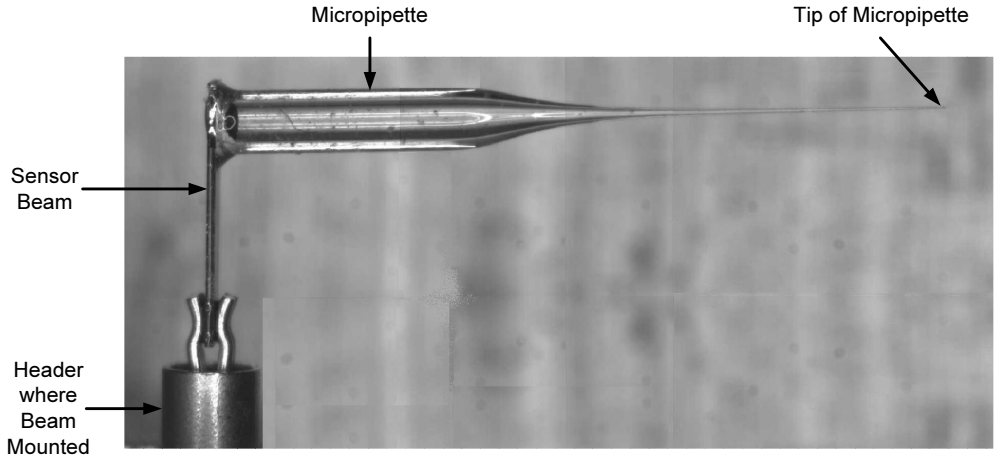

Figure 6.4: Side view of the modified piezoresistive micro-force sensor with the micropipette.

The force sensor was calibrated as follows. The force sensor was mounted on a piezoelectric positioning stage (Melles Griot, NanoMax HS 3-axis stage with piezoelectric drive with feedback) and moved in steps, with each increment of 20 *nm*, to press against a hard stationary surface. Taking the commonly applied approach of determining force based on a beam-deflection model (e.g., [66]), the resulting deflection of the beam was converted into a signal representing the force acting on the beam through the equation: $F = dEbh^3/4l^3$, where F is the force acting on the beam, E is the modulus of elasticity of the deflection beam, b, h, l are the width, height and active length of the beam, respectively, and d is the deflection of the beam due to F. This force signal was then plotted against the voltage reading from the sensor, which was measured by a high resolution dynamic strain-meter (Tokyo Sokki Kenkyuio Co. Ltd, TML DC-92D). Figure 6.5 shows the results of three calibration trials. Through linear fitting, the sensitivity

of the integrated probe sensor was estimated to be 1.865 mN/mV. The results also show good linearity of the sensor (with non-linearity estimated to be under 0.3%). The resolution of the modified micro-force sensor was calculated to be 40 μN.

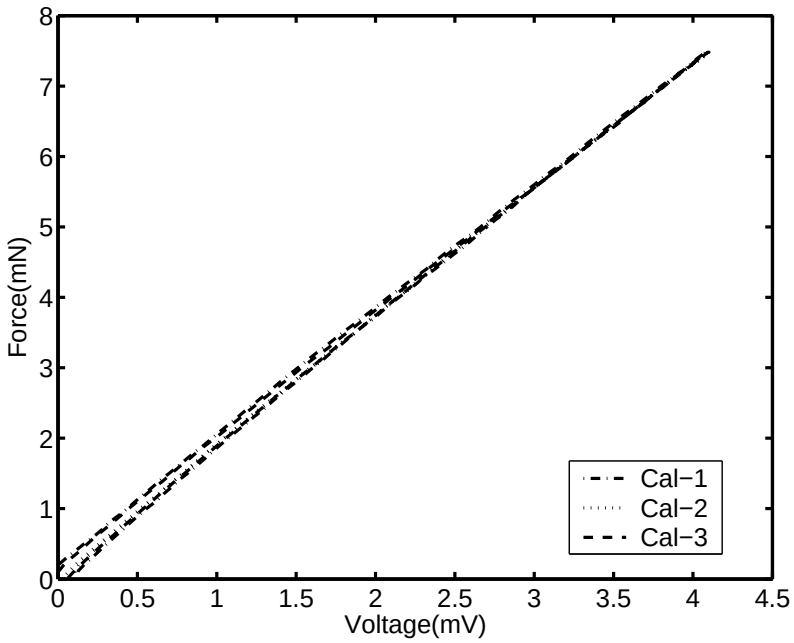

Figure 6.5: Calibration results of the micro-force sensor.

6.2.3 Force Augmented Position Control

There are several strategies to control the penetration process [99]. The simplest to implement is pure position control without any feedback. Suppose that the micropipette and an embryo has been properly aligned and that the distance *d* between the current position of the micropipette tip and the chorion of the embryo is known. Moving the micropipette directly towards the embryo by a distance much larger than *d* would normally result in the chorion being penetrated under excessive deformation. However, in this simple approach, there is no feedback during the process to indicate whether the

penetration is successful. For instance, sometimes the micropipette may just slip on the surface of the chorion and thus does not penetrate it. Although vision feedback may be implemented to monitor the penetration process, the practicality of such a vision-based method is hindered by the difficulty in identifying the tip of the micropipette correctly and quickly, because of the difficulty in determining whether the tip is inside or outside (but laying on the surface of) the transparent chorion, and the high computational load associated with real-time image processing.

The method of force augmented position control is proposed to overcome this difficulty. The measured penetration force is used to augment the position control strategy by dynamically determining the stopping point of the tip of the micropipette. This is done by exploiting the unique characteristics of the force signal in the penetration process. Figure 6.6(a)-(c) shows the sequential pictures of the penetration of the zebrafish embryo during a trial microinjection of a zebrafish embryo, while Figure 6.6(d) shows the force trajectory (with respect to time) of this penetration process. As shown in Figure 6.6(d), at point *a* the penetration force reached 1 *mN*, and then dropped drastically to below 0 *mN* at point *b*, indicating that the chorion was penetrated. As the micropipette continued its penetration of the embryo, the yolk was subsequently pierced, as indicated by the slight jump in the force between points *b* and *c*. The point at which penetration of the chorion occurs can be determined by detecting the sharp drop in the penetration force after its initial rise (e.g., between points *a* and *b* in Figure 6.6(d)).

The position of penetration can be obtained by analyzing the first-order and second-order derivatives of the penetration force with respect to time, as shown in Figures 6.7(a)

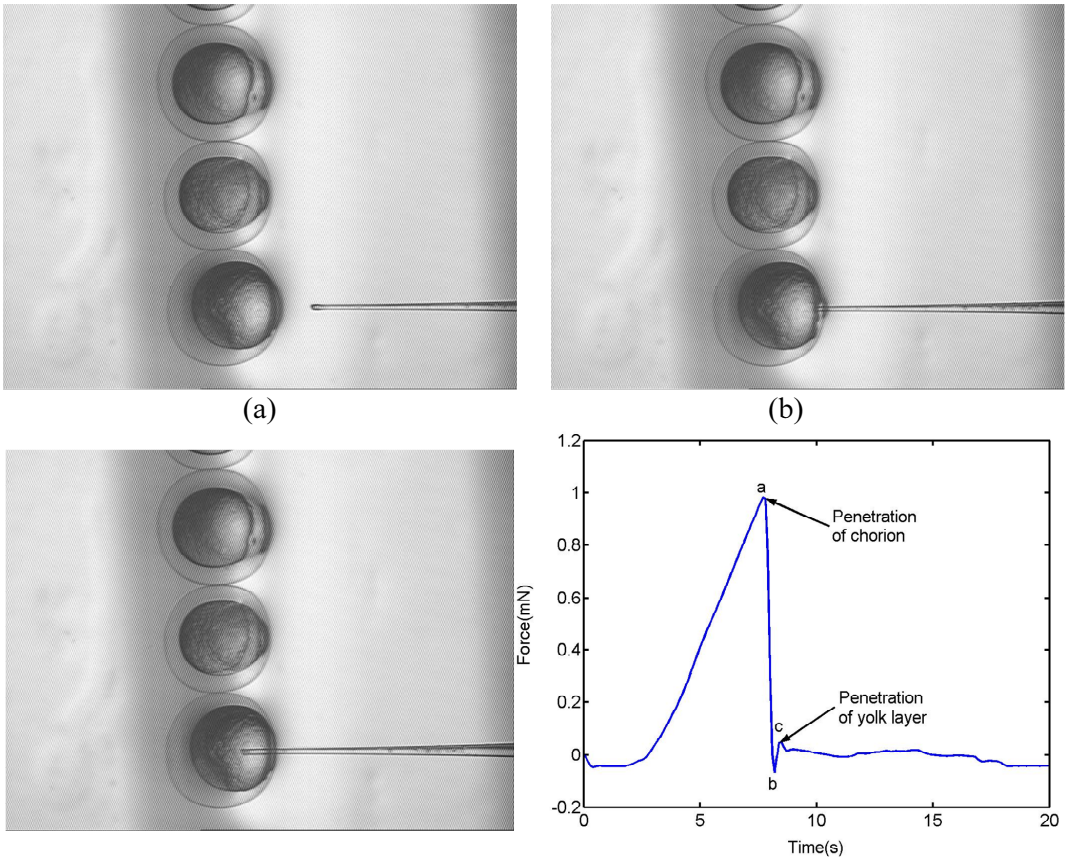

Figure 6.6: Penetration of zebrafish embryo (a) before contact (b) contact (c) penetration (d) force trajectories of the penetration process.

and 6.7(b), respectively. When the value of the first-order derivative is smaller than 0 (point *d*) and the value of the second-order derivative is larger than 0 (point *e*), the corresponding force is between point *a* and *b* shown in Figure 6.6(d). This brief interval (between *a* and *b*) indicates that the chorion is being penetrated, with *b* signifying the end of the penetration.

In the application of the method of force augmented position control, the position of the micropipette and penetration force are sampled in two different real-time processes, with the force sampled at a much higher frequency. The first-order and second-order

derivatives of the penetration force are computed in real-time. When their values meet the requirements, the force augmented position control will command the micropipette to stop. The stopping position should be inside the embryo, slightly further inward from the point of penetration.

It is usually not necessary to control the penetration of the yolk. With a sharp micropipette and a properly selected penetration point, the yolk will be penetrated subsequently as long as the micropipette continues its motion inwards for a few hundred microns upon penetrating the chorion. (This can also be determined more systematically by exploiting the slight jump in the force signal from *b* to *c* as shown in the force profile in Figure 6.6(d).) Upon penetrating the yolk, the micropipette is retracted quickly to extricate itself from the embryo.

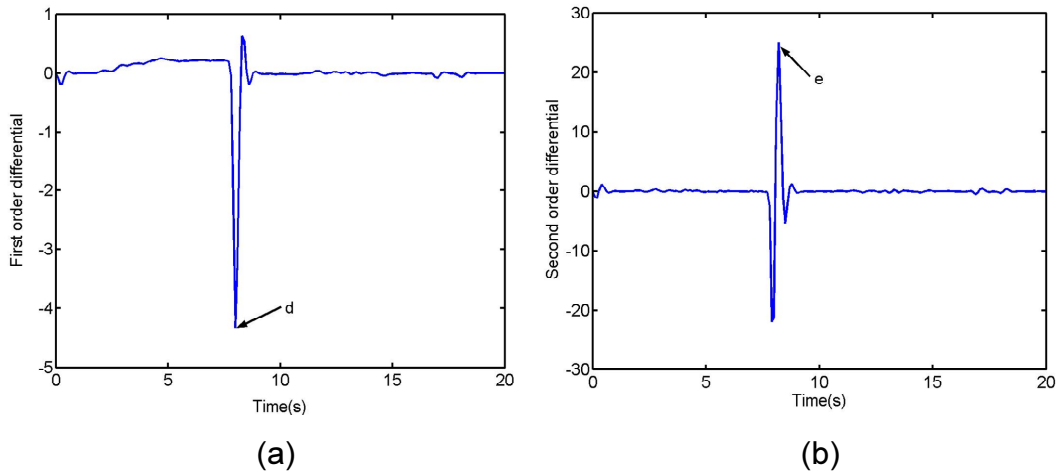

Figure 6.7: Derivative of penetration force (a) first order derivative (b) second order derivative.

6.3 Experiment Setup and results

To demonstrate the effectiveness of the proposed approach for batch microinjection with force feedback, an experiment involving the penetration of a group of zebrafish embryos using the prototype automatic micromanipulation system was designed and conducted. All the zebrafish embryos used in the experiment were collected in accordance with the standard embryos preparation procedures; they were at the state between four to six hours after fertilization.

6.3.1 Setup

The prototype micromanipulation system consists of a petri dish with a custom-design holder, a modified piezoresistive force sensor bonded to a micropipette, two sets of high-precision motion stages, an imaging unit and a dynamic strain-meter. All the instruments were mounted on a vibration isolation table. Figure 6.8 shows an overall view of this system.

The gel in the petri dish was made of 2% agarose. It was first dissolved by heating it in the water and then poured into the petri dish. To produce the desired pattern, a V-groove model was pressed on the gel surface, and removed after the gel has cooled down. The petri dish was mounted on a six degrees-of-freedom (DOF) high precision stage, which has a travel range of 4 mm in its X, Y, and Z axes, with a step resolution of 37.5 nm in the X and Y axes, and 25 nm in the Z axis, and a rotation range of 6 degrees with a resolution of 25 seconds in the θ_x, θ_y, and θ_z axes. The modified piezoresistive force sensor was

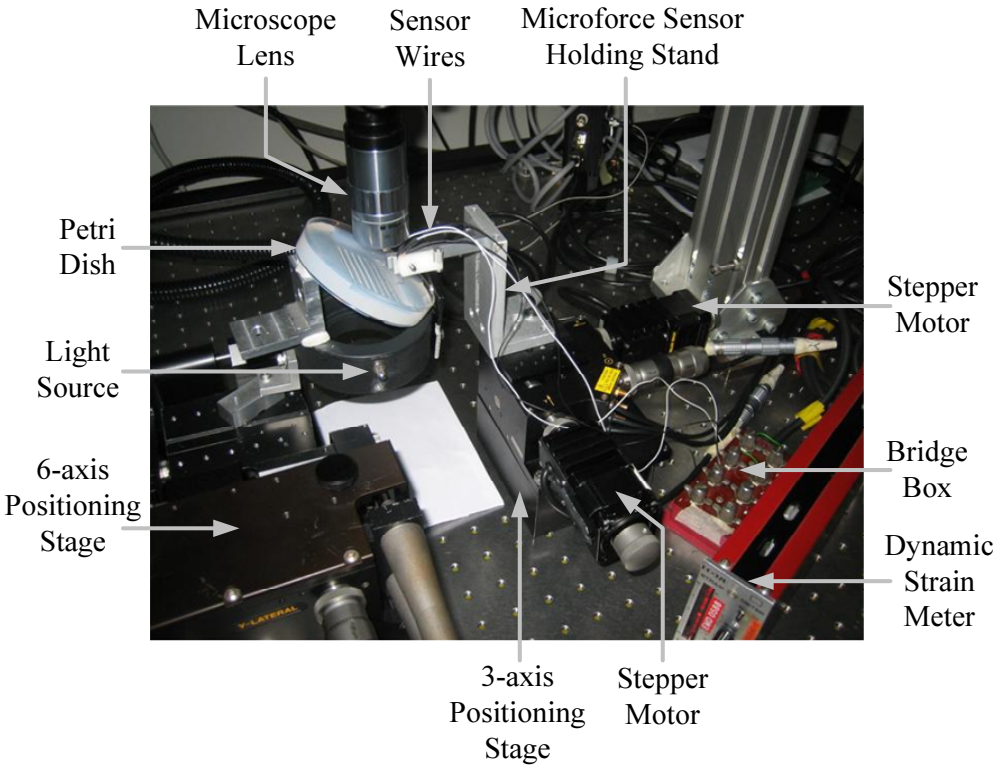

Figure 6.8: Setup of the micromanipulation system for batch microinjection.

held by a stand mounted on a 3-DOF high precision stage with a travel range of 4 *mm* in each of the X, Y, and Z axes and a step resolution of 25 *nm*. The imaging unit included one set of microscope with a CCD camera. It was mounted upright above the petri dish. Upon calibration, the resolution of each pixel was around 10.6 μm. Figure 6.9 shows a close-up view of the microinjection area. The zebrafish embryos were arrayed in the parallel V-grooves. The micropipette was manually adjusted in vertically (as indicated in Figure 6.1) to align with the center of the embryo. The petri dish was tilted to reduce the mobility of the embryos during injection.

The software that run in this system was written in LabVIEW, which was fully integrated for data communication with all instruments. The normalized two-dimensional cross-correlation algorithm was programmed using MATLAB and embedded in the control

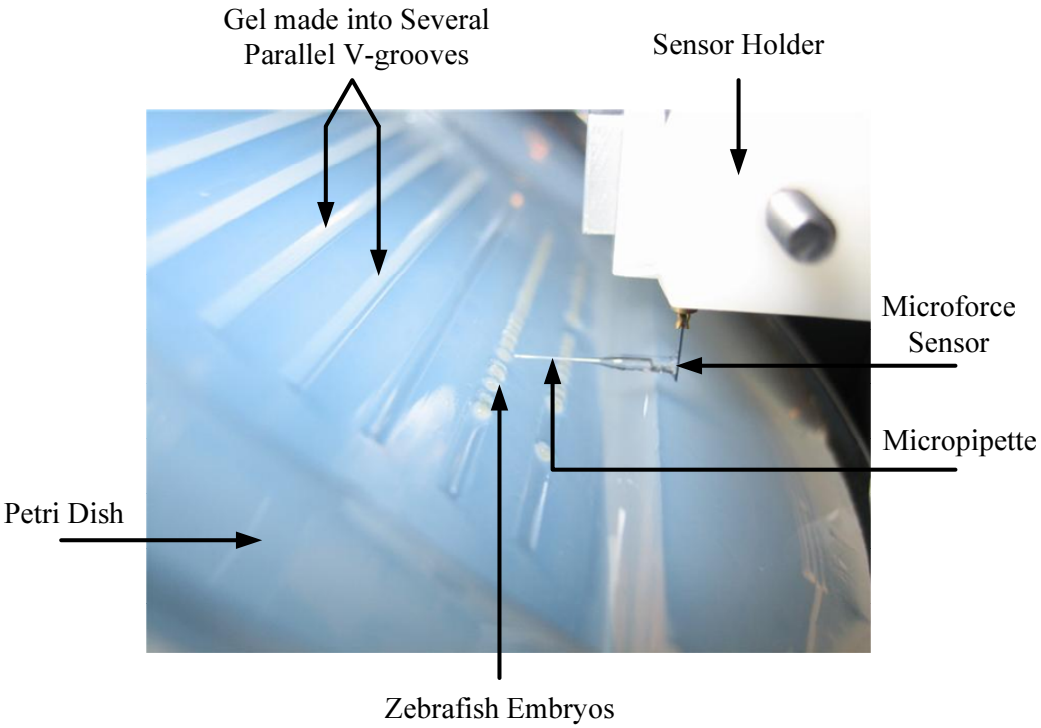

Figure 6.9: Close view of the microinjection area.

system.

6.3.2 Results

This batch microinjection experiment involved three zebrafish embryos, which is within the range of the limited view of the lens of the microscope. The horizontal starting position of the tip of the micropipette was set to be about 300 μm away from the chorion of the embryo. At the start of the experiment, the stage moved the micropipette towards the embryo at a speed of 0.1 mm/s in steps of 10 μm each. When the chorion was penetrated, the stage continued its motion for an additional distance of 100 μm to penetrate the yolk, then the stage reversed its motion at a speed of 0.4 mm/s with a step size of 40 μm to extricate the micropipette from the embryo quickly. The sampling fre-

quency of the force measurement loop was three times higher than that for the position control loop. The threshold values of the first-order and second-order derivatives of the penetration force were set as discussed in Section II.

The machine vision algorithm first located the centerline of the micropipette and each yolk. Then the micropipette was moved by 0.43 *mm*, 1.69 *mm* and 2.96 *mm* to align with the centerline of each yolk respectively. For each embryo, penetration was started upon each alignment. Figure 6.10 shows the trajectories of the penetration force of the three embryos. It can be seen from the figure that the maximum penetration force for embryo 1, 2 and 3 were 1.1 *mN*, 0.75 *mN*, and 1.3 *mN*, respectively. Although these values are different, all three embryos were successfully pierced with dynamic feedback of the penetration force. In the experiment, the average penetration time for each embryo was around 15 seconds.

6.4 Summary and Discussion

In this chapter, we have described the design and construction of a prototype micromanipulation system for automatic batch microinjection of the zebrafish embryos. Such an automatic batch process is made possible by (i) the development of a machine vision algorithm to identify the number of embryos in a batch and to locate the centerline of each embryo, (ii) the integration of a piezoresistive micro-force sensor with a micropipette to measure the penetration force of the embryo in real-time, and (iii) the synthesis of an augmented position control with dynamic force feedback by exploiting the characteris-

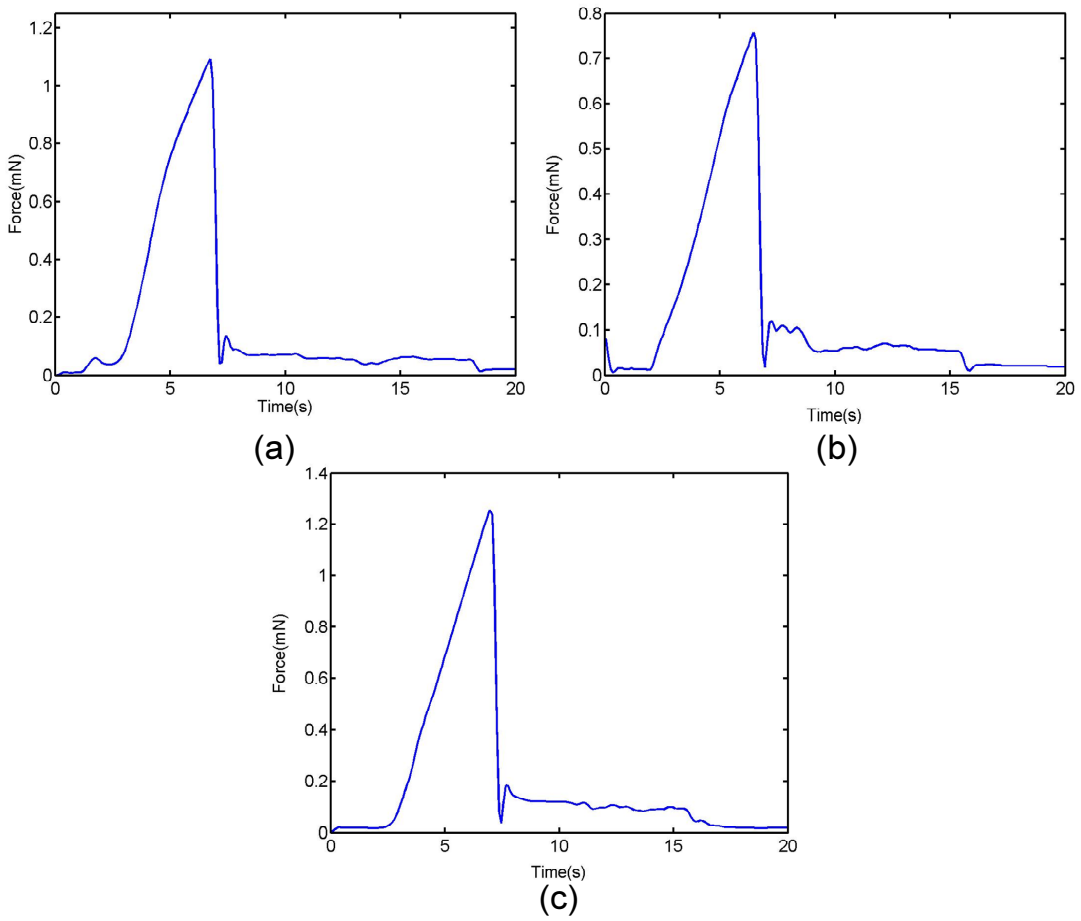

Figure 6.10: Penetration force trajectories of group embryos (a) embryo 1 (b) embryo 2 (c) embryo 3.

tics of the force profile associated with the microinjection process. The effectiveness of this prototype micromanipulation system has been demonstrated in an experiment involving automatic identification and penetration of a group of zebrafish embryos. The experimental results demonstrate that the technique of force augmented position control with dynamic penetration-force feedback is practicable for automatic batch microinjection applications.

To improve the applicability of this micromanipulation system, several research issues are to be pursued. The first issue concerns the design of a mechanism to transmit the

force experienced by the micropipette to the micro-force sensor. Currently, injection upon penetration is not implemented because the cavity of the micropipette is blocked by the glue that bonds the micro-force sensor to the micropipette. Such a mechanism should ensure easy separation of the micropipette from the fixture of the sensor to allow quick replacement of the micropipette (because of the wear and tear resulted from repeated use); it should also provide protection to the micro-force sensor against excessive force.

The second issue concerns the protection of the embryo by reducing its unnecessary deformation during penetration. Usually, penetration by the micropipette results when the chorion of the embryo is deformed to an extent that the strain in the chorion exceeds a certain limit. In a penetration process under pure positioning control with the micropipette moving at a constant speed, the entire embryo may undergo an unnecessarily large deformation until the chorion is penetrated. To resolve this problem, a frictionless compound flexure stage can be used (instead of positioning stage) to enable direct control of the penetration force, so that the micropipette can be moved at variable speed and fast acceleration. This could lead the ideal situation that only the membrane close to the injection point will deform during penetration.

The third issue concerns the installing of an additional camera to provide the side view of the penetration area. Currently, the Z axis (as indicated in Figure 6.1) of the micropipette was adjusted manually to align with the centerline of the embryo in Z axis. With this additional camera, such an adjustment can be automated. The last issues concerns the reduction of the time required in identifying the embryos and locating the micropipette. This can be done by implementing the machine vision algorithm using advanced coding

techniques and computational resources.

Chapter 7

Experiment III: A Micro-assembly System for Automation of the Pick-up and Assembly Process in Scaffold Assembly

This chapter presents an experiment to use micro-force sensing and control to automate the pick-up and assembly of the micro-part used in scaffold assembly. An explicit force-feedback control system is developed for the automation of the scaffold assembly in tissue engineering. It illustrates the direct force control represents an effective alternative to position-based force control in micro-assembly.

7.1 Background

Tissue generation by autogenous cell transplantation is a promising technique in the area of life sciences because it would eliminate the problems of donor site scarcity, immune rejection and pathogen transfer [119]. To provide the necessary support for cells to proliferate and replicate, a scaffold is usually needed [120]. A scaffold is a porous 3D structure made of biodegradable material and attached with necessary growth factors to form a biomimetic surface. When cells multiply and finally grow into the new tissues, the scaffold will discompose and be absorbed by human body.

In order to cater to the patients with particular receptor profiles, it is necessary to manufacture diverse scaffolds with different constructions. This involves modification of scaffold pore size, mechanical properties, degradation and resorption kinetics during each manufacture. Implantation on different parts of a human bone requires different scaffolds with customized biological properties. One approach to meet this requirement is to assemble micro-parts (made of biomaterial and coated with desired cells and agents) to form a scaffold. This approach of scaffold assembly is desirable as there is no thermal, electrical and chemical reaction involved in production process.

Manual scaffold assembly has been reported in [121]. A scaffold was assembled manually with a positioning stage without any reference to the force involved in the process. To avoiding damaging the micro-parts, the assembly was conducted at low speed. Moreover, such a manual assembly process induces stress (for fear of damaging the micro-parts) and fatigue (due to repetitive maneuvers that require high accuracy) in the

human operator. Automation of such micro-assembly through force-feedback control can improve the effectiveness and efficiency of the process, in terms of likelihood of part damage and speed of assembly, respectively.

7.2 Experimental Setup

To achieve automation of the pick-up and assembly process in scaffold assembly, we developed an explicit force-feedback control system for micro-assembly. The force-feedback system is incorporated with a compound flexure stage (discussed in Chapter 4.1), which is driven by a voice-coil actuator and designed to provide frictionless translation motion along one axis. A force sensor measures the interaction force between the micromanipulator and its environment, while an explicit force controller (discussed in Chapter 4.2) controls the interaction force to follow a desired force trajectory. The experiment setup is shown in Figure 7.1.

A voice-coil actuator (Model LA-13-000A, BEI) was used to directly drive the compound flexure stage. It has a peak force of 15.6 N with a sensitivity of 9.79 mN/mA. This sensitivity is ensured in a small motion range ($\pm 500\ \mu m$). A DC current source (Model 220, KEITHLEY) with a range from 1 nA to 100 mA was used to supply a stable input current. The step size of the current under 100 mA range is 50μA. This current source can be directly controlled from a PC through a GPIB interface.

A 6-DOF strain gauge force/torque sensor (Model Nano17, ATI) was mounted on the upper movable platform of the flexure stage. It has a resolution of 12.5 mN with a range

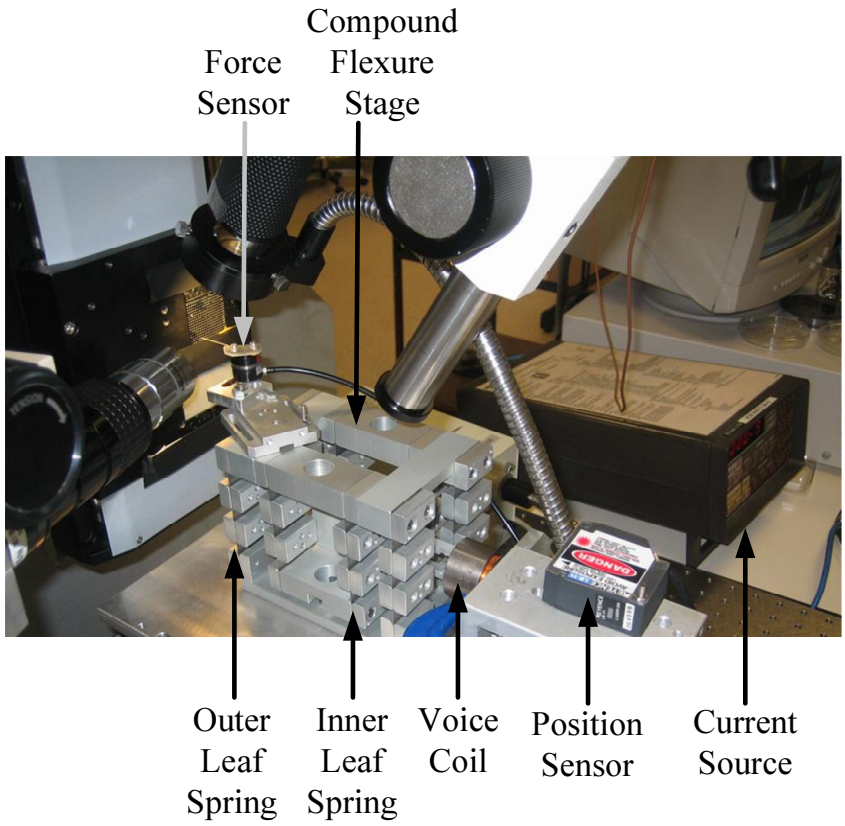

Figure 7.1: Setup of the force-feedback control system for micro-assembly.

of $\pm 12\,N$. A micro-machined manipulator in the shape of a needle was fixed on the force sensor to perform the tasks of picking up a micro-part and assemble it onto a particular support structure. Since the flexure stage can provide translation movement in a single axis only, the measured force was also restricted to that axis.

The force-feedback control system was fixed on a 3-axis high precision positioning stage (Model M-511.DD and M-501.1PD, Physik Instrumente (PI)). Each of the X and Y axes has an accuracy of 0.2 μm per 50 mm, while the Z axis has a resolution of 8 nm with a travel range of 12.5 mm. The Y-axis was set up to be the insertion direction. Another vertical positioning stage (Model M-501.1PD, Physik Instrumente (PI)) was used to hold the base wafer and the zero plate. These positioning stages enable long-range

conveyance and (visually guided) alignment of a micro-part.

The micro-parts, whose design and fabrication are described in [121], are made of SU8, a biocompatible polymer. These fragile building blocks were conceived to be assembled into scaffolds for tissue engineering with optimal growth properties [122]. Figure 7.2 shows a drawing of a micro-part. The overall dimensions of the micro-part are $500\mu m \times 500\mu m \times 200\mu$ with a wall-thickness of 60 μm. Each micro-part is pre-fabricated on a wafer with a weak joint between the micro-part and the wafer. There is a hole of 100 μm in diameter at the center of the micro-part. On each flank is a notch 60 μm in width. The purpose of the center hole is to permit the part to be picked up by inserting into it a properly sized needle and then retracting this needle, thus breaking the weak joint between the part and the wafer. The purpose of the notch is to enable a micro-part to be assembled onto a so-called “zero plate” by mating the notch with the pre-fabricated walls on the zero plate. Fabrication of the micro-parts was carried out in the Micro-Machines Center at the Nanyang Technological University, Singapore.

Figure 7.3 shows a close-up view of the pick-up and assembly area. The needle is a tungsten rod with a diameter of 500 μm. The tip of the rod (about 180 μm in length) was etched to a diameter of 100 μm. A clear shoulder was formed at the boundary between the etched section and the unetched section. The force acting on the micro-part takes effect on this edge. The design and fabrication of the wafer, the zero plate, and the needle will be reported elsewhere [121].

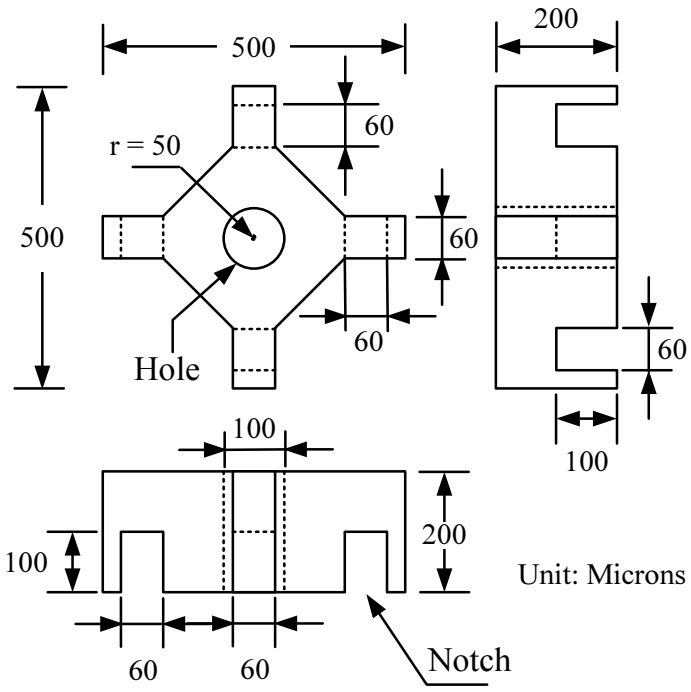

Figure 7.2: Dimension of a 3D micro-part.

7.3 Experimental Results

Two experiments, one involves a pick-up operation and the other an assembly, were conducted in this application of explicit force-feedback control for automatic micro-assembly. In the first experiment, the tungsten needle was first moved by the positioning stage to a location at a distance of about 20 μm above the center hole of the micro-object, as shown in Figure 7.4(a). It was determined experimentally that a compressive force greater than 100 *mN* applied from the top of the micro-part would break the joint between the micro-part and the base wafer. A desired force with the magnitude of 150 *mN* was then input to the force controller. Under the integral control with $K_i = 0.05$, the force-transmission stage was actuated to apply the force. The actual force experienced by the micro-part, as measured by the force sensor, increased until it reached the desired

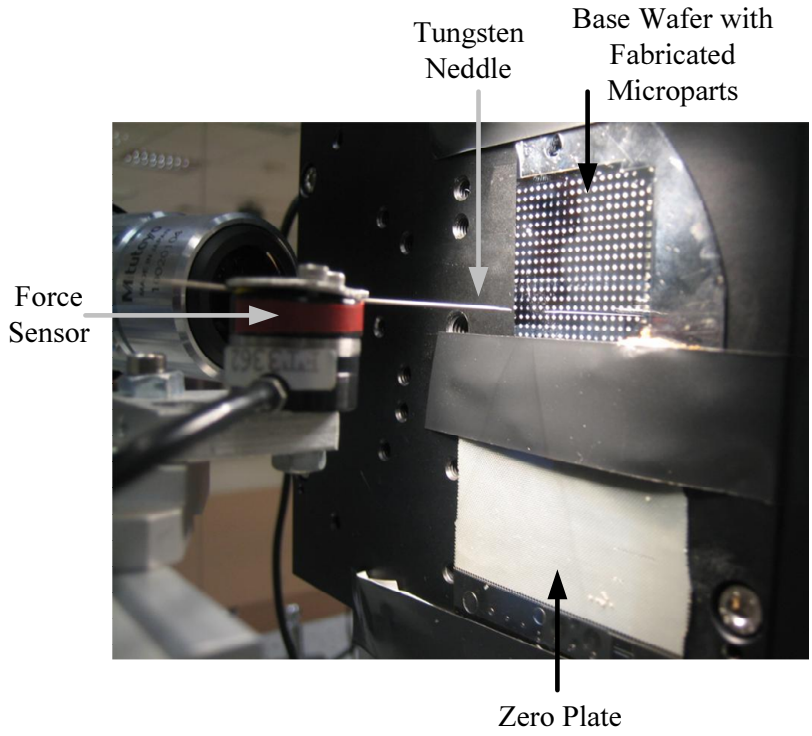

Figure 7.3: Prototype force-control system.

magnitude of 150 *mN*, as shown on the rising solid line in Figure 7.4(d). The photo in Figure 7.4(b) confirms that the joint was indeed broken after the force reached 150 *mN*.

Once the actual force had stabilized at 150 *mN* for about five seconds, another desired force with a magnitude of 0 *mN* was subsequently input to the force controller. This was to extract the micro-part from the wafer. Under the same integral force control, the actual force dropped to 0 quickly, as indicated by the sharp decline in the solid line in Figure 7.4(d). The photo in Figure 7.4(c) shows the position of the micro-part after the extraction. It clearly shows that the micro-part is detached from the base wafer and attached to the tungsten needle. The complete force trajectories are shown in Figure 7.4(d), where the dashed line represents the desired force and the solid line represents the actual contact force. For a series of five pick-up operations conducted during the

experiment, the average duration was around 25 seconds for each operation.

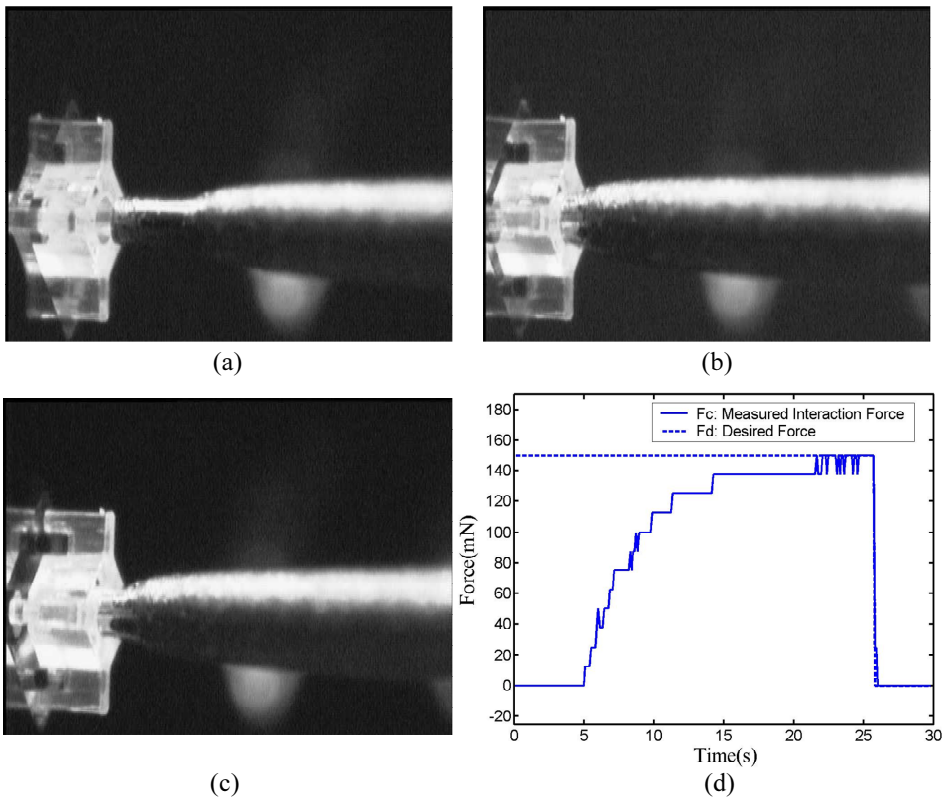

Figure 7.4: (a) Tungsten needle positioned 20 μm above the center hole of the micro-part; (b) micro-part with broken joint upon application of 150 *mN* force; (c) position of micro-part after extraction; (d) force trajectories of pick-up process.

In the second experiment, a micro-part was automatically assembled onto the zero plate. This was accomplished by pushing the micro-part down onto the wall on the zero plate such that the notch at the bottom of the micro-part fitted onto the wall. It was found, experimentally, that a 400 *mN* force exerting on the top of the micro-part would be sufficient to ensure a successful assembly, which was ascertained by observing the gap between the notch of the micro-part and the wall on the zero plate. In the experiment of automated assembly, the notch of the micro-part was first aligned with the wall on the zero plate, as shown in Figure 7.5(a). Then a desired 400 *mN* force was input to the

force controller. Under the same integral control, the actual contact force increased until it stabilized at 400 *mN*, as shown on the rising solid line in Figure 7.5(d). This force represents the friction between the notch of the micro-part and the wall on the zero plate. The photo in Figure 7.5(b)shows that the notch of the micro-part fully engaged the wall on the zero plate when the force reached 400 *mN*.

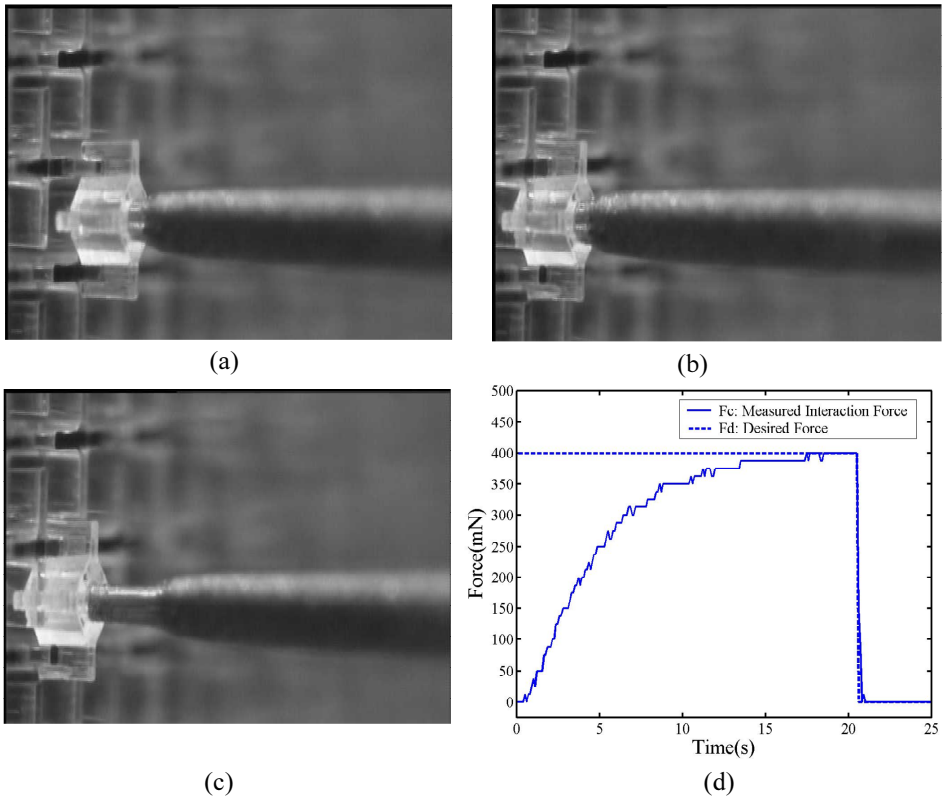

Figure 7.5: (a) Notch of the micro-part aligned with wall on zero plate; (b) notch of micro-part fully mated to wall when force reached 400 *mN*; (c) tungsten needle separated from micro-part; (d) force trajectories of assembly process.

Once the actual force had stabilized at 400 *mN* for about five seconds, a 0 *mN* desired force was input to the force controller. This was to extricate the tungsten needle from the micro-object while leaving the micro-object on the zero plate. It is noted that simply retracting the needle would result in its extraction from the hole on the micro-part, be-

cause by design the force between the tip of the tungsten needle and the inner wall of the hole on the micro-object is much smaller than that between the notch of the micro-part and the wall on the zero plate. Force control is not crucial in this particular situation. The system was kept under force control during the extraction process mainly as an extra measure to avoid damaging the part. The sharp decline in the solid line in Figure 7.5(d) shows the actual force drops to zero quickly. The photo in Figure 7.5(c) confirms that the micro-part was successfully assembled to the zero plate and the tungsten needle separated from the micro-part. The complete force trajectories are shown in Figure 7.5(d), where the dashed line represents the desired force and the solid line represents the measured contact force. The average assembly time was around 25 seconds.

7.4 Summary and Discussion

To complement pure positioning-based approaches for scaffold assembly, we have proposed and developed an explicit force-feedback system capable of controlling the dynamic interaction force between a micro-manipulator and the micro-part. This force-control system is a compound flexure stage that transmits force by frictionless translational motion with low stiffness along one axis, while exhibiting high stiffness in all other axes. Under the action of an integral control law, the interaction force can be controlled to follow a desired trajectory. The effectiveness of this force-control system has been demonstrated in the automatic pick-up and assembly of the micro-part used in tissue engineering.

Two main research issues are to be pursued to improve the applicability of the force-feedback control system for micro-assembly. The first concerns enabling faster assembly operations by improving the capability of the force controller. The second concerns the improvement of the force sensor and the flexure stage.

In the reported experimental application, the average durations for pick-up and assembly were both around 25 seconds, mainly due to the slow approach (of the manipulator) to the pick-up and assembly area. Such speeds are obviously not suitable for high volume production. The main reason for keeping the speed of the needle low during the approach was to avoid damaging the parts. This over-cautious approach can be accelerated by improving the capability of the force control loop. For instance, the approaching speed can be increased by incorporating a force controller to deal with the impact force under high-speed motion, while the pick-up and assembly speeds can be increased by properly tuning K_i.

The capability of the force-transmission stage can be improved to deal with finer motion and hence smaller force. This specifically concerns the resolution of the voice-coil actuator, and the travel range of the force-transmission stage. Currently, the resolutions of the voice-coil actuator and the force sensor used in this work are still in the order of *mN*. This can be improved by using the smaller voice-coil actuator and the high resolution micro-force sensor in the order of μN in the future. Compared to the displacement range of a few hundred microns (or less) in a typical micro-assembly operation, the travel range (in the order of *mm*) of the current force-transmission stage is rather large, mainly due to the fact that the stiffness of the flexure stage is relatively low. Although

such low stiffness permits the flexure stage to be readily moved by a small driving force from the actuator, it also makes the translational movement of the stage more liable to be adversely affected by vibration. This trade-off between resistance to vibration and ease of actuation should be taken into account in the design of next-generation flexure stages.

Chapter 8

Conclusion

8.1 Contribution of This Work

The work in this thesis has made the following contributions:

Develop a piezoresistive-based probe micro-force sensor

Significant results have been reported in the literature on various applications using piezoresistive force sensors. However, few works have been done to specifically deal with the design or modification of piezoresistive-based probe micro-force sensors. A commercial piezoresistive force sensor was selected for modification. A probe with a small diameter was integrated to the sensing beam as an extension. An important consideration in adding an extension to the core sensor is that the mechanical property of the probe should be close to that of the piezoresistive force sensor. This is to ensure that the extension is strong enough to transfer forces from the measurement to the sensor without

affecting its frequency response. A single-mode optical fiber meets this requirement.

According to the elastic bending theory, the deflection of the cantilever beam is linear to the force perpendicularly acting on the beam. This relationship can be modelled analytically. Such an analytical model is useful, as it can be used to determine the theoretical value of critical force that needs to be observed when using the sensor. This critical force arises due the fact that loading condition of the tip of the beam will be more severe with an integrated fiber extension than without. To prevent overloading (and thus causing damage to) the sensor, careful analysis has been done to calculate the maximum allowable force at the tip of the sensor beam.

Develop a Force Transmission Stage for Direct Force-feedback Control

Direct force-feedback control represents an effective alternative to position-based force control in micro-assembly. Implementation of direct force-feedback control requires effective force-transmission. The means for force transmission proposed in this research is in the form of a force-transmission stage. It is desirable that the force-transmission stage generates low frictional effect and has high immunity against noise (due to vibration, for instance). This ensures that no matter how small the output force from the actuator, the system still exhibits a high signal-to-noise ratio. A force-transmission stage, designed and built based on a compound flexure configuration, has been developed to provide frictionless translation with low stiffness motion along one axis while exhibiting high stiffness in all other axes.

The design and integration of force transmission stage for explicit force control could

serve as an impetus for stimulating further interests in the subsequent generation of practical tools and systems in this field, leading to possible commercial development of components and subsystems that are instrumental in micromanipulation, such as frictionless stage, high-resolution actuator, multi-axis micro-force sensors, etc.

Achieve Fast Coarse Alignment in Fiber Pigtailing

Optimization of coarse alignment seems to have received little attention. This is particularly unfortunate because coarse alignment is actually a very important step in fiber pigtailing. It is the prerequisite to successful fine alignment. When the apparent separate processes of coarse alignment and fine alignment are taken as a whole, a properly optimized coarse alignment process could greatly enhance the efficiency of fiber pigtailing. It is therefore desirable to develop optimization methods for coarse alignment.

The method of 2-D blind raster scan is usually used in coarse alignment. In this method, the signal of light intensity is measured to check whether the first light is found. The fiber scans (by back-and-forth search or rectangular spiral search) over an area where is assumed that the input channel of the optical device is located. Estimation of position and area size of search directly affect the efficiency of this method. However, the estimation is difficult to make without any assistances.

An approach using force information is developed to locate the small area. A micro-force sensor with a sharp tip is used to sweep the input facet of the optical device. The resulting micro-force measured by the sensor will continuously provide useful information about the surface features as long as the tip of the sensor is in contact with the input

facet. These surface features (as characterized by the micro-force signal in real-time) provide useful clues in guiding the fiber to rapidly locate the actual optical path of the optical device.

Achieve Automation of the Embryos Injection Process

In a manual microinjection process, the skill and experience of the operator play a crucial role in achieving a successful injection. It usually takes several months of training and practice for an operator to become proficient in performing such a task. However, even for an experienced operator, the success rate of such manual microinjection may still be very low. This is mainly due to the fact that to execute various steps in a manual microinjection requires fine control of both position and force, which is difficult for a human operator to accomplish consistently. Another reason for the low success rate of manual microinjection is that in general manual manipulation has poor repeatability. In a research laboratory, for instance, it is not uncommon to require more than a hundred embryos be injected one after another in quick succession. The repetitive maneuvers associated with such a high throughput microinjection process inevitably causes fatigue in the human operator, and so may easily lead to a low success rate. Automating these maneuvers is a desirable means of improving success rate for batch microinjection.

A prototype micromanipulation system for automatic batch microinjection of the zebrafish embryos is designed and constructed. Such an automatic batch process is made possible by (i) the development of a machine vision algorithm to identify the number of embryos in a batch and to locate the centerline of each embryo, (ii) the integration of a piezoresistive micro-force sensor with a micropipette to measure the penetration force

of the embryo in real-time, and (iii) the synthesis of a augmented position control with dynamic force feedback by exploiting the characteristics of the force profile associated with the microinjection process. The effectiveness of this prototype micromanipulation system has been demonstrated in an experiment involving automatic identification and penetration of a group of zebrafish embryos.

Achieve Automation of the Pick-up and Assembly Process in Scaffold Assembly

To provide the necessary support for cells to proliferate and replicate, a scaffold is usually needed. Conventionally, the scaffold is assembled manually with a positioning stage without any reference to the force involved in the process. To avoiding damaging the micro-parts, the assembly was conducted at low speed. Moreover, such a manual assembly process induces stress (for fear of damaging the micro-parts) and fatigue (due to repetitive maneuvers that require high accuracy) in the human operator. Automation of such micro-assembly through force-feedback control can improve the effectiveness and efficiency of the process, in terms of likelihood of part damage and speed of assembly, respectively.

An explicit force-feedback control system for micro-assembly is developed to achieve automation of the pick-up and assembly process in scaffold assembly. This force-control system is a compound flexure stage that transmits force by frictionless translational motion with low stiffness along one axis, while exhibiting high stiffness in all other axes. Under the action of an integral control law, the interaction force can be controlled to follow a desired trajectory. The effectiveness of this force-control system has been demonstrated in the automatic pick-up and assembly of the micro-part used in tissue

engineering.

The prototype systems and experiments developed in this research may serve as an experimental foundation for further advancing micromanipulation techniques to a higher level, where direct and automated control of interaction processes is possible. This would lead to more practical applications of force-based techniques, such as in the realization of lab-level 3D hybrid MEMS devices in mass fabrication and the automation of the volume-injection of the zebrafish eggs.

8.2 Future Works

Several directions are available for future research based on the work in this thesis.

Sensor-Manipulator Connection Mechanism Design

Design a mechanism to transmit the force from the micromanipulator to the micro-force sensor. In certain applications, the micromanipulator is used as a probe or as an injection pipette. It has a sharp tip diameter around a few microns. This makes the micromanipulator become very fragile and easily damaged due to ordinary wear and tear. Traditionally, the micromanipulator and the micro-force sensor are fixed together. The sensor is waste after the rapid wear and tear of the micromanipulator. So it is preferred to separate the micro-force sensor and the micromanipulator. The mechanism should ensure the repeated change of the micromanipulator with the fixture of the sensor. This mechanism will also provide protection to the sensor against excessive force.

Micro-force Sensor Design

The result of the comparison of different types of one-axis micro-force sensors (piezoresistive, piezoelectric and capacitive) showed that the piezoresistive micro-force sensor is preferred as it has both a large measurement range and a high resolution. A one-axis piezoresistive micro-force sensor will be designed and fabricated with a resolution around 20 micro-Newton and a range of tens of milli-Newton. The maximum allowable deflection of the tip of the sensor should be larger than tens of microns.

Frictionless Flexure Based Stage Design

Design a flexure based stage to provide frictionless transmission of the micro-level force from the actuator, which the output force is in the order of a few micro-Newton. The flexure stage is preferred as it allows the application of explicit force-feedback control system in micromanipulation. The travel range of this stage should be in a few millimeters. The design of the stiffness of the stage is an important issue. Although a low stiffness design permits the flexure stage to be readily moved by a small driving force from the actuator, it also makes the translational movement of the stage more liable to be adversely affected by vibration. The trade-off between resistance to vibration and ease of actuation should be taken into account in the design.

Development of an Inspection System

Develop an inspection system based on the micro-force sensing and position control to measure the topography of the wire bonding pads and the firmness of the bonding wire between the two wire bonding pads. A group of sharp probes (tip diameter around a few

microns) with micro-force sensors will be used to scan over the wire bonding pads and drag the bonding wire, the measured force is then used to analyze the topography and firmness results. The dimension of the pads is in a few micron scales and the dragging force is estimated around a few milli-Newton. This system will dramatically shorten the inspection time required in other current industrial inspection system.

Development of a Micro-injection System with Haptic Interface

Develop a micro-injection system based on the micro-force sensing and control to automate the embryos injection process (such as zebrafish injection). Using a combined system constituting of a haptic device and an explicit force control module, the injection force will be felt and controlled precisely to reduce the possible injection damage to the eggs. The scale of the measured and controlled force is in tens of micro-Newton level. This system may be widely applied to the intracytoplasmic sperm injection (ICSI) to ensure its successful rates.

Improvement of the Force Scaling Factor in Tele-Micromanipulation

Improve the existent haptic device to facilitate the human intervention of the micromanipulation task through the sensed micro-level interaction force. The selection of the force scaling parameter is going to be investigated. This force scaling will preserve the dynamic similarity and minimizes the distortion (such as density and velocity) with the existence of nonlinear adhesion forces in the micro-world. The haptic device will be tested in the micro-injection task.

Bibliography

[1] R. P. Feynman. There's plenty of room at the bottom. *J. Microelectromech. Syst.*, 1:60–66, 1992.

[2] An industry in transition: 2006 mems forecast. Technical report, In-Stat, 2006.

[3] Micro- and nanomedicine: Technologies, applications, industry, and markets worldwide. Technical report, MedMarket Diligence, LLC, 2006.

[4] S. C. Ng, A. Bongso, H. Sathananthan, and S.S. Ratnam. Micromanipulation: its relevance to human in vitro fertilization. *Fertil. Steril.*, 53(2):203–219, 1990.

[5] A. V. Steirteghem, P. Nagy, and H. Joris. The development of intracytoplasmic sperm injection. *Hum. reprod.*, 8:59–72, 1996.

[6] K. Yanagida, H. Katayose, H. Yazawa, Y. Kimura, K. Konnai, and A. Sato. The usefulness of a piezo-micromanipulator in intracytoplasmic sperm injection in humans. *Hum. reprod.*, 14(2):448–453, 1998.

[7] N. Dechev, W. L. Cleghorn, and J. K. Mills. Microassembly of 3-d mems structures utilizing a mems microgripper with a robotic manipulator. In *IEEE Int. Conf. on Robot. and Automat.*, pages 3193–3199, 2003.

[8] M. J. Madou. *Fundamentals of microfabrication*. CRC Press, 1997.

[9] M. Elwenspoek and H. V. Jansen. *Silicon micromachining*. New York : Cambridge University Press, 1998.

[10] B. Danny. *Microengineering, MEMS, and interfacing : a practical guide*. FL : Dekker/CRC Press, 2006.

[11] J. G. Jason and G. D. Nicholas. Force control of linear motor stages for microassembly. In *Proc. ASME Int. Mechanical Eng. and Congress*, pages 1–9, 2003.

[12] Z. Lu, P. C. Y. Chen, A. Ganapathy, G. Y. Zhao, J. H. Nam, G. L. Yang, E. Burdet, C. L. Teo, Q. N. Meng, and W. Lin. A force-feedback control system for microassembly. *J. Micromech. Microeng.*, 16:1861–1868, 2006.

[13] J. Dreschler. Automation advances life sciencese microscopy. In 130-133, editor, *Scientific and Technical Information*, Oct. 2005.

[14] K. Stephen. Automated alignment equipment in test and measurement. Technical report, Melles Griot, 2001.

[15] J. T. Feddema and R. W. Simon. Cad-driven microassembly and visual servoing. In *IEEE Int. Conf. on Robot. and Automat.*, pages 1212–1219, 1998.

[16] Y. Song, M. T. Li, L. N. Sun, and J. H. Ji. Global visual servoing of miniature mobile robot inside a micro-assembly station. In *Proc. IEEE Int. Conf. Intell. Mechatron. and Automat.*, pages 1586–1591, 2005.

[17] Y. Zhou and B. J. Nelson. The effect of material properties and gripping force on micrograsping. In *Proc. IEEE Int. Conf. on Robot. and Automat.*, pages 1115–1120, 2000.

[18] D. H. Kim, Y. Sun, S. Yun, S. H. Lee, and B. Kim. Investigating chorion softening of zebrafish embryos with a microrobotic force sensing system. *Journal of Biomechanics*, 38(6):1359–1363, 2005.

[19] Z. Lu, P. C. Y. Chen, and W. Lin. Force sensing and control in micromanipulation. *IEEE Trans. Syst., Man, and Cybern. C*, 36:713–724, 2006.

[20] A. Menciassi, A. Eisinberg, I. Izzo, and P. Dario. From macro to micromanipulation: models and experiments,. *IEEE/ASME Trans. Mechatron.*, 9:311–320, 2004.

[21] T. Sato, T. Kameya, H. Miyazaki, and Y. Hatamura. Hand-eye system in nano manipulation world. In *Proc. IEEE Int. Conf. on Robot. and Automat.*, pages 59–66, 1995.

[22] R. S. Fearing. Survey of sticking effects for micro parts handling. In *Proc. IEEE/RSJ Int. Conf. on Intell. Robot. and Syst.*, pages 212–217, 1995.

[23] F. Arai, D. Andou, T. Fukuda, Y. Nonoda, and T. Oota. Micro manipulation based on micro physicscstrategy based on attractive force reduction and stress measurement. In *Proc. IEEE/RSJ Int. Conf. on Intell. Robot. and Syst.*, pages 236–241, 1995.

[24] F. Arai, D. Andou, Y. Nonoda, T. Fukuda, H. Iwata, and K. Itoigawa. Integrated

microendeffector for micromanipulation. *IEEE/ASME Trans. Mechatron.*, 3:17–23, 1998.

[25] F. Arai, D. Andou, and T. Fukuda. Adhesion force reduction for micmanipulation based on micro physics. In *Proc. IEEE Micro-electro-Mechanical Syst. Conf.*, pages 349–354, 1996.

[26] P. R. Scheeper, J. A. Voorthuyzen, W. Olthius, and P. Bergveld. Investigation of attractice forces between pecvd silicon nitride microstructures and an oxidized sillicon substrate,. *Sens. Actuators*, 30:231–239, 1992.

[27] P. Lambert, P. Letier, and A. Delchambre. Capillary and surface tension forces in the manipulation of small parts. In *Proc. 5th IEEE Int. Symposium on Assembly and Task Planning*, pages 54–59, 2003.

[28] S. Tsuchitani et al. Measurement of the surface force in microstructures and its reduction. *Trans. Soc. Instrm. Contr. Eng.*, 30:136–142, 1994.

[29] M. Gauthier, B. Lopez-Walle, and C. Clevy. Comparison between micro-objects manipulations in dry and liquid mediums. In *Proc. IEEE Int. Symposium on Comp. Intell. in Robot. and Automat.*, pages 707–712, 2005.

[30] W. Zesch, M. Brunner, and A. Weber. Vacuum tool for handling microobjects with a nano-robot. In *Proc. IEEE Int. Conf. on Robot. and Automat.*, pages 1761–1766, 1997.

[31] F. Arai, A. Kawaji, T. Sugiyama, Y. Onomura, M. Ogawa, T. Fukuda, H. Iwata,

and K. Itoigawa. 3d micromanipulation system under microscope. In *IEEE Int. Symposium on Micromechatronics and Human*, pages 127–134, 1998.

[32] H. V. Brussel, J. Peris, D. Reynaerts, A. Delchambre, G. Reinhart, N. Roth, M. Weck, and E. Zussman. Assembly of microsystems. *CIRP Annals*, 2:451–472, 2000.

[33] F. Dionnet, D. S. Haliyo, and S. Regnier. Autonomous micromanipulation using a new strategy of accurate release by rolling. In *Proc. IEEE Int. Conf. on Robot. and Automat.*, pages 5019–5024, 2004.

[34] T. Tanikawa and T. Arai. Development of a micromanipulation system having a two-fingered micro-hand. *IEEE Trans. Robot. Automat.*, 15:152–162, 1999.

[35] D. S. Haliyo, G. Venture, S. Regnier, and J. C. Guinot. An overview of the micromanipulation system [mu] mad. In *IEEE/ASME Int. Conf. Adv. Intell. Mechatron.*, pages 390–395, 2005.

[36] K. W. C. Lai, P. S. Chung, M. Li, and W. J. Li. Automated microassembly of surface mems mirrors by centrifugal force. In *Proc. IEEE Int. Conf. Intell. Mechatron. and Automat.*, pages 880–885, 2004.

[37] A. Menciassi, A. Eisiberg, M. C. Carrozza, and P. Dario. Force sensing microinstrument for measuring tissue properties and pulse in microsurgery. *IEEE/ASME Trans. Mechatron.*, 8:10–17, 2003.

[38] S. Fahlbusch, A. Shirinov, and S. Fatikow. Afm-based micro-force sensor and

haptic interface for a nanohandling robot. In *Proc. IEEE Int. Conf. on Robot. and Automat.*, pages 1772–1777, 2002.

[39] W. Hoffmann, S. Loheide, T. K. Besten, U. Brand, and A. Schlachetzki. Method of characterising micromechanical beams and its calibration for the application in micro force measurement systems. In *Proc. MicroTec.*, pages 819–823, 2000.

[40] Z. Lu, H. Luo, P. C. Y. Chen, and W. Lin. An integrated probe sensor for micro-force measurement. *Meas. Sci. Technol.*, 17:869–875, 2006.

[41] P. Berkelman, L. L. Whitcomb, R. H. Taylor, and P. Jensen. A miniature micro-surgical instrument tip force sensor for enhanced force feedback during robot-assisted manipulation. *IEEE Trans. Robot. Automat.*, 19:917–922, 2003.

[42] Y. Yamamoto, R. Konishi, Y. Regishi, and T. Kawakami. Prototyping ubiquitous micromanipulation system. In *IEEE/ASME Int. Conf. on Adv. Intell. Mechatron.*, pages 709–714, 2003.

[43] S. Butefisch, T. Buttgenbach, T. Kleine-Besten, and U. Brand. Micromechanical three-axial tactile force sensor for micromaterial characterisation. *Microsystem Technologies*, 7:171–174, 2001.

[44] P. Ruther, J. Bartholomeyczik, S. Trautmann, M. Wandt, O. Paul, W. Dominicus, R. Roth, K. Seitz, and W. Strauss. Novel 3d piezoresistive silicon force sensor for dimensional metrology of micro components. *Sensors J.*, pages 1006–1009, 2005.

[45] D. V. Dao, T. Toriyama, J. Wells, and S. Sugiyama. Micro force-moment sensor

with six-degree of freedom. In *IEEE Int. Symposium on Micromechatronics and Human Science*, pages 93–98, 2001.

[46] M. S. Bartsch, W. Federle, R. J. Full, and T. W. Kenny. Small insect measurement using a custom mems force sensor. In *IEEE Int. Conf. on Transducers, Solid-State Sensors, Actuators and Microsystems*, pages 1039–1042, 2003.

[47] D. H. Kim, B. Kim, and H. J. Kang. Development of a piezoelectric polymer-based sensorized microgripper for micromanipulation and microassembly. *Microsystem Technologies*, 10(4):275–280, 2004.

[48] J. Dargahi, M. Parameswaran, and S. Payandeh. A micromachined piezoelectric tactile sensor for an endoscopic grasper - theory, fabrication and experiments. *J. of Microelectromech. Syst.*, 9:329–335, 2000.

[49] Y. T. Shen, N. Xi, W. J. Li., and Y. X. Wang. Dynamic performance enhancement of pvdf force sensor for micromanipulation. In *Proc. IEEE/RSJ Int. Conf. on Intell. Robot. and Syst.*, pages 2827–2832, 2005.

[50] C. K. M. Fung, I. Elhajj, W. J. Li, and N. Xi. A 2-d pvdf force sensing system for micromanipulation and micro-assembly. In *Proc. IEEE Int. Conf. on Robot. and Automat.*, pages 1489–1494, 2002.

[51] S. Fahlbusch and S. Fatikow. Micro-force sensing in a micro-robotic system. In *Proc. IEEE Int. Conf. on Robot. and Automat.*, pages 3435–3440, 2001.

[52] Y. Sun, K. T. Wan, K. P. Roberts, J. C. Bischof, and B. J. Nelson. Mechanical

property characterization of mouse zona pellucida. *IEEE Nanobioscience*, 2:279–286, 2003.

[53] E. T. Enikov and B. J. Nelson. Three-dimensional microfabrication for a multi-degree-of-freedom capacitive force sensor using fiber-chip coupling. *J. of Microelectromech. Syst.*, 10:492–497, 2000.

[54] T. Kenny. Nanometer-scale force sensing with mems devices. *Sensors J.*, 1:148–157, 2001.

[55] Y. Sun, D. P. Potasek, D. Piyabongkarn, R. Rajamani, and B. J. Nelson. Actively servoed multi-axis microforce sensors. In *Proc. IEEE Int. Conf. on Robot. and Automat.*, pages 294–299, 2003.

[56] B. J. Nelson, Y. Zhou, and B. Vikramaditya. Sensor-based microassembly of hybrid mems devices. *IEEE Control Syst. Mag.*, 18:35–45, 1998.

[57] R. Resch, A. Bugacov, C. Baur, B. E. Koel, A. Madhukar, A. A. G. Requich, and P. Will. Manipulation of nanoparticles using dynamic force microscopy: simulation and experiments. *Appl. Phys. A*, 67:265–271, 1998.

[58] L. T. Hansen, A. Kuhle, A. H. Sorensen, J. Bohr, and P. E. Lindelof. A technique for positioning nanoparticles using an atomic force microscope. *Nanotechnology*, 9:337–342, 1998.

[59] A. A. G. Requicha, S. Meltzer, F. P. T. Arce, J. H. Makaliwe, H. Siken, S. Hsieh, D. Lewis, B. E. Koel, and M. E. Thompson. Manipulation of nano-scale com-

ponents with the afm: principles and applications. In *Proc. IEEE conf. on Nanotechnology*, pages 81–86, 2001.

[60] G. Y. Li, N. Xi, M. M. Yu, F. Salem, D. H. Wang, and J. P. Li. Manipulation nano-scale biological specimen in liquid. *Proc. IEEE conf. on Nanotechnology*, 2:68–71, 2003.

[61] M. Sitti. Micro- and nano-scale robotics. In *Proc. American Control Conf.*, pages 1–8, 2004.

[62] M. Sitti. Atomic force microscope probe based controlled pushing for nanotribological characterization. *IEEE/ASME Trans. Mechatron.*, 8:343–349, 2004.

[63] G. Y. Li, N. Xi, and M. M. Yu. Assembly of nanostructure using afm based nanomanipulation system. In *Proc. IEEE Int. Conf. on Robot. and Automat.*, pages 428–433, 2004.

[64] X. J. Tian, N. D. Jiao, L. Q. Liu, Y. C. Wang, Z. L. Dong, N. Xi, and W. J. Li. An afm based nanomanipulation system with 3d nano forces feedback. In *Proc. IEEE Int. Conf. Intell. Mechatron. and Automat.*, pages 18–22, 2004.

[65] J. Park, S. Kim, D. H. Kim, B. Kim, S. J. Kwon, J. O. Park, and K. I. Le. Identification and control of a sensorized microgripper for micromanipulation. *IEEE/ASME Trans. Mechatron.*, 10:601–606, 2005.

[66] M. A. Greminger and B. J. Nelson. Vision-based force measurement. *IEEE Trans. Pattern Anal. Machine Intell.*, 26:290–298, 2004.

[67] A. Eisinberg, A. Menciassi, D. Campolo, M. C. Carrozza, and P. Dario. Pi force control of a microgripper for assembling biomedical microdevices. In *Proc. IEEE Int. Circuits Devices Syst.*, pages 348–352, 2001.

[68] A. Pillarisetti, W. Anjum, J. P. Desai, G. Friedman, and A. D. Brooks. Force feedback interface for cell injection. In *First Joint Eurohaptics Conf. and Symposium on Haptic Interfaces for Virtual Environment and Teleoperator Systems*. 391-400, 2005.

[69] J. Y. Lew. Contact control of flexible micro/macro-manipulators. In *Proc. IEEE Int. Conf. on Robot. and Automat.*, pages 2850–2855, 1997.

[70] Y. Yamamoto, T. Hashimoto, T. Okubo, and T. Itoh. Measurement of force sensory information in ultraprecision assembly tasks. *IEEE/ASME Trans. Mechatron.*, 7:186–189, 2002.

[71] L. G. Chen, L. N. Sun, W. B. Rong, and X. Q. Bian. Hybrid control of vision and force for mems assembly system. In *IEEE Int. Conf. on Robot. and Biomimetics*, pages 136–141, 2004.

[72] P. Kallio, Q. Zhou, and H. Koivo. Control issues in micromanipulation. In *IEEE Int. Symposium on Micromechatronics and Human Science*, pages 135–141, 1998.

[73] T. Fukuda and F. Arai. Prototyping design and automation of micro/nano manipulation system. In *Proc. IEEE Int. Conf. on Robot. and Automat.*, pages 192–197, 2000.

[74] K. Inoue, T. Arai, T. Tanikawa, and K. Ohba. Dexterous micromanipulation supporting cell and tissue engineering. In *IEEE Int. Symposium on Micro-NanoMechatronics and Human Science*, pages 197–202, 2005.

[75] M. Gauthier and E. Piat. Control of a particular micro-macro positioning system applied to cell micromanipulation. *IEEE Trans. Automat. Science and Eng.*, 3:264–271, 2006.

[76] P. Yen, R. D. Hibberd, and B. L. Davics. A telemanipulator system as an assistant and training tool for penetrating soft tissue. *Mechatronics*, 6:423–436, 1996.

[77] M. Mitsuishi, Y. Lizuka, H. Watanabe, H. Hashizume, and K. Fujiwara. Remote operation of a micro-surgical system. In *Proc. IEEE Int. Conf. on Robot. and Automat.*, pages 1013–1019, 1998.

[78] J. E. N. Jaspers and C. A. Grimbergen. Mechanical manipulator for intuitive control of endoscopic instruments with seven degrees of freedom. In *Proc. IEEE Int. Conf. on Syst., Man and Cybern.*, pages 2479–2485, 2004.

[79] E. A. Y. Murakami, T. Kondo, and K. Ito. Man-machine dynamic characteristics related to position and force control tasks in micro-teleoperation system. In *SICE Annual Conference*, pages 1620–1625, 2003.

[80] J. E. Colgate. Robust impedance shaping telemanipulation. *IEEE Trans. Robot. Automat.*, 9:374–384, 1993.

[81] K. Kaneko, H. Tokashiki, K. Tanie, and K. Komoriya. Impedance shaping based

on force feedback bilateral control in macro-micro teleoperation system. In *Proc. IEEE Int. Conf. on Robot. and Automat.*, pages 710–717, 1997.

[82] M. Goldfarb. Dimensional analysis and selective distortion in scaled bilateral telemanipulation. In *Proc. IEEE Int. Conf. on Robot. and Automat.*, pages 1609–1641, 1998.

[83] M. Sitti and H. Hashimoto. Teleoperated touch feedback from the surfaces at the nanoscale: modeling and experiments. *IEEE/ASME Trans. Mechatron.*, 8:287–298, 2003.

[84] Y. Zhou, B. J. Nelson, and B. Vikramaditya. Fusing force and vision feedback for micromanipulation. In *Proc. IEEE Int. Conf. on Robot. and Automat.*, pages 1220–1225, 1998.

[85] Y. T. Shen, N. Xi, and W. J. Li. Contact and force control in microassmbly. In *IEEE Int. Symposium on Assembly and Task Planning*, pages 60–65, 2003.

[86] Y. T. Shen, N. Xi, U.C. Wejinya, W. J. Li, and J. Z. Xiao. Infinite dimension system approach for hybrid force position control in micromanipulation. In *Proc. IEEE Int. Conf. on Robot. and Automat.*, pages 2912 – 2917, 2004.

[87] M. C. Carrozza, A. Eisinberg, A. Menciassi, D. Campolo, S. Micera, and P. Dario. Towards a force-controlled microgripper for assembling biomedical microdevices. *J. Micromech. Microeng.*, 10:271–276, 2000.

[88] J. Y. Park, S. M. Kim, D. H. Kim, B. Kim, S. J. Kwon, J. O. Park, and K. I. Lee.

Identification and control of a sensorized microgripper for micromanipulation. *IEEE/ASME Trans. Mechatron.*, 10:601–606, 2005.

[89] J. Prmares and F. Torres. Movement-flow-based visual servoing and force control fusion for manipulation tasks in unstructured environments. *IEEE Trans. Syst., Man, and Cybern. C*, 35:4–15, 2005.

[90] A. Cohen. *Biomedical signal processing*. Boca Raton, FL: CRC, 1986.

[91] U. Brand, T. K. Besten, and H. Schwenke. Development of a special cmm for dimensional metrology on microsystem components. In *ASPE 15th Annual Meeting*, pages 542–546, 2000.

[92] E. Lebrasseur, J. B. Pourciel, T. Bourouina, and T. Masuzawa. A new characterization tool for vertical profile measurement of high-aspect-ratio microstructures. *J. Micromech. Microeng.*, 12:280–285, 2002.

[93] S. M. Namara, A. S. Basu, J. H. Lee, and Y. B. Gianchandani. Ultracompliant thermal probe array for scanning non-planar surfaces without force feedback. *J. Micromech. Microeng.*, 15:237C243, 2005.

[94] Y. Sun and B. J. Nelson. Mems for cellular force measurements and molecular detection. *Int. J. of Information Acquistion*, 1:23–32, 2004.

[95] K. Inohaya, S. Yasumasu, K. Araki, K. Naruse, K. Yamazaki, I. Yasumasu, I. Iuchi I, and K. Yamagami. Species-dependent migration of fish hatching gland cells that express astacin-like proteases in common. *Dev. Growth Differ.*, 39:191–197, 1997.

[96] D. Stainier. Zebrafish genetics and vertebrate heart formation. *Nature Rev. Genetics*, 2:39–48, 2001.

[97] K. Y. Lee, H. Huang, B. Ju, Z. Yang, and S. Lin. Cloned zebrafish by nuclear transfer from long-term-cultured cells. *Nature Biotechnol.*, 20:795–799, 2002.

[98] Y. Kimura and R. Yanagimachi. Intracytoplasmic sperm injection in the mouse. *Biol. Reprod.*, 52(4):709–720, 1995.

[99] K. K. Tan and S. C. Ng. Computer-controlled piezoactuator for cell manipulation. In *IEEE Proc. Nanobiotechnology*, pages 15–20, 2003.

[100] O. T. Strand, M. E. Lowry, S. Y. Lu, D. C. Nelson, D. J. Nikkel, M. D. Pocha, and K. D. Young. Automated fiber pigtailing technology. In *Proc. of Electronic Components and Tech. Conf.*, pages 1000–1003, 1994.

[101] P. Karioja, J. Ollila, V. P. Putila, K. Keranen, J. Hakkila, and H. Kopola. Comparison of active and passive fiber alignment techniques for multimode laser pigtailing. In *Proc. of Electronic Components and Tech. Conf.*, pages 244–249, 2000.

[102] B. C. Gibson, S. T. Huntington, and J. D. Love. Self-aligning method of fiber-to-waveguide pigtailing. *Opt. Lett.*, 30(21):2858–2860, 2005.

[103] G. Yang, J. A. Gaines, and B. J. Nelson. A flexible experimental workcell for efficient and reliable wafer-level 3d microassembly. In *IEEE Int. Conf. on Robot. and Automat.*, pages 133–138, 2001.

[104] D. Popa, H. K. Byoung, S. Jeongsik, and Z. Jie. Reconfigurable micro-assembly

system for photonics applications. In *Proc. IEEE Int. Conf. on Robot. and Automat.*, pages 1495–1500, 2002.

[105] V. Richard and K. Pradeep. A theoretical and experimental investigation of explicit force control strategies for manipulators. *IEEE Trans. Automat. Contr.*, 38:1634–1650, 1993.

[106] H. Zhang, Y. Bellouard, E. Burdet, R. Clavel, A. N. Poo, and D. W. Hutmacher. Shape memory alloy microgripper for robotic microassembly of tissue engineering scaffolds. In *Proc. IEEE Int. Conf. on Robot. and Automat.*, pages 4198–4124, 2004.

[107] J. Agnus, P. Nectoux, and N. Chaillet. Overview of microgrippers and design of a micromanipulation station based on a mmoc microgripper. In *IEEE Int. Symposium on Compu. Intell. on Robot. and Automat.*, pages 117–123, 2005.

[108] M. Mizukami, M. Hirano, and K. Shinjo. Simultaneous alignment of multiple optical axes in a multistage optical system using hamiltonian algorithm. *Opt. Eng.*, 40(3):448–454, 2001.

[109] R. Zhang and F. G. Shi. A novel algorithm for fiber-optic alignment automation. *IEEE Trans. Adv. Packag.*, 27(1):173–178, 2004.

[110] Y. Sun, S. N. Fry, D. P. Potasek, D. J. Bell, and B. J. Nelson. Characterizing fruit fly flight behavior using a microforce sensor with a new comb-drive configuration. *J. of Microelectromech. Syst.*, 14:4–11, 2005.

[111] A. Pillarisetti, M. Pekarev, A. D. Brook, and J. P. Desai. Evaluating the role of

force feedback for biomanipulation tasks. In *Symposium on Haptic Interfaces for Virtual Environment and Teleoperator Systems*, pages 11–18, 2006.

[112] D. Y. Cho and J. H. Shim. A new micro biological cell injection system. In *Proc. IEEE/RSJ Int. Conf. on Intell. Robot. and Syst.*, pages 1642–1647, 2004.

[113] L. Mattos, E. Grant, and R. Thresher. Semi-automated blastocyst microinjection. In *Proc. IEEE Int. Conf. on Robot. and Automat.*, pages 1780–1785, 2006.

[114] D. H. Kim, C. N. Hwang, Y. Sun, S. H. Lee, B. Kim, and B. J. Nelson. Mechanical analysis of chorion softening in prehatching stages of zebrafish embryos. *IEEE Trans. Nanobiosci.*, 5(2):89–94, 2006.

[115] Y. Sun and B. J. Nelson. Biological cell injection using an autonomous microrobotic system. *The International Journal of Robotics Research*, 21(11):861–868, 2002.

[116] S. Zappe, M. Fish, M. P. Scottb, and O. Solgaard. Automated mems-based drosophila embryo injection system for highthroughput rnai screens. *Lab Chip*, 6:1–9, 2006.

[117] M. Tortonese, H. Yamada, R. C. Barrett, and C. F. Quate. Atomic force microscopy using a piezoresistive cantilever. In *Int. Conf. on Transducers*, pages 448–451, 1991.

[118] G. Villanueva, J. Bausells, J. Montserrat, and F. Perez-Murano. Polysilicon piezoresistive cantilevers for intermolecular force detection. In *Spanish Conf. on Electron Devices*, pages 495–498, 2005.

[119] D. W. Hutmacher. Scaffolds in tissue engineering bone and cartilage. *Biomaterials*, 21:2529–2543, 2000.

[120] R. Langer and J. Vacanti. Tissue engineering. *Science*, 260:920–926, 1993.

[121] H. Zhang. *Robotic microassembly of tissue engineering scaffold*. PhD thesis, Mechanical Engineering Department, National University of Singapore, 2005.

[122] H. Zhang, E. Burdet, D. W. Hutmacher, and A. N. Poo. Robotic microassembly of scaffolds for tissue engineering (video). In *Proc. IEEE Int. Conf. on Robot. and Automat.*, 2003.